LATE HOLOCENE SEISMO-TURBIDITE INVESTIGATION IN THE SEDIMENTS OF GULF OF AQABA

A THESIS SUBMITTED TO
THE GRADUATE SCHOOL OF NATURAL AND APPLIED SCIENCES
OF
MIDDLE EAST TECHNICAL UNIVERSITY

BY

ZEYNEP BEKTAŞ

IN PARTIAL FULFILLMENT OF THE REQUIREMENTS
FOR
THE DEGREE OF MASTER OF SCIENCE
IN
GEOLOGICAL ENGINEERING

FEBRUARY 2021

Approval of the thesis:

LATE HOLOCENE SEISMO-TURBIDITE INVESTIGATION IN THE SEDIMENTS OF GULF OF AQABA

submitted by **ZEYNEP BEKTAŞ** in partial fulfillment of the requirements for the degree of **Master of Science in Geological Engineering, Middle East Technical University** by,

Prof. Dr. Halil Kalıpçılar
Dean, Graduate School of **Natural and Applied Sciences**

Prof. Dr. Erdin Bozkurt
Head of the Department, **Geological Engineering**

Assoc. Prof. Dr. Ulaş Avşar
Supervisor, **Geological Engineering, METU**

Examining Committee Members:

Prof. Dr. Nuretdin Kaymakcı
Department of Geological Engineering, METU

Assoc. Prof. Dr. Ulaş Avşar
Department of Geological Engineering, METU

Prof. Dr. Aurélia Hubert-Ferrari
Department of Geography, University of Liège

Prof. Dr. Sigurjón Jónsson
Physical Sciences and Engineering Division,
King Abdullah University of Science and Technology
(KAUST)

Prof. Dr. Yann Klinger
Lithosphere Tectonics and Mechanics,
Institut de Physique du Globe de Paris (IPGP)

Date: 12.02.2021

I hereby declare that all information in this document has been obtained and presented in accordance with academic rules and ethical conduct. I also declare that, as required by these rules and conduct, I have fully cited and referenced all material and results that are not original to this work.

Name, Last name: Zeynep Bektaş

Signature:

ABSTRACT

LATE HOLOCENE SEISMO-TURBIDITE INVESTIGATION IN THE SEDIMENTS OF GULF OF AQABA

Bektaş, Zeynep
Master of Science, Geological Engineering
Supervisor: Assoc. Prof. Dr. Ulaş Avşar

February 2021, 135 pages

The Gulf of Aqaba is located at the southern part of the Dead Sea Fault (DSF), the length of which is reaches approximately to 1200 km, extending up to Amuq valley in southern Turkey. The gulf is characterized by three pull-apart basins accommodating trans-tensional deformation. Although paleo-seismological information on the past devastating earthquakes that occurred on the on-shore part of DSF is available, it is lacking for the off-shore part of the DSF. In order to fill this information gap and to improve our knowledge about the location, 3D geometries and seismic potentials of the active fault segments in the region, the "Interdisciplinary earthquake hazard study - GAST Project" was initiated in the Gulf of Aqaba and Strait of Tiran in 2017. In this context, 23 short cores were collected from the gulf to investigate sedimentary traces of past earthquakes. Among these, 18 cores with lengths ranging between 35 and 107 cm were scanned by ITRAX micro-XRF scanner at a resolution of 0.5 mm. Radiographic imaging was carried out on 4.2 cm-wide and 0.8 cm-thick u-channels, which allows better evaluation of sedimentary structures. The radiographic images reveal that primary sedimentary structures are completely destroyed by extensive bioturbation, hampering the use of soft-sediment deformations for detecting past earthquakes. Turbidites, on the other hand, are clearly seen in the radiographs since they were deposited in a very short time and are least affected by bioturbation. In the radiographic images, fining upwards bedding is very common and the uppermost parts of the sequences appear finer and more homogeneous. Turbidites manifested geochemical anomalies in the ITRAX profiles, such as Zr/Ca, Ti/Ca, Rb/Ca confirming the relatively very quick deposition that did not allow almost any significant bio/geochemical contribution from the water column. Magnetic Susceptibility measurements were performed at 0.5 cm intervals along the full length of the cores. Dating of the deposits was performed by radionuclide (^{210}Pb and ^{137}Cs) and radiocarbon (^{14}C) dating. High-resolution inter-core and inter-basinal stratigraphical correlations allowed the identification of turbidites triggered by AD 1068, 1212, 1588, 1839, and 1995 earthquakes. In addition, studies have enabled the source segments of these historical earthquakes to be understood. The segments in the Gulf of Aqaba are thought to have a recurrence interval of about 800 years.

Keywords: Marine paleoseismology, Dead Sea Fault, Seismo-turbidite, Bioturbation, ITRAX micro-XRF scanning, U-channel radiography.

ÖZ

AKABE KÖRFEZİ SEDİMANLARINDA GEÇ HOLOSEN SİSMO-TÜRBİDİT ARAŞTIRMASI

Bektaş, Zeynep
Yüksek Lisans, Jeoloji Mühendisliği
Tez Yöneticisi: Doç. Dr. Ulaş Avşar

Şubat 2021, 135 sayfa

Akabe Körfezi, Türkiye'nin güneyindeki Amik vadisine kadar uzanan, uzunluğu yaklaşık 1200 km'yi bulan Ölü Deniz Fayı'nın (ÖDF) güney kesiminde yer almaktadır. Körfez, sıkışmalı-genişlemeli hareketi temsil eden üç adet çek-ayır havzası ile karakterizedir. ÖDF kıyı kesiminde meydana gelen geçmiş yıkıcı depremlerle ilgili paleosismik bilgi fayın kara bölümünde mevcut olsa da, ÖDF'nin açık deniz kısmı için bilgi eksiktir. Bu bilgi boşluğunu doldurmak ve bölgedeki aktif fay segmentlerinin konumu, 3 boyutlu geometrileri ve sismik potansiyelleri hakkındaki bilgilerimizi artırmak amacı ile 2017 yılında "Akabe Körfezi ve Tiran Boğazı'nda disiplinler arası deprem tehlikesi araştırması - GAST Projesi" başlatılmıştır. Bu bağlamda, bölgedeki geçmiş depremlerin sedimanter izlerini araştırmak için körfezden 23 adet kısa karot alınmıştır. Bunlardan, uzunlukları 35 ile 107 cm arasında değişen 18 karot 0.5 mm çözünürlükte ITRAX micro-XRF tarayıcı ile taranmıştır. Radyografik görüntüleme 4,2 cm genişliğinde ve 0,8 cm kalınlığındaki u kanallarda gerçekleştirildi, bu da tortul yapıların daha iyi değerlendirilmesine olanak sağlamaktadır. Radyografik görüntüler, ilksel sedimanter yapıların, geçmiş depremleri tespit etmek için yumuşak sediman deformasyonlarının kullanılmasını engelleyen kapsamlı biyoturbasyonla tamamen tahrip edildiğini ortaya koymaktadır. Türbiditler ise, aniden çökeldikleri ve dolayısıyla biyoturbasyondan en az etkilendikleri için radyografik görüntülerde açıkça görülmektedir. Radyografik görüntülerde, yukarı doğru incelen tabakalanma çok yaygındır ve sekansların en üst kısımları daha ince ve daha homojen görünmektedir. Türbiditler, ITRAX profillerinde Zr/Ca, Ti/Ca, Rb/Ca gibi jeokimyasal anormallikler göstererek, su kolonundan neredeyse hiçbir önemli biyo/jeokimyasal katkıya izin vermeyen nispeten çok hızlı çökelmeyi doğrulamaktadır. Manyetik Duyarlılık ölçümleri, karotların tüm uzunluğu boyunca 0.5 cm aralıklarla gerçekleştirilmiştir. Sediman tarihlendirmesi, radyonüklid (^{210}Pb ve ^{137}Cs) ve radyokarbon (^{14}C) tarihleme ile yapılmıştır. Yüksek çözünürlüklü karotlar-arası ve havzalar-arası stratigrafik korelasyonlar, M.S. 1068, 1212, 1588, 1839 ve 1995 tarihsel depremlerinin türbiditlerinin tanımlanmasına olanak sağlamıştır. Ayrıca, yapılan çalışmalar bu tarihsel depremlerin kaynak segmentlerinin de anlaşılmasına olanak sağlamıştır. Akabe Körfezi'ndeki segmentlerin yaklaşık 800 yıllık bir tekrarlanma aralığına sahip olduğu düşünülmektedir.

Anahtar Kelimeler: Deniz paleosismolojisi, Ölü Deniz Fayı, Sismo-türbidit, Biyoturbasyon, ITRAX mikro-XRF taraması, U kanallı radyografi.

To my family

ACKNOWLEDGMENTS

This study has been conducted within the scope of the “Interdisciplinary Earthquake Hazard Research in Gulf of Aqaba and Strait of Tiran – GAST” project, which was funded by the King Abdullah University of Science and Technology (KAUST).

Many people have contributed to this study and I would like to thank them all individually. First of all, I would like to express my sincere thanks to my supervisor Assoc. Prof. Dr. Ulaş Avşar for his invaluable supports and patience throughout the study. I am very grateful for his guidance and contribution to my academic career.

Secondly, I am deeply grateful to Prof. Dr. Sigurjón Jónsson and Prof. Dr. Yann Klinger for their continual support and providing the opportunity to work on GAST project. I would also like to extend my gratitude to all jury members, Prof. Dr. Sigurjón Jónsson, Prof. Dr. Yann Klinger, Prof. Dr. Nuretdin Kaymakcı, and Prof. Dr. Aurelia Hubert-Ferrari taking their time and improving my thesis.

Also, I would like to thank my dear friends and colleagues Özlem Karadaş, Akın Çil, Ferhat Kalkan, and Meryem Dilan İnce for their support and help during the lab work and thesis writing process. I am also very grateful to Gamze Tanık, who contributed to the determination of the species of planktonic foraminifera samples extracted for radiocarbon dating.

Finally, I would like to thank my parents Meryem and Talip Solakoğlu, my dear brother Ziya Solakoğlu for their unconditional love and support. Also, I would like to thank my husband Recep Bektaş for his endless support. His presence at all matters in my life increased my motivation and played an important role in the realization of this thesis.

TABLE OF CONTENTS

CHAPTERS

APPENDICES

LIST OF TABLES

TABLES

LIST OF FIGURES

FIGURES

CHAPTER 1

INTRODUCTION

It is an undeniable fact that natural events and disasters have caused deaths and property losses of millions of people throughout history. Earthquakes, tsunamis, fires, floods, landslides, volcanic eruptions, droughts are just a few of these disasters. The damage is not only limited to loss of life and property but also causes serious damage to the economies of countries. Considering the size of the damage, it is not difficult to see that earthquakes take their place in the top rankings of natural hazards. Major deadly earthquakes that have been experienced and recorded can be exemplified as follows: 1999 Earthquake in Turkey (17.118 dead), 2001 Earthquake in India (20.023 dead), 2003 Earthquake in Iran (31.000 dead), 2004 Earthquake in Indonesia (>250.000 dead), 2005 Earthquake in Pakistan (80.361 dead) and 2008 Earthquake in Sichuan province in China (69.000 dead) (US National Earthquake Information Center). The losses caused by earthquakes have been recorded in different ways at different times. For example, by the invention of writing, people have started to note their feelings and losses they experienced after earthquakes. In their chronicles, many clergymen frequently recorded the destructive effects of the earthquakes, and the extent of losses (Subaşı, 2015). Although providing no information on the magnitude of earthquakes, such records are invaluable for recording the timing of historical earthquakes.

The advances in science and technology, on the other hand, facilitated studying earthquakes quantitively. The discipline investigating past earthquakes is called “paleoseismology”. The main reason for many paleoseismology studies is social and economical concerns arising from devastating earthquakes. To mitigate future losses, the characteristics of these earthquakes and their sources, the faults, ought to be well understood. Such information comprises detailed information about the location, timing, and size of the earthquake for predicting possible future earthquakes. In this context, paleoseismological studies play a key role in understanding the behavior, and recurrence intervals aid the authorities in the mitigation of future earthquakes.

Paleoseismological studies are multidisciplinary in nature and use information obtained from various disciplines such as; structural geology, sedimentology, seismology, geochemistry, and historical geology. By definition, paleoseismology is a science aiming at identifying earthquakes that occurred in the past and revealing the seismic potential of active faults by investigating the origins of them (Gràcia et al., 2013). It can be shortly explained as the study of past earthquakes by using special methods.

Due to the relatively recent advent of modern seismology, accumulated seismological data is still not sufficient for determining the recurrence intervals of most earthquakes in the long term. Paleoseismological studies, on the other hand, cover longer time spans and integrates available seismic records and historical data as well geological information and observations based on field and laboratory analyses to understand the long term seismic behavior of an area. Unraveling the seismic history of a region can be used to predict future earthquakes and helping to take necessary precautions.

Deciphering paleoearthquakes can also be possible by using various paleoseismological methods. Dendroseismology, which is based on finding the traces of past earthquakes on tree rings, can reveal past earthquakes by studying damages in tree root systems and trunks or sudden asymmetric growth in tree rings, or suppressions in the growth of a branch of trees (Avşar, 2013; Fan et al., 2020). Although it is difficult to find a long and complete record of earthquakes with this method, tree ring chronology is one of the most precise methods used in paleoseismological investigations. This method is suitable for faults where paleoseismic trenching is not possible and especially for faults located in forested areas (Kozacı, 2012).

Speleoseismology involves finding the traces of past earthquakes with the data obtained from cave deposits (Avşar, 2013; Kagan et al., 2017; Mendecki & Szczygieł, 2019). The most conspicuous earthquake damage that may occur in caves is the breaking of stalactites and stalagmites. Besides, these structures can be deformed or displaced by an earthquake, and also some growth anomalies might develop due to seismic activity (Becker et al., 2006). Timing of past earthquakes can be determined by dating the breaking points. This method makes a valuable contribution to paleoseismological studies by providing precise and accurate correlations at locations where far-field effects of earthquakes can be studied.

Archeoseismology is another widely used branch of paleoseismology. The objects made by people in ancient times, the tools they have used, or architectural structures are also affected by earthquakes. It is possible to find traces of past earthquakes in all kinds of archaeological sites (Silva et al., 2005; Korzhenkov et al., 2016). For example, the walls of damaged or destroyed ancient buildings and displaced structures carry the fingerprints of paleoearthquakes. Sometimes, residential areas that people have left suddenly may also be caused by a natural disaster such as an earthquake (Avşar, 2013).

The most commonly used method in many paleoseismology studies on land is on-fault trenching (Kelsey et al., 1998; Masana et al., 2004; McCalpin, 2009; Klinger et al., 2015). Since it is widely used, it has been improved over time and kept up with the developing technology. Finding the physical, chemical, and morphological traces of earthquakes on sedimentary deposits using trenching provides a wide range of knowledge about the seismic background of a study site. Trenching means opening a research pit exactly on the fault at a depth pre-determined according to the purpose of the study. It is essential to follow the stratigraphic horizons in these trenches because the basic motivation behind on-fault trenching is to detect surface rupture-related stratigraphic horizons and to date their timing (Avşar, 2013). By doing so, paleoseismologists can easily recognize the amount of replacement of the rock units and gather all necessary data related to that faulting. However, erosional processes sometimes may limit the capability of trenching method. Any erosion that takes place on the trench site may cause chronological errors for paleoseismological investigations. Nevertheless, the earthquake magnitude is the most important factor to create surface ruptures during and earthquakes, although there are numerous mechanisms behind the earthquakes' potential. In addition, it is a known fact that earthquakes with a magnitude of about M 5.6-5.8 cannot be very effective in producing surface rupture (Villamor & Berryman, 2001; Pavlides & Caputo, 2003), which limits the applicability of trenching method. Therefore, trenches on such faults may not provide paleoseismological information. Another important point related to on-fault trenching is that this method is applicable only to the faults on land. For subaqueous faults, like in the case of Aqaba, on fault trenching ceases to be a viable method for paleoseismology.

Many large and destructive earthquakes take place in marine environments, especially in subduction zones (e.g. 17.02. 2010 Chile earthquake (Mw 8.8) and 25.12.2004 Sumatra earthquake (Mw 9.1) and constitute a large part of the most destructive and major earthquakes in the world. In this context, it can be said that the most dangerous places in the world in terms of seismicity are the coastal regions. In order to study the seismicity of subaqueous faults, the 'Subaqueous Paleoseismology' method is used. Subaqueous paleoseismology involves the study of the effects of past earthquakes on sediments of marine or lacustrine environments. For this purpose, all physical and chemical changes created by earthquakes on the subaqueous sedimentation are used as earthquake detection tools. In this context, earthquake-induced soft-sediment deformations and subaqueous mass wasting products are the two most common proxies (Monecke et al., 2004; Goldfinger, 2009; Avşar et al., 2016). Additionally, it is also possible to detect catchments response to a significant earthquake, as geochemical changes in background sedimentation or a large volume of sediment influx the basin (Avşar et al., 2016). The sediment influx from the catchment to the lake basin is expected to increase due to the large volume of loose material during ground shaking.

When land and subaqueous paleoseismological studies are compared in terms of methods applied and the results obtained, it is clearly seen that there are some prominent advantages of subaqueous paleoseismology. One advantage is that there is a continuous deposition underwater since oceans and seas are calm and relatively stable environments, so it is possible to obtain a continuous sedimentation record (McHugh et al., 2006; Avşar et al., 2014a; De Batist et al., 2017). Since the aqueous environments have continuous sedimentation records and relatively slow sedimentation rates when compared to land, longer-term and more precise chronology can be constructed compared to the on-fault trenching method (McHugh et al., 2014; Goldfinger, 2011). Another prominent aspect of subaqueous paleoseismology is that faults that do not have large enough magnitudes to create surface rupture cannot be studied by trenching method. However, such earthquakes can still create some sedimentological or geochemical anomalies in the continuous sedimentation of subaqueous environments. This means that the traces of many earthquakes that cannot be detected on land may not be missed out by subaqueous paleoseismological studies.

In-situ soft-sediment deformations and coeval mass wasting events are the most prominent earthquake markers according to main subaqueous paleoseismology studies (Inouchi et al., 1996; Gorsline et al., 2000; Goldfinger et al., 2003a, 2003b, 2009, 2011; Monecke et al., 2004; Patton et al., 2013, 2015; Avşar et al., 2014a, 2015, 2016; McHugh et al., 2014; Moernaut et al., 2014; Ikehara et al., 2016). In addition, a significant increase in the petrography, size, volume of terrigenous material shedding to the lake from its catchment due to earthquake-induced landslides is also an important indicator used in subaqueous paleoseismology, especially in lacustrine paleoseismology (Howarth et al., 2012; 2014; Avşar et al., 2016).

It is important to note that some of the sedimentological markers of earthquakes such as turbidity currents or underwater landslides can also occur due to other natural phenomena (i.e., storms, natural slope failure, flooding, etc.). For this reason, it is necessary to assess the triggering mechanism of these natural phenomena. One of the most reliable criteria would be the assessment of such natural phenomena that took place only at one place or in a large area simultaneously throughout the basin.

In other words, synchronicity and the number of turbidites or submarine landslides occurring at the same time must be checked and temporally correlated (Goldfinger et al., 2007). Another important issue related to subaqueous paleoseismology is chronology. Radiocarbon dating is the most widely used method for obtaining sediment chronology in Quaternary deposits. Uncertainties in radiocarbon dating may result in an inaccurate chronology. These uncertainties will be discussed in detail in “section - 3.6.2. Radiocarbon Dating”.

1.1 Purpose and Scope

The main purpose of this thesis is to unravel traces of the historical earthquakes that occurred in the last thousand years and recorded within the sediments of the Gulf of Aqaba and to characterize the southern part of the Dead Sea Fault (DSF) within the Gulf of Aqaba.

Previously, the DSF has been studied by geophysical investigations and paleoseismic trenches (Qatar Site, Klinger et al., 2015; Avrona Site, Amit et al., 1999; Zilberman et al., 2005; Shehoret Site, Amit et al., 2002; and Eilat Site, Kanari et al., 2020). Moreover, morphology and fault traces of the Araba Valley were mapped out using aerial photographs and satellite images (Amit et al., 1999). According to previous paleoseismology studies, the DSF is a left-lateral strike-slip fault (Quennel, 1958) having approximately 5 ± 1 mm/yr slip rate (Le Beon et al., 2010) and more than 1200 km length. The fault starts with the Bitlis-Zagros suture in the north and ends with the Red Sea extension in the south (Al-Tarazi, 1999; Amit et al., 1999, 2002; Gomez et al., 2003; Ben Avraham et al., 2008; Klinger et al., 2015; Kanari et al., 2020). However, the difficulties in opening trenches at the shoreline where DSF enters the Gulf of Aqaba, subaqueous paleoseismology is the most plausible alternative to obtain information about the long-term paleoseismic record from the submerged continuation of the fault.

Only one segment in the Gulf of Aqaba has ruptured during the 1995 Nuweibaa Earthquake (Ribot et al., 2021) meaning that more stress is accumulated on the other unbroken segments and they have the potential to cause large earthquakes in the near future. This demands a detailed study of the past earthquake records in the gulf.

Motivated by previous studies, the Gulf of Aqaba Strait of Tiran (GAST) project was initiated to understand the underwater character of the DSF and to unravel reveal its long term paleoseismological record for the Gulf of Aqaba. Within the scope of this project, a rigorous coring program and high-resolution multi-beam bathymetric imaging to aid in determining core locations is performed. On the obtained cores, various analyses such as grain-size analyses, ITRAX micro-XRF scanning, and radiographic imaging are applied. Moreover, temporal correlation of turbidites with historically known earthquakes is performed by C^{14} dating techniques.

1.2 Study Area: The Gulf of Aqaba

The Gulf of Aqaba is located in the northern part of the Red Sea and it separates the Arabian plate and the Sinai microplate from each other by the left lateral DSF. The length of the gulf is approximately 180 km and its width reaches up to 25 km at its widest part. It is located between $27^{o}57'36''$N-$29^{o}32'50''$N latitudes and $34^{o}27'35''$E-$35^{o}58'29''$E longitudes. The coastlines and waters of the gulf are shared by four countries; Egypt, Israel, Jordan, and Saudi Arabia. The Gulf of Aqaba is the southernmost of the three pull-apart basins formed along DSF due to the interaction between Red Sea extension and DSF itself. Other important pull-apart basins formed along the DSF are the Dead Sea and Sea of Galilee from south to north respectively.

The southernmost segment of the Dead Sea Fault system just before entering the gulf is called the Wadi Araba Fault (WAF). This fault runs along the Arava Valley between the Dead Sea and the Gulf of Aqaba and enters the gulf by passing through the city of Eilat (Figure 1.1 - b). The WAF has been examined in detail by a series of paleoseismic trenches at certain locations from the city of Rahma in the north to the city of Eilat in the south, and traces of historical earthquakes that had caused surface ruptures on this fault segment have been identified. These trench locations are represented on the map by the letters a, b, c, and d, from north to south, respectively.

The trench shown with 'a' in Figure 1.1b was excavated at the Qatar site which is located in Jordan and 30 km north of the city of Aqaba (Klinger et al., 2015). It got its name from its location because it is close to a village called Qatar. The paleoseismic trench excavated in this area was approximately 25 m long and 4 m wide. Its depth was about 3 m due to the high groundwater table. Besides, the long axis of the trench was opened perpendicular to the fault, so it was aimed to find the traces of the surface rupture. As a result of the detailed analyses made in this trench site, 9 distinct levels described as ‘events’ are determined, but only a few of them coincide with historical earthquakes. In addition, the exact locations of historical earthquakes found in this trench site are still uncertain. The surface rupture of the historical AD 1588 earthquake, which affected the areas from Madinah to Cairo, cannot be found in the Qatar paleoseismic trench. Therefore, it was concluded that the AD 1588 earthquake may have been confined before it reaches the Gulf of Aqaba. At the end of this study, just like the AD 1588 earthquake, the traces of the AD 1293 and AD 1546 earthquakes were not observed. In this study, it was revealed that the historical earthquakes of AD 1458, 1212, 1068, 746 -757, and 363 have ruptured along the WAF.

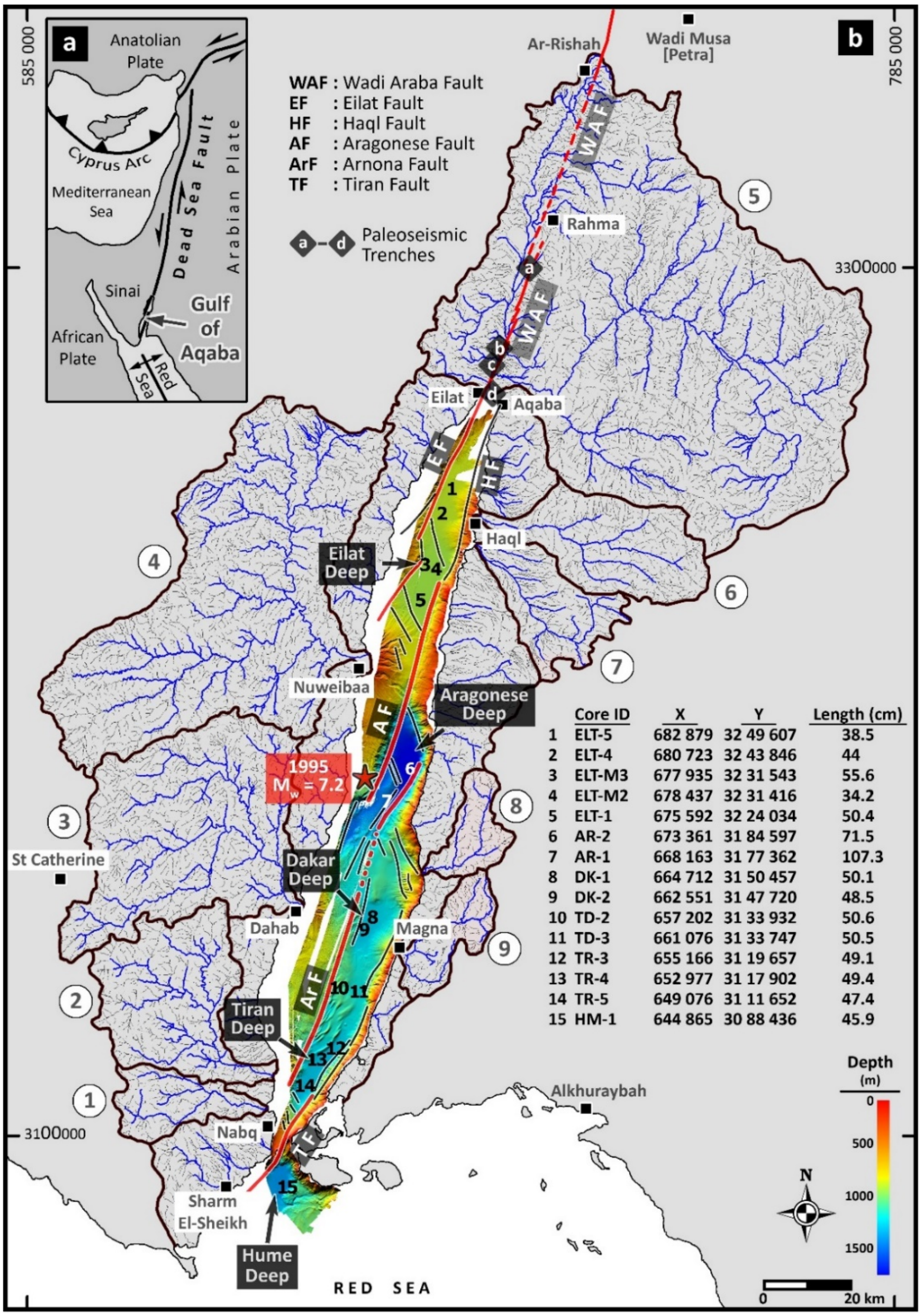

	Core ID	X	Y	Length (cm)
1	ELT-5	682 879	32 49 607	38.5
2	ELT-4	680 723	32 43 846	44
3	ELT-M3	677 935	32 31 543	55.6
4	ELT-M2	678 437	32 31 416	34.2
5	ELT-1	675 592	32 24 034	50.4
6	AR-2	673 361	31 84 597	71.5
7	AR-1	668 163	31 77 362	107.3
8	DK-1	664 712	31 50 457	50.1
9	DK-2	662 551	31 47 720	48.5
10	TD-2	657 202	31 33 932	50.6
11	TD-3	661 076	31 33 747	50.5
12	TR-3	655 166	31 19 657	49.1
13	TR-4	652 977	31 17 902	49.4
14	TR-5	649 076	31 11 652	47.4
15	HM-1	644 865	30 88 436	45.9

Figure 1.1. a) Regional tectonic setting and the location of Gulf of Aqaba. b) Bathymetric map of the Gulf of Aqaba, paleoseismic trench studies (a,b,c,d), active fault branches, and drainage map of the Gulf of Aqaba.

There were 2 important paleoseismic investigations done in Avrona Site (Figure 1.1b). In the first study, Amit et al. (1999) argue that the only damaging earthquake that occurred during the BC 184 - AD 1992 time period was the AD 1212 earthquake, and they suggested its epicenter as the Arava Valley. Therefore, they designate Avrona Playa, which is located in the southern Arava Valley, as their study site. After the morphology of the Avrona Playa was mapped using aerial photographs and satellite images, other necessary geophysical studies were completed. According to the data obtained from these preliminary studies, trench locations that were adjusted to cross tectonic features were determined. The lengths of the excavated trenches range between 10 m and 70 m and have a width of 1.5 m and a depth of up to 5 m. While 2 of the 3 paleoseismic trenches excavated within the scope of this study cuts the fault scarps, the third one cuts the elevated ridge in the easternmost part of the playa. At the end of their study, Amit et al. (1999) concluded that the most recent tectonic activity in the region resulted in the relief inversion for the Avrona Playa. In other words, they concluded that the topographically lowest part of the playa was converted to the highest topographic position. They also drew attention to the seismic quiescence of the region and emphasized that an earthquake that is likely to occur on the Avrona fault segment in the near future may have a great potential to cause serious damage to the cities of Eilat and Aqaba. The second paleoseismic study conducted at the same location is Zilberman et al. (2005). In this study, the paleoseismic trenches that were excavated in 1999 by Amit et al. (1999) were used. In addition to the results obtained from the previous study (Amit et al., 1999), it has been proven by paleoseismic, geophysical, and archaeological evidences that the devastating earthquake that caused the change in the form of the Arava Playa was the historical AD 1068 earthquake. Moreover, the location of the historical earthquake of AD 1068 is said to be south of the Arava Valley, not in the Tabuk area as it is said in Ambraseys (1994) meaning that the last two destructive earthquakes that are AD 1068 and 1212 were related to the DSF. Since recurrence intervals of major large earthquakes experienced during the Holocene on the Eilat fault were identified as about 1.2 ± 0.3 ky, the fact that almost 1000 years had passed since the last major earthquake proves that the Eilat-Aqaba region is in a high seismic hazard zone.

The third paleoseismic trenching study was conducted by the same team (Amit et al., 2002) in Shehoret Site which is located in the southwest of the Avrona Playa and the trench site is indicated as 'c' on the map (Figure 1.1b). Eilat fault zone was selected as the study area and 5 fault segments were determined for paleoseismic analysis. After necessary preliminary mapping and geophysical studies, trench excavation was done to cut each of these 5 fault segments at least once. As a result of the study, when the recurrence intervals of the major earthquakes along the Late Pleistocene and Holocene are compared and examined in detail, it was noted that these intervals decreased from 2.8 ± 0.7 ka to 1.2 ± 0.3. This means that quite a long time has passed since the last major earthquake in the Eilat fault segment (AD 1068), and this may indicate a locking in this fault segment. In short, it has been pointed out that the Eilat fault segment has a high potential to create large earthquakes in the near future, just like in the previous paleoseismic trenching works.

Kanari et al. (2020) is the most recent paleoseismic trenching study conducted on land just before entering the Gulf of Aqaba. The trench area determined in this study is Eilat Site and it is marked with 'd' on the map (Figure 1.1b). Seismic reflection and paleoseismic trenching were performed to reveal the seismic hazard potential of the Eilat Fault segment in terms of the welfare of the cities Eilat and Aqaba. While two of the paleoseismic evidences found at the end of the study were in the form of surface ruptures, two of them were stated as sand blows due to paleoliquefaction caused by earthquakes. It is indicated that the first of the surface ruptures found in the paleoseismic trenches belonged to the historical AD 1068 earthquake and the second to the AD 1458 or 1588 earthquakes. On the other hand, paleoliquefaction, which is the second paleoseismic evidence, was attributed to the AD 1458 or 1588 earthquakes as a result of the dating the sand blows caused by this liquefaction. Another result obtained is that the surface rupture of the AD 1068 earthquake was minimum of 37 km and its magnitude was between M 6.6-7.1. Similar to previous studies, in this study, it was pointed out that the Eilat fault segment has been silent for approximately 430-550 years and that there is a high seismic hazard in the Eilat-Aqaba region.

Previous studies have revealed that the Gulf of Aqaba consists of a coalescence of pull-apart basins (Ben-Avraham et al., 1979, 2008; Tibor et al., 2010; Ribot et al., 2021) (Figure 1.1b). The northernmost basin of the gulf is called the Eilat Deep (Figure 1.1b) and is controlled by the Eilat Fault (EF) having strike-slip character along its western flanks and by Haql Fault (HF) having normal dip-slip character along its eastern coasts. Also, the Aragonese Fault (AF), which passes through the south of the Eilat Deep, is in contact with the Eilat Deep and plays an important role in the basin geometry. The Eilat Deep, with an average depth of 900 m, has a classic pull-apart basin geometry (Ribot et al., 2021). It has relatively gentle slopes in the eastern parts, while on the west coast it has steep slopes that are considered as fault scarps. In the south of the Eilat Deep, there is the Aragonese Deep (Figure 1.1b), which has a classic pull-apart basin geometry with a long axis almost parallel to the long axis of the Gulf of Aqaba (about N20) (Ben-Avraham, 1985, 2008; Ribot et al., 2021), just like the Eilat Deep. The Aragonese Deep, bordered by the Aragonese Fault (AF) in the northwest and the Arnona Fault (ArF) in the southeast, has a small secondary basin, having approximately 1500 m water depth, on the west flank called Arnona Deep. Both the Aragonese and Arnona deeps have steep slopes indicating that the strike-slip faults that comprise them have also some normal components. The Dakar Deep (Figure 1.1b) is located south of the Aragonese Deep and its average depth is 1285 m. While it is bounded by ArF in the west, it is under the influence of normal fault activity on its eastern side. In the western part of the Dakar Deep, there is a plain called Dahab Plateau. In addition, when the detailed seafloor morphology is examined, salt diapirs and cylindrical folds were found in the eastern part. It is possible to say that the exact location of the Arnona fault passes through the Dahab Plateau and the point where these salt diapirs separate from each other. The southernmost basin in the Gulf of Aqaba is the Tiran Deep (Figure 1.1b), which has an average water depth of 1270 m, and the gulf is connected to the Strait of Tiran with this small deep. Since the Tiran Deep is where the gulf is narrowing, its width is quite limited. ArF is effective in the north of the Tiran Deep and Tiran Fault (TF) in the south. Hume deep with average water of about 1400 m is located where the Strait of Tiran connects to the northern Red Sea. Detailed analysis and descriptions of fault geometry and basins are provided by Ribot et al., 2021.

15 sediment cores varying in length from 34.2 cm to 107.3 cm, were taken (Figure 1.1b) in the cruise conducted from May 20th to June 7th, 2018 along the Gulf of Aqaba. A high-resolution bathymetric survey along the eastern half of the Gulf of Aqaba (within Saudi waters) and the Strait of Tiran was performed on shipboard the R/V Thuwal. The sediment coring sites are shown in Figure 1.1b with their exact geographic locations.

Considering that the Gulf of Aqaba has a total catchment area of 19260 km^2 and a well-developed drainage pattern (Figure 1.1b), it is a straightforward indicator that the gulf is exposed to intense sediment influx. In a study conducted by Moernaut (2010) in Lake Calafquén, 96 sublacustrine landslides were examined in terms of morphological parameters. According to the results of this study, 6.1° was stated as the threshold slope angle for most of the subaqueous slopes to fail. When the Gulf of Aqaba is considered in terms of slope steepness like in this study (Moernaut, 2010), it is seen that the submarine morphology of the gulf mimics the steep topography of its surrounding mountains (Ribot et al., 2021). Average slope angles for sub-basins of the Gulf of Aqaba were calculated and presented in Table 1.1. For example, in Tiran Basin, the edge of the basin plain (ca. 1280 m) is approximately 4000 m from the eastern coastline of the Gulf, which corresponds to an average slope amount of 17.7°. Similarly, in the Aragonese Basin, the edge of the basin plain (ca. 1760m) is approximately 3000 m from the eastern coastline of the Gulf, which corresponds to an average slope amount of 30.4° and it is much greater than 6.1°. That is, steep-sloped submarine topography and its exposure to excessive sediment influx because of its big catchment with a well-developed drainage pattern indicate that the Gulf of Aqaba is quite susceptible to submarine mass-wasting events.

Table 1.1. Average slope angles are calculated according to geometric information of the sub-basins within the Gulf of Aqaba.

	Depth of Basin Plain (m)	Distance between the edge of the basin plain and coastline (m)	Average Slope (Degrees)
Eilat	920	4500	11.6
Aragonese	1760	3000	30.4
Dakar	1270	7000	10.3
Tiran	1280	4000	17.7
Hume	1400	3000	25

1.2.1 Regional Tectonics

On a regional scale, the Gulf of Aqaba is the southern tip of the DSF (Figure 1.1a), which acts as a bridge between the Bitlis-Zagros Suture zone in the north and the Red Sea extension zone in the south (Ben Avraham, 1985; Barjous & Mikbel, 1990; Girdler, 1990; Klinger et al., 1999; Ben Avraham et al., 2008; Le Béon et al., 2012). The compression between the Arabian Plate and the Eurasian Plate and the anti-clockwise rotation of the Arabian plate cause the continuation of the DSF with a left lateral strike deformation. The interaction between this compressional and extensional movement in the region resulted in the formation of several pull-apart basins along the DSF such as the Sea of Galilee, the Dead Sea, the Gulf of Aqaba, and some smaller ones in the gulf (Klinger et al., 2000). When the long axis of the Aqaba Gulf is examined carefully, it is clearly seen that it is almost parallel to the strike of the fault, proving that it is one of the pull-apart basins formed along the DSF. The gulf is connected to the Red Sea by the Strait of Tiran in the south.

1.3 Background Seismicity of the Gulf of Aqaba

In paleoseismology studies, as well as establishing a precise chronology, it is also crucial to check this chronological record by making a proper correlation with the historical and instrumental earthquake records experienced in the studied region. In this way, the quality and reliability of the work are also assessed. Also, unless historical records do not match geological and seismic data, earthquakes can not be beyond being sad memories.

The Gulf of Aqaba is a seismically active region due to its location and has been exposed to many earthquakes throughout history. Historical and instrumental earthquakes and their sources are presented below (Table 1.2). The historical earthquakes of AD 1068 and 1212 can be given as examples of the earthquakes that have been proven by the existence of surface ruptures found in paleoseismic studies (Zilberman et al., 2005; Klinger et al., 2015).

The instrumental seismicity along the DSF with moderate and large scale was recorded in 1927 Jericho (ML 6.1) and 1995 Nuweibaa (Mw 7.2). Although the number of instrumental earthquakes is limited, there are many historical earthquakes in the region recorded in earthquake catalogs. Records of historical earthquakes are generally based on damaged structures, buildings, churches, property loss, or fatalities in that area, rather than faulted surface ruptures. Since geologists investigate the sedimentological and geological traces of the earthquakes, they often have trouble matching historical earthquakes with ruptured faults. This issue can only be overcome by precise dating and correlation (Marco & Klinger, 2014).

Table 1.2. Some of the major historical and instrumental earthquakes on DSF.

Date	Affected Area	References
AD 749		Marco et al., 2003; Ambraseys, 2009
AD 859	Northern Yammouneh	Badawy & Horvath, 1999; Akyüz et al., 2006; Marco & Klinger, 2014
AD 1068	South Arava	Ben-Menahem, 1991; Badawy & Horvath, 1999; Klinger et al., 2000; Zilberman et al.,2005; Ambraseys, 2009; Marco & Klinger, 2014
AD 1202	South Yammouneh	Daeron et al., 2007; Badawy & Horvath, 1999; Marco & Klinger, 2014
AD 1212	Northern Arava	Al-Tarazi, 1999; Badawy & Horvath, 1999; Klinger et al., 2000; El-İsa, 2012; Marco & Klinger, 2014
AD 1293	Northern Wadi Araba	Klinger et al., 2000, 2015; Marco & Klinger, 2014
AD 1408	Northern Yammouneh	Akyüz et al., 2006; Marco & Klinger, 2014
AD 1458	Northern Wadi Araba	Klinger et al., 2000, 2015; El-İsa, 2012; Marco & Klinger, 2014
AD 1588	Southern Wadi Araba	Badawy & Horvath, 1999; Klinger et al., 2015
AD 1759	Jordan Gorge	Ben-Menahem, 1991; Al-Tarazi, 1999; Marco & Klinger, 2014
AD 1837	Roum Fault	Ben-Menahem, 1991; Al-Tarazi, 1999; Marco & Klinger, 2014
AD 1872	Northern Yammouneh	Akyüz et al., 2006; Marco & Klinger, 2014
AD 1927	Northern Red Sea	Ben-Menahem, 1991; Al-Tarazi, 1999
AD 1995	Gulf of Aqaba	Klinger et al., 1999

Almost all earthquakes that occurred before the instrumental period, known as historical earthquakes, are available in written sources. At that time, although the earthquakes cannot be identified quantitatively, the earthquakes have been recorded in the areas where they have caused damage and many destruction and fatalities. In light of the information obtained from these historical written sources, the existence of these earthquakes is confirmed by new paleoseismic methods. Historical earthquakes, with their sedimentary, geophysical, and geochemical traces, enable the determination of the large earthquake-generating intervals of active faults.

1.4 Previous Studies along the DSF System

The Eastern Mediterranean region has been studied for many years in terms of tectonics and seismology. For the first time, in 1869 Lartet realized that the Arabian and African plates were separated from each other and the Red Sea was formed. Later, in 1932, Dubertret agreed with Lartet's idea and additionally mentioned a 160 km left-lateral shear movement along the DSF and also suggested the existence of a 6º rotation between the Arabian Plate and the African plate. Subsequently, in 1938, Wellings explained the validity of this hypothesis proposed so far with the offset between the marine Cambrian and Jurassic beds. Then, this left lateral movement explained by a scientist group was supported by Quennell with facies changes and dislocation along DSF. According to Quennell (1956), 107 km dislocation was found in Pre-Cambrian rocks. Freund (1965) also found a 100 km offset between two peer units and supported this dislocation hypothesis. Unfortunately, the political situation of that time did not allow these scientists to go to work to confirm the hypotheses in the region.

Dead Sea Rifting System has been considered as a boundary between the Zagros-Taurus collision zone and Red Seafloor spreading since earlier times (Ben Avraham, 1985; Barjous, 1990). In his study, Ben Avraham (1985) mentioned the existence of 3 pull-apart basins in the Gulf of Aqaba. It was also observed that magnetic anomalies in the geophysical studies carried out in this region changed from land to sea rather than from one shore to another which implies the presence of shearing. At the end of the study, it was seen that there is a transition between the Dead Sea transform and the Red Sea spreading center along the Gulf of Aqaba.

In 1989, Z.H. El İsa and A. Al Shanti conducted a study around the Gulf of Aqaba. When the seismology studies carried out in the Arabian and African regions were considered, it was clearly observed that recorded earthquakes in this region were associated with plate boundaries. For this reason, scientists began to study the Red Sea among the world's rift systems. This region was previously known as aseismic; however, it was found to be seismically active by conducting micro-earthquake studies. Considering that the western part of Saudi Arabia is seismic hazard studies in the region have been mentioned as an urgent need in this paper.

Ben Menahem, 1991 conducted a study that was very similar to this thesis. The main purpose was to reveal 4000 years of seismic record along the Dead Sea. During the study, many independent dating methods have been used such as geological, archaeological, biblical, historical, and seismological methods. Also, historical records have been researched. As a result, it has been concluded that there is an uninterrupted north-south trending seismic movement on the Dead Sea Transform Fault Zone, which has been acting as a boundary between African and Arabian plates, at least for the last 4000 years. Some traces of seismic zones that continue under the sea and parallel to the coastal line of the Eastern Black Sea were detected. It is known that the Dead Sea Transform Zone is still active today and produces continuous earthquakes, so more extensive works are needed to get more information.

Klinger et al., 1999 documented information about the 22 November 1995 Earthquake that occurred in Nuweibaa. Also, this study stated that the 1995 earthquake was associated with the spatial distributions of 1983, 1990, and 1993 swarms which have already been documented in the region. When looking at the seismic background of the gulf, it is seen that seismicity is scarce and characterized by swarms. One of the conclusions from the same study is that the Gulf of Aqaba region is an arid region and it is extremely difficult to create a complete historical earthquake catalog in such desert environments. Also, Klinger et al., 2015 identified some historical earthquakes such as AD 1068, 1212, and 1458 earthquakes.

The studies conducted around the southernmost segment of the DSF system which is the Gulf of Aqaba and Strait of Tiran region are quite limited. The fact that the Gulf of Aqaba is in a desert environment and the tectonic processes in this region are faster than erosional processes have restricted the paleoseismology studies. The deficiency of marine paleoseismology studies in the Gulf of Aqaba has great importance in terms of emphasizing the necessity of this study.

CHAPTER 2

SEISMO-TURBIDITE ANALYSIS

Turbidites are a typical form of deposition normally seen on the active continental margins where regular sedimentation occurs. When every submarine slope reaches a certain weight and can no longer carry its own weight, it slides periodically and causes the formation of a dense sediment cloud called ‘turbidite’. Turbidites can either occur naturally or can be triggered by any catastrophic event. Seismo-turbidites are the turbidity current deposits that occur as a result of any seismic events such as earthquakes. In this chapter, turbidites of seismic origin and their most prominent features will be explained in detail.

2.1 An Overview of Turbidites

Turbidites are dense sediment clouds deposited as a result of subaqueous mass wasting events. Since they are not a product of stable sedimentation, they are examined under the heading of event-deposits.

These types of events may occur due to various reasons. The most common reason for slopes to fail and cause turbidite depositions is excessive loading. Where the rivers open to the seas or oceans, the materials transported long distances are deposited on continental shelves and slopes. After a certain period of time, these deposited materials reach a level that can not carry their own weights. At this level, excessively loaded slopes fail and slide along the sea bottom. This sliding mass keeps its movement until a flatness. As the topography is gradually flattened, the sediment cloud can no longer move and begins to accumulate the sediments it carries. This dense material is called turbidite.

Turbidites contain particles of different sizes and characteristics. One of the most prominent features of turbidites is the gravitational segregation that occurs during the deposition of dense sediment clouds. In gravitational segregation, relatively coarser particles are deposited first, while finer-grained materials are deposited after being suspended for some time. Fining upward sequence is the most probably expected result for a turbidite. In this context, Bouma Sequence, which is interpreted mainly as a typical turbidite sequence, can be examined closely (Shanmugam, 1997).

In a typical Bouma sequence, there are five distinct sections of sediments (Figure 2.1) named Ta-e, Tb-e, Tc-e, Td-e, and Te from the starting point of a turbidite to its termination, respectively. In other words, this turbidite model was developed based on 'proximal' to 'distal' turbidity current depositions. The first section (Ta) includes massive sand-sized materials. As the energy of transportation decreases, sand-sized clasts start to accumulate. Secondly, in the Tb section, plane parallel laminations of sediments are observed on top of massive sands. After that, the ripples (in Tc) formed due to the movement of turbidity current along the seafloor are the expected structures in a typical turbidite. The grain size is getting finer towards the top of a turbidite sequence and laminated mud-sized materials are encountered (Td). At top of the sequence (Te), the suspended sediments are deposited. That is, muddy material is accumulated at the top of a turbidite. This is a very classical and most accepted version of subaqueous gravity flow depositions.

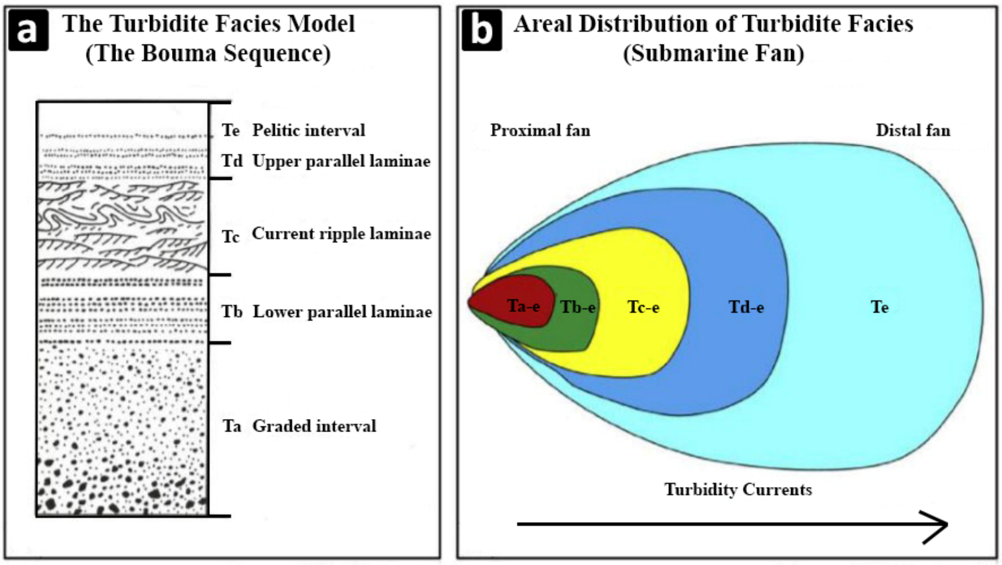

Figure 2.1. Schematic representation of the Bouma sequence. a) Columnar section view and b) Map view of a typical turbidite in the Bouma sequence (From Shanmugam, 2016).

2.2 Seismo-turbidites

Turbidites do not form only as a result of excessive sediment loading on top of submarine slopes. There are many different mechanisms behind subaqueous gravity flow depositions. The most prominent ones are storms, crustal earthquakes, slab earthquakes, tsunamis, excessive sediment loads, hyperpycnal flows, volcanic explosions, cyclones, or bolide impacts (Adams, 1990; Goldfinger et al., 2003a, 2011; Patton, et al., 2013). Apart from all these mechanisms, there are many other mechanisms such as tectonic oversteepening, depositional oversteepening, glacial loading, biological erosion, or sea-level lowering. However, they are rare events that are not regional and synchronous (Inouchi et al., 1996; Goldfinger et al., 2007; Patton et al., 2013). To test the seismic origin of turbidites, the turbidite records are checked if they are regional and synchronous, and at the same time, these records' consistency with historical or other historical and instrumental earthquake records is examined (Goldfinger et al., 2007; Gràcia et al., 2010; Patton et al., 2013; Moernaout et al., 2014).

Among the above-mentioned subaqueous landslide triggering mechanisms, seismic ground shaking is the most investigated one and this item has been studied for many different regions of the world (Heezen & Ewing, 1952; Adams, 1990; Goldfinger, et al., 2003a; Shanmugam, 2008; Polonia, et al., 2012). Subaqueous mass wasting event deposits formed due to a seismic activity are said to be seismo-turbidites. In other words, turbidity current depositions that are formed as a result of catastrophic events and have a unique interior order and composition are called 'seismo-turbidites' (Mutti et al., 1984).

In general, seismo-turbidites differ from classical turbidites in some aspects (Mutti et al., 1984; Nakajima & Kanai, 2000; Goldfinger, 2011; Migeon et al., 2017). Multiple coarse fractions within the cores, irregular and abrupt grain size variations and mineral-based provenance, observability in a wide area, multi-source materials, and greater mass are some of these aspects. Classical turbidites are generally observed as a single bed and have an internal structure that more or less fits the Bouma sequence. However, amalgamated layers are formed in seismically-induced turbidites and cause the formation of a more irregular and incomplete appearance. In turbidites with a non-seismic origin, grading is in the form of a fining upward sequence in accordance with the general criteria whereas in the case of seismo-turbidites, inverse grading or grain size break events may also be observed (Nakajima & Kanai, 2000). The compositional variation between beds or within a bed is more uniform in a turbidite having a non-seismic origin. However, variable compositions may be encountered in seismo-turbidites. The source is also an important criterion to make a comparison between non-seismic and seismically induced turbidites. Turbidites with non-seismic origin generally result from a single source whereas seismo-turbidites may have variable sources due to the shaking of large areas during an earthquake.

Turbidite Paleoseismology is a new approach to investigate pre-historical and historical earthquakes, and have been studied for a few decades (Inouchi et al., 1996; Gorsline et al., 2000; Goldfinger et al., 2003a, 2003b, 2011; Patton et al., 2013, 2015; Avşar et al., 2014b, 2015; McHugh et al., 2014; Moernaut et al., 2014; Ikehara et al., 2016). In this context, turbidites are utilized as a tool to detect past earthquakes that occurred in and around a study area.

Some criteria are taken into consideration to distinguish seismo-turbidites from classical turbidites. First of all, ground shaking that can create a slope failure affects a wide area along the seafloor. Therefore, it is expected for each earthquake having severe magnitudes to cause more than one slope to fail simultaneously which causes the formation of many turbidites within the study area. In other words, when the seismically induced turbidites are investigated, coeval turbidites that occurred in a large area are examined in detail (Goldfinger, 2009; McCalpin, 2009; Avşar et al., 2014b). Secondly, multiple coarse fraction pulses of various provenance are expected to be seen in a typical seismo-turbidite sequence. Ground shaking causes many different regions and also different sediments to slide or slump at the same time. On a regional scale, coeval coarse fractions belonging to various provenance can be observed during an earthquake. As a third point, seismically induced turbidites have usually greater volumes and larger thicknesses than the ones having non-seismic origins (Goldfinger, 2011; Polonia et al., 2012; Bernhardt et al., 2015). Turbidites other than non-seismically induced ones generally do not reach abnormal thicknesses. If turbidite deposits of abnormal thickness and width are observed, this often causes suspicion of a seismic or tectonic event (Mutti et al., 1984). In addition to all these, temporal correlations of the suspected sedimentary sequence with the historical or instrumental earthquakes in the study area contribute substantially to associate that suspected subaqueous mass wasting depositions with a seismic event. To make an accurate and precise correlation, it is crucial to take more than one sediment core from the study area and to know the historical and instrumental earthquake records in the same region (Avşar, 2019b).

Despite turbidites are a good proxy for paleoseismology investigations, all earthquakes may not create submarine mass wasting events. Various studies have been carried out in this context. According to these studies, earthquakes with Mw>5 are known as earthquakes having the potential to create mass wasting (Keeper, 1984; Patton et al., 2013).

Considering that the major destructive earthquakes in the world are generally localized in the subduction zones, marine environments are very suitable areas for studying turbidite paleoseismology. Using turbidites as a proxy for paleoseismic investigations has been tested in many different locations in the world; Cascadia Subduction Zone and San Andreas Fault (Adams 1990; Goldfinger & Nelson, 1999; Goldfinger et al., 2003a, 2003b, 2012; Nelson et al., 2006), Japan Sea (Inouchi et al., 1996; Nakajima & Kanai, 2000; Shiki et al., 2000), Portugal (Gràcia et al., 2010), Dead Sea (Niemi & Ben Avraham, 1994) and North Anatolian Fault (Polonia et al., 2012; McHugh et al., 2006; Sarı & Çağatay, 2006; Çağatay et al., 2012).

Since marine environments consist of a shelf, a slope, and a huge abyssal plain, the seismo-turbidites formed in these environments are generally characterized by sediments from one direction (Figure 2.2). Sediments that are deposited on shelves and slopes slide along the seafloor by being shaken in case of an earthquake. This sliding occurs from the slopes to the abyssal plain. Therefore, when the turbidites are examined after an earthquake, the turbidite thickness is higher in places where the abyssal plain is closer to the slope, whereas this thickness decreases in more distant places. If this change in turbidite thickness is examined on a single line, it is possible to see sliding sediment comes from a single point in open marine environments.

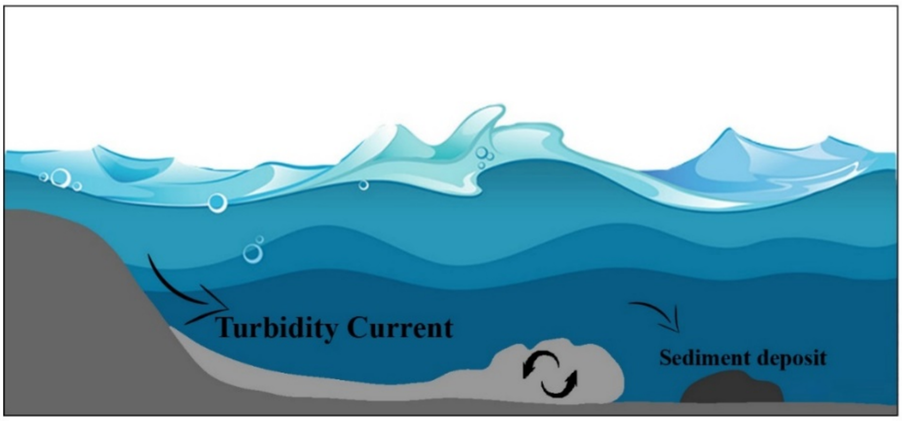

Figure 2.2. Schematic diagram summarizing the submarine slopes slipping due to earthquake or any other reason to create turbidite deposition.

However, this may not always be the case, because nature is not so perfect. For example, in submarine canyons with advanced channel systems and many tributaries (Figure 2.3), more than one slope may slide simultaneously after a seismic event. Also, the sediments in these sliding slopes may overlap in some locations. In such cases, turbidites coming from very different directions but originating from the same event, called multi-source turbidites (Avşar et al., 2015) may be encountered in the sedimentary sequences of the cores taken from the locations that such overlapping occurs.

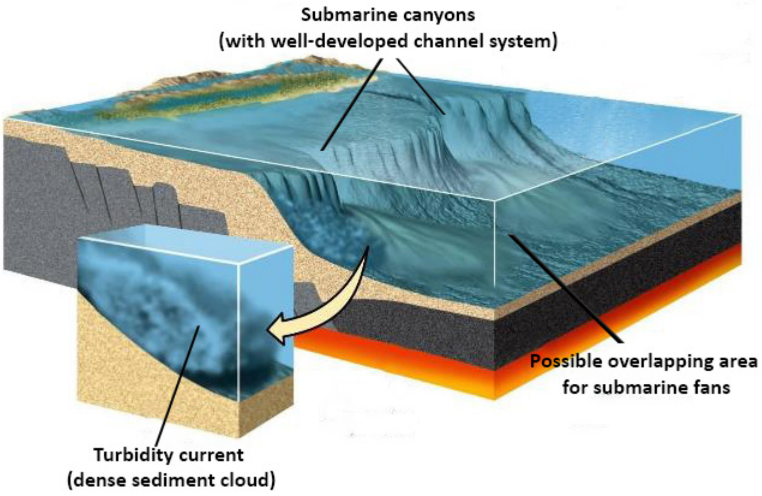

Figure 2.3. Schematic diagram of submarine canyons with well-developed channel system (Modified from Grotzinger & Jordan, 2010).

Although lakes are smaller water bodies in comparison with seas and oceans, no matter how small the lake is, turbidite paleoseismology can be applied in lacustrine environments as well. Especially the lakes on a major fault zone are good locations to study turbidite paleoseismology. Lakes located on the North Anatolian Fault (Yeniçağa, Ladik, Boraboy, Zinav, and Göllüköy) (Avşar, 2013) and lakes in South Central Chile (Villarrica, Calafquén, Panguipulli, and Riñihue) (Moernaut et al., 2017) are two major locations where lacustrine turbidite paleoseismology was investigated. In the former study, sedimentary imprints of earthquakes were investigated in five small and shallow lakes located on the North Anatolian Fault

(NAF) by using lacustrine paleoseismology techniques. This study showed that even small and shallow lakes can have the potential to record earthquakes, as well as the deeper and larger lakes (Avşar, 2013). In the latter study, sedimentary records of the giant 1960 AD (Mw 9.5) Chile earthquake were analyzed by surficial slope remobilization in four South Central Chilean lakes. Two main implications can be obtained from this study. One of them is that surficial slope sediment remobilization can explain why many studies in oceans and lakes may have encountered continuous and sensitive turbidite paleoseismic records all around the world. The second implication is that turbidite volume can be related to the strength of the triggering mechanism and the nature of slope sedimentation (Moernaut et al., 2017).

Turbidites formed in lacustrine environments are generally characterized by multi-source depositions (Figure 2.4). Since lakes are smaller water bodies than their marine equivalents (such as seas or oceans), they have many opposing slopes all-around their perimeters. These slopes may consist of units that are lithologically different from each other. Or, the topography surrounding the lake may consist of high mountains on one side of the lake and a flat coastal area on the other side. In the case of an earthquake, or any other landslide triggering mechanism, those slopes can slide and different types of sediments coming from different directions in the lake perimeter can accumulate and form turbidite depositions at the bottom of the lake. Sometimes zig-zag shaped coeval turbidites may be encountered depending on the sediment core-site. In such cases, careful interpretation of these mass wasting events plays an important role in correct conclusions. Otherwise, it is quite possible to interpret the coeval turbidites as if they were the result of two different events.

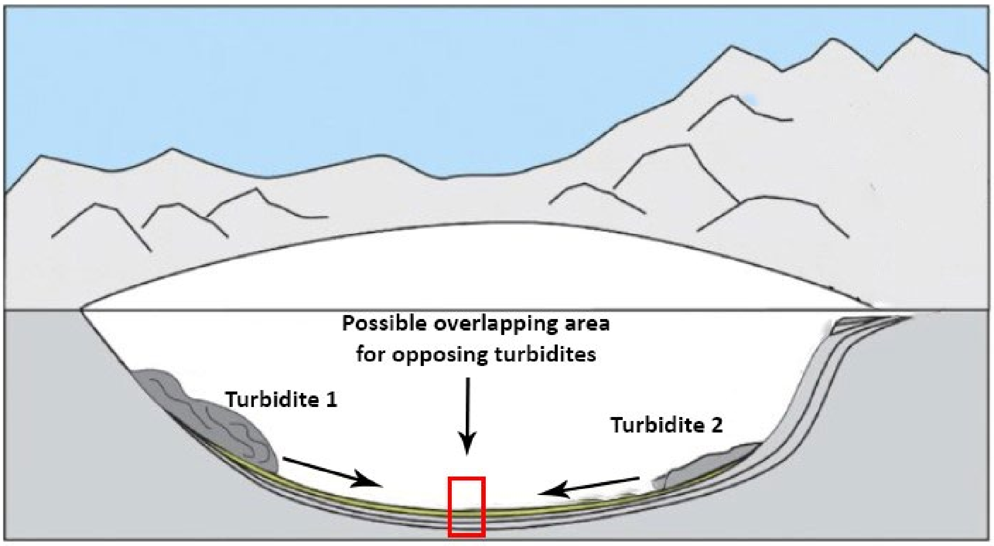

Figure 2.4. Schematic diagram showing possible underwater landslides that may occur in lakes (Simplified from Leithold et al., 2017). When a core is taken from the location indicated by the red rectangle, it is quite possible to encounter multi-source turbidite deposits.

Also, when looking at lacustrine paleoseismology literature, catchment area response is used as a tool to detect past earthquakes (Howarth et al., 2012, 2014; Avşar et al., 2014a). In other words, sediment enhancement due to the increase in erosion caused by earthquakes in the areas surrounding and feeding the lake is interpreted as the catchment area response, and it is mentioned as one of the clear evidences of past earthquakes. This is noticeable with the increase of mineralogical clastic material (enhancement in the amounts of some elements such as Ti, Zr, Si, Fe, Ni) and the size of the grain in the sedimentary cores taken (Howarth et al., 2012; Avşar et al., 2014a; 2019). Therefore, knowledge about the channels feeding the lake and the size of the catchment area plays an important role in getting information about the possible landslides that might be triggered due to earthquakes and the amount of sediment influx to the lake.

CHAPTER 3

MATERIALS AND METHODS

The main purpose of this study is to investigate sedimentological imprints of the historical and instrumentally recorded earthquakes in the Gulf of Aqaba and the Strait of Tiran region. All methods utilized to collect data for this purpose will be introduced and explained in this chapter. Multi-beam bathymetry has been conducted as a pioneer in all studies. In this part, a multi-beam sounder has been used and bathymetric mapping has been performed. According to the bathymetry data, basins and active fault branches have been determined and 23 short sediment cores have been collected to make detailed sedimentological investigations. These cores have been cut in half and one half has been used for ITRAX – Micro XRF core scanning, while the other halves have been stored as a spare in the cold room at METU Sediment Coring and Analyses Laboratory. U-channels with 4.2 cm width and 0.8 cm height have been extracted from the half cores. These U-channels have been scanned by the ITRAX-Micro XRF core scanner in the ITRAX Laboratory at the Marine Research Department of the General Directorate of Mineral Research and Exploration (MTA). During the scanning, radiographic imaging has been performed in the widest possible frame by shifting the channels one cm to the right and one cm to the left. The ITRAX-Micro XRF scanning has provided the indications of geochemical data in the cores. After all these steps have been completed, the next step has been establishing a precise chronology of the sediment cores. From numerous dating techniques available in the literature, both radionuclide (^{210}Pb-^{137}Cs) dating and radiocarbon (^{14}C) dating have been used in this study. Levels suitable for radiocarbon dating have been determined based on the results of radiographic images and samples have been collected from these levels. However, for radionuclide dating, sampling levels have been determined before U-channel extraction from half cores. The samples taken for radionuclide dating were bulk sediment samples, but when encountered organic matters (i.e. mixed planktonic foraminifera consisting of mostly *Trilobatus sacculifer* (Brady, 1877) and *Globigerinoides ruber* (d'Orbigny, 1839)) have been extracted from the sampling levels for radiocarbon dating to achieve more accurate results. Detailed information about the above-mentioned methods will be given in the following sections.

3.1 Multibeam Bathymetry and Sediment Coring

Multibeam bathymetry is a very modern technique to detect submarine topography. It is mainly used to obtain high-resolution and precise data related to sea bottom characterization. In addition to mapping the seafloor, it is a very significant tool used for analyzing the character of fault branches, their locations, and physical properties (Bandy et al., 2010; Cui et al,2020).

The first task carried out in this study has been the bathymetric survey. Before core collection, it is critical to decide on the location of each core, so that the location of the retrieved sedimentary sequence would be susceptible to the possible effects of earthquakes and at the same time unsusceptible to other natural effects. To make this decision correctly, first, it is very essential to understand the submarine morphology in the study area. Within the scope of this study, a multibeam bathymetric survey was completed using a Kongsberg EM 710-MK2 multi-beam echo sounder (R / V Thuwal 59 cruise, 20 May - 7 June 2018).

According to the bathymetric survey, sub-basins in the Gulf of Aqaba have been identified as Eilat, Aragonese, Dakar, Tiran, and Hume deeps from north to south, respectively. Besides, the submarine morphology of the gulf and the locations of active fault strands have been determined as a result of the bathymetric survey.

The work done right after bathymetry was sediment coring. Several criteria are taken into account when deciding on the core locations. First of all, the determination of the core location as far away from the submarine slopes as possible allows avoiding any hiatus problems that may be encountered in the core taken. More clearly, in the case of coring from any slope, it is suspicious whether the sediment sequence taken is complete or not, since there are no stable depositions on the slopes and they are subjected to irregular mass movements. Second, while deciding on the coring location, avoiding submarine fans, like slopes, contributes to more accurate results. Submarine fans cause sediments to transport and displace as their channels erode the fans over time. Therefore, when cores are taken from the submarine fans, it becomes questionable whether the resulting sediment sequence is complete or not. Briefly, the most suitable location for coring is the basin flat, away from the submarine slopes and fans. On the other hand, coring from a basin flat that is too far from submarine slopes and fans makes it difficult to detect mass wasting events caused by earthquakes, which are the main subject of marine paleoseismology studies. Moreover, another reason why the basin flat, which is the deepest possible point, is preferred as the core location is that the sediment sequence in the cores taken from here represents a much longer span of time.

In this study, the above-mentioned issues have been considered and the core locations have been carefully determined. First, the main sub-catchments around the gulf have been established. Then, the percentage of their areas to the total catchment area is calculated (Table 3.1). The percentage is used as an indicator of sediment amount brought from each sub-catchment to the gulf. The close-up views of the exact locations of the cores are shown in Figure 3.1 - Figure 3.4.

The location of the ELT-1 core has been selected so that, it would record turbidites resulting from both the Nuweibaa submarine fan, which is fed by sub-catchment #4 and the eastern slopes. The most suitable locations for ELT-4 and ELT-5 cores have been determined by considering the same criteria. The sub-catchment areas numbered 6 and 7, which constitutes 4.3% and 2.9% of the total catchment area with their 842 km ^{2} and 552 km^2 areas (Table 3.1), respectively, enable the development of the northern and southern Haql submarine fans. Especially the ELT-4 core location has been determined so that its sedimentary sequence would record the turbidites that may come from these two submarine fans. Similarly, the location of the ELT-5 core has been determined in a way that it does not coincide with any submarine slope or fan and taking into account the proximity to slopes. In order to determine the parameters to be used for both inter-core and inter-basin correlations throughout the entire gulf, ELT-M2 and ELT-M3 cores have been taken very close to each other (the distance between them is 515 m) (Figure 3.1). In short, all Eilat cores have been collected from the deepest points of the basin and significant care has been taken to keep these locations far enough from the submarine slopes and fans.

Table 3.1. The areas of main sub-catchments of the Gulf of Aqaba and their percentage to the total catchment area.

Sub-catchment ID	Area (km^2)	% of the Whole Catchment
1	367	1.9
2	1071	5.5
3	2081	10.8
4	3543	18.3
5	6618	34.3
6	842	4.3
7	552	2.9
8	265	1.5
9	321	1.7
The rest	3600	18.7
Whole Catchment	19260	100

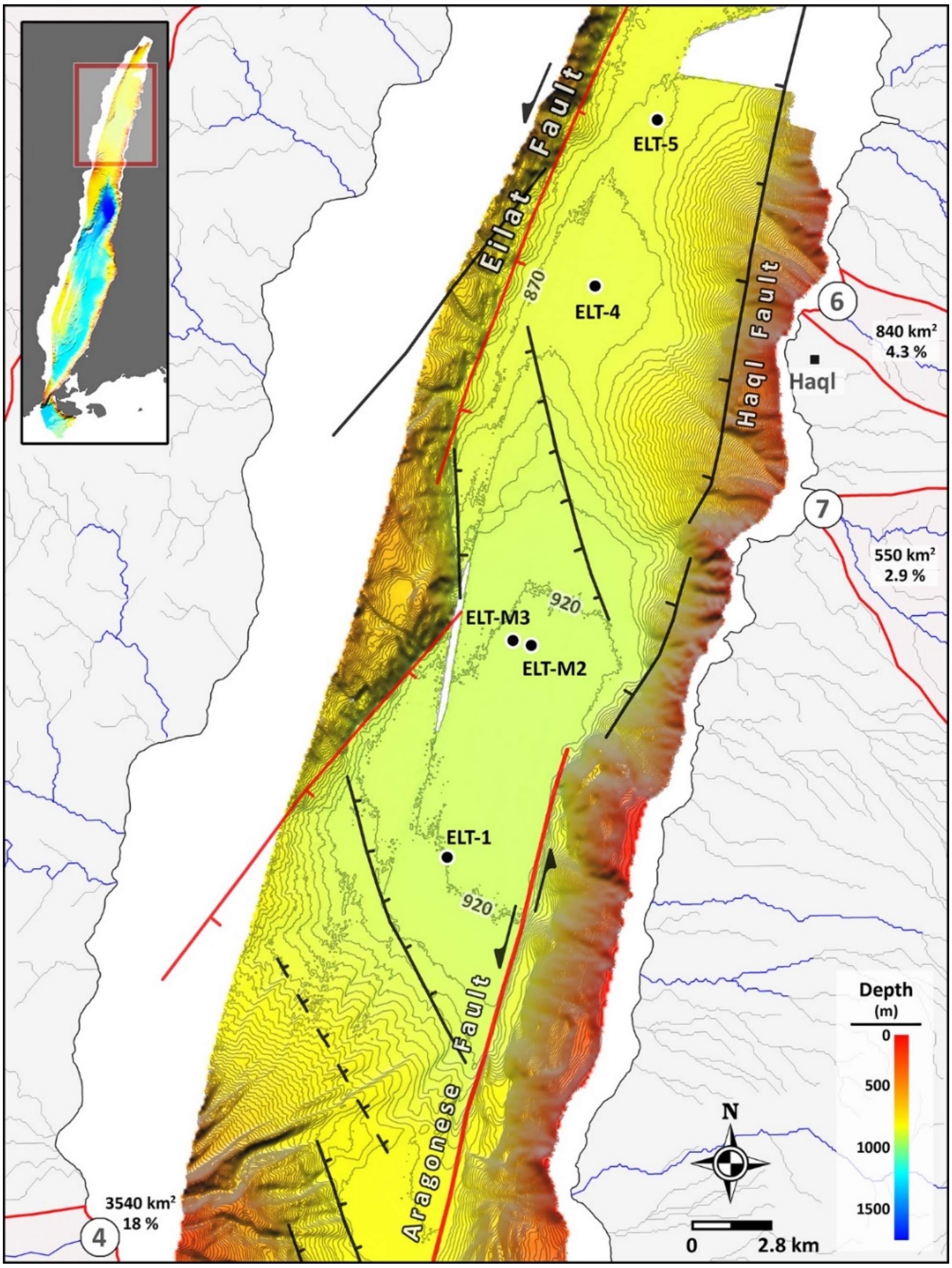

Figure 3.1. Close-up bathymetry of the Eilat Deep and exact locations of the ELT-1, ELT-M2, ELT-M3, ELT-4, and ELT-5 sediment cores which were taken from here (Contour interval is 10 m). The Eilat Deep is rich in sediment sources because sediment influx provided by 3 different sub-catchments makes up 25.5 % (4.3%, 2.9%, and 18.3%) of the total catchment area of the gulf.

AR-1 and AR-2 cores have been collected from the Aragonese Deep, which is the deepest basin in the Gulf of Aqaba (Figure 3.2). The Aragonese Deep is suitable for the deposition of turbidites resulting from the large Nuweibaa submarine fan in the west and many small fans in the east. The AR-2 core has been taken exactly from the basin flat and the deepest point of the Aragonese Deep. However, the general submarine morphology of the Aragonese Deep and the fact that it is surrounded by very steep slopes make this area very susceptible to landslides. Since the Aragonese Deep is bounded by the Arnona and Aragonese faults, any earthquake that may occur due to the rupture of these faults is very likely to cause seismically-induced landslides in the region. Therefore, to eliminate the possibility of the AR-2 core being a complete turbidite deposit, the AR-1 core has been taken from a different part of the basin (Figure 3.2).

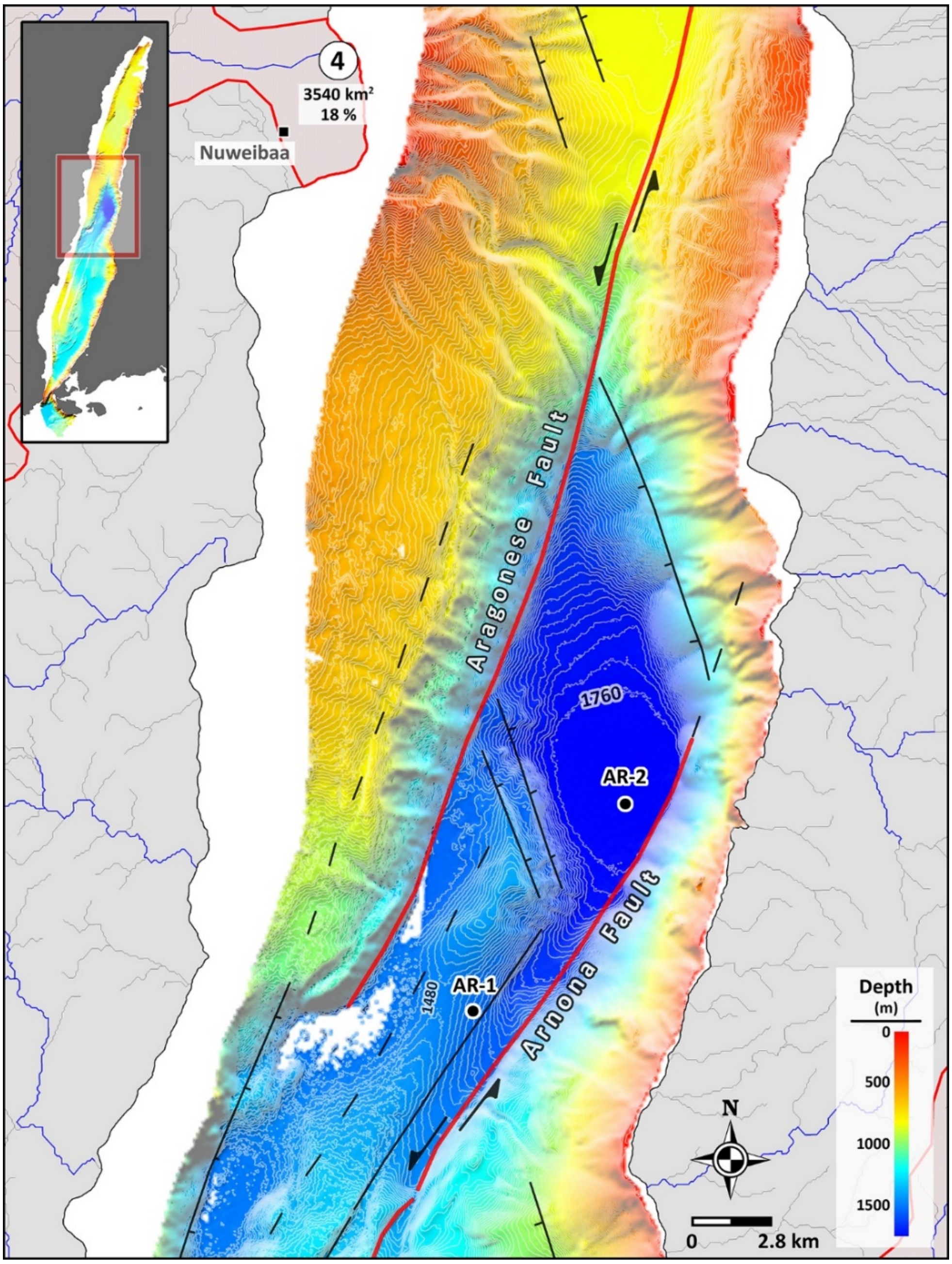

Figure 3.2. Close-up bathymetry of the Aragonese Deep and exact locations of the AR-1 and AR-2 sediment cores which were taken from here (Contour interval is 10 m). The main sediment source for the Aragonese Deep is the large Nuweibaa submarine fan having a sub-catchment area of 3543 km^2 and it constitutes a significant portion (18.3%) of the total catchment area of the Gulf of Aqaba.

DK-1 and DK-2 cores have been collected from the basin flat of the Dakar Deep, which has a water depth of approximately 1270 m (Figure 3.3). Core locations are affected by submarine fans formed due to sub-catchment areas numbered 3, 8, and 9, which have areas of 2081 km^2, 265 km^2, and 321 km^2 respectively (Table 3.1). In other words, it is quite possible that the DK-1 and DK-2 cores contain turbidites that may result from these three sub-catchment areas. Also, the presence of the strike-slip Arnona Fault to the west and the normal-dip-slip Dakar Fault to the east indicate that the turbidites that can be recorded here are most likely seismo-turbidites triggered by the earthquakes resulting from the rupture of these faults. On the other hand, in the south of the Dakar Deep, TD-2 and TD-3 cores have been collected from two small basins bounded by topographic highs (Figure 3.3), which have formed as a result of the salt tectonics in this region and are defined as 'diapiric folds' (Ribot et al., 2021). In general, the core locations have been arranged so that they would not miss the turbidites that may come from the slopes.

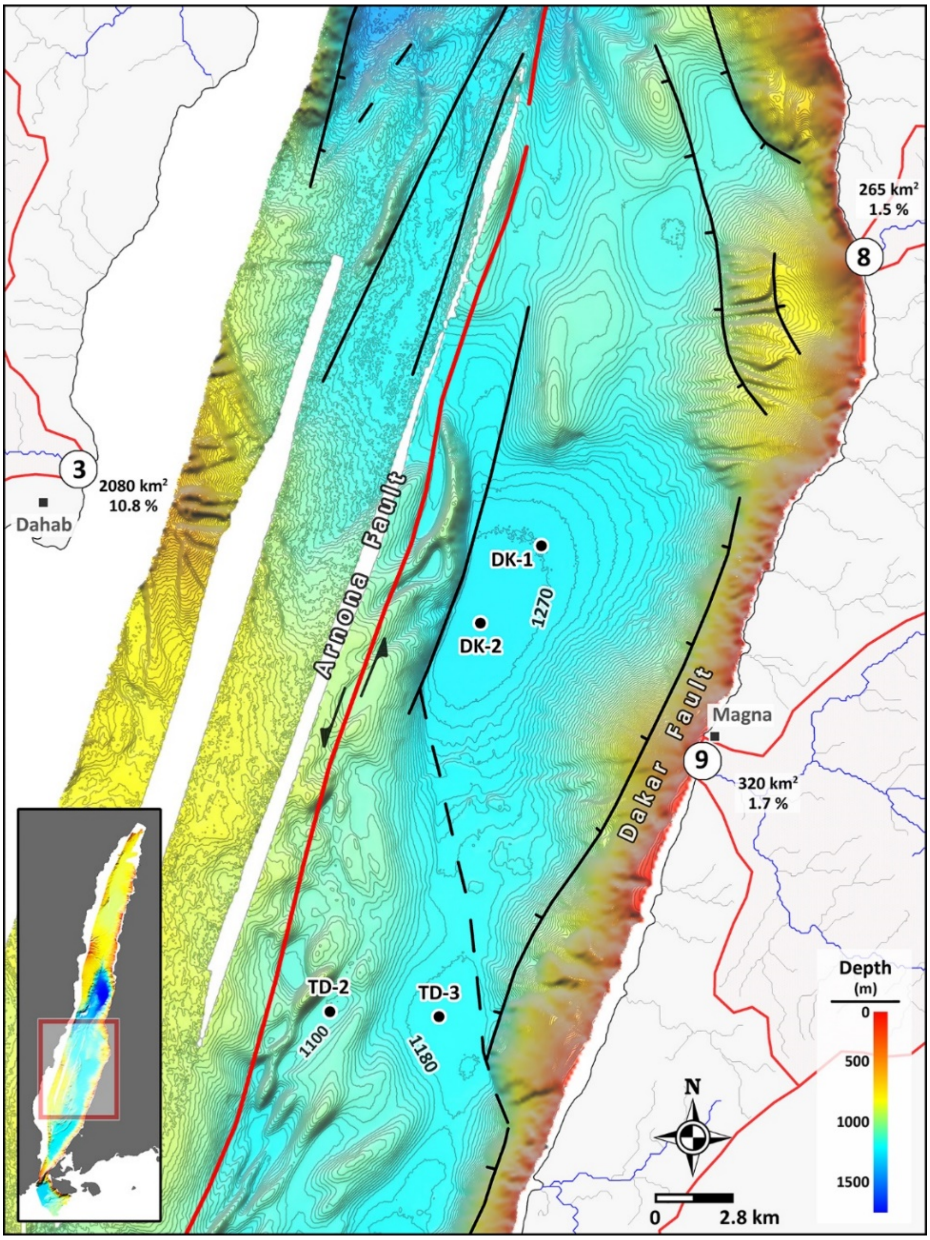

Figure 3.3. Close-up bathymetry of the Dakar Deep and exact locations of the DK-1 and DK-2 sediment cores which were taken from here. TD-2 and TD-3 cores were taken from the region between Dakar and Tiran deeps (Contour interval is 10 m). Dahab sub-catchment (3) has an area of 2081 km², which accounts for a significant portion (10.8%) of the total catchment of the Gulf of Aqaba. Magna sub-catchment (9) has an area of 321 km² and this constitutes 1.7% of the total catchment. 3 and 9 have well-developed submarine fans in front of the entrance to the gulf. Although sub-catchment, indicated by 8, with an area of 265 km², accounts for only 1.5% of the total catchment, it also provided the formation of a well-developed submarine fan which is useful in turbidite paleoseismology. These three sub-catchments are the main sediment sources for the Dakar Deep.

The exact locations of the cores taken from the Tiran and Hume deeps in the southernmost part of the Gulf of Aqaba, where it connects to the Strait of Tiran, are shown in Figure 3.4. The water depth was around 1280 m at TR-3, TR-4, and TR-5 core locations at the Tiran Deep, and 1400 m at HM-1 core location at Hume Deep. As described above, core locations have been kept as far as possible from submarine slopes and fans. Since Tiran Deep is located in the narrowing part of the Gulf of Aqaba, the slopes on the west and east coasts of the gulf are very close to each other. For this reason, great care has been taken to keep an almost equal distance from both coasts while determining the core locations. The cores TR-3 and TR-4 are bounded by the normal dip-slip Dakar Fault to the east, and by diapiric folds to the northwest (Ribot et al., 2021). TR-5 core is expected to have a relatively higher sediment influx compared to TR-3 and TR-4 locations due to its proximity to the catchment areas 2 and 3 (Figure 3.4). Especially considering the sediment influx coming from sub-catchment area 2, which constitutes 5.5% of the total catchment area (Table 3.1), and the fact that the western coast of the gulf has steeper slopes than the eastern coast, it can be claimed that the possible earthquake-induced landslides in the TR-5 core are more affected from the west coast of the gulf. Nevertheless, at the HM-1 core location (Figure 3.4), the possible earthquake-induced landslides would have been originated from the steep slopes in the east. The HM-1 core was taken from a place close to the eastern slope due to the maritime traffic in the Strait of Tiran.

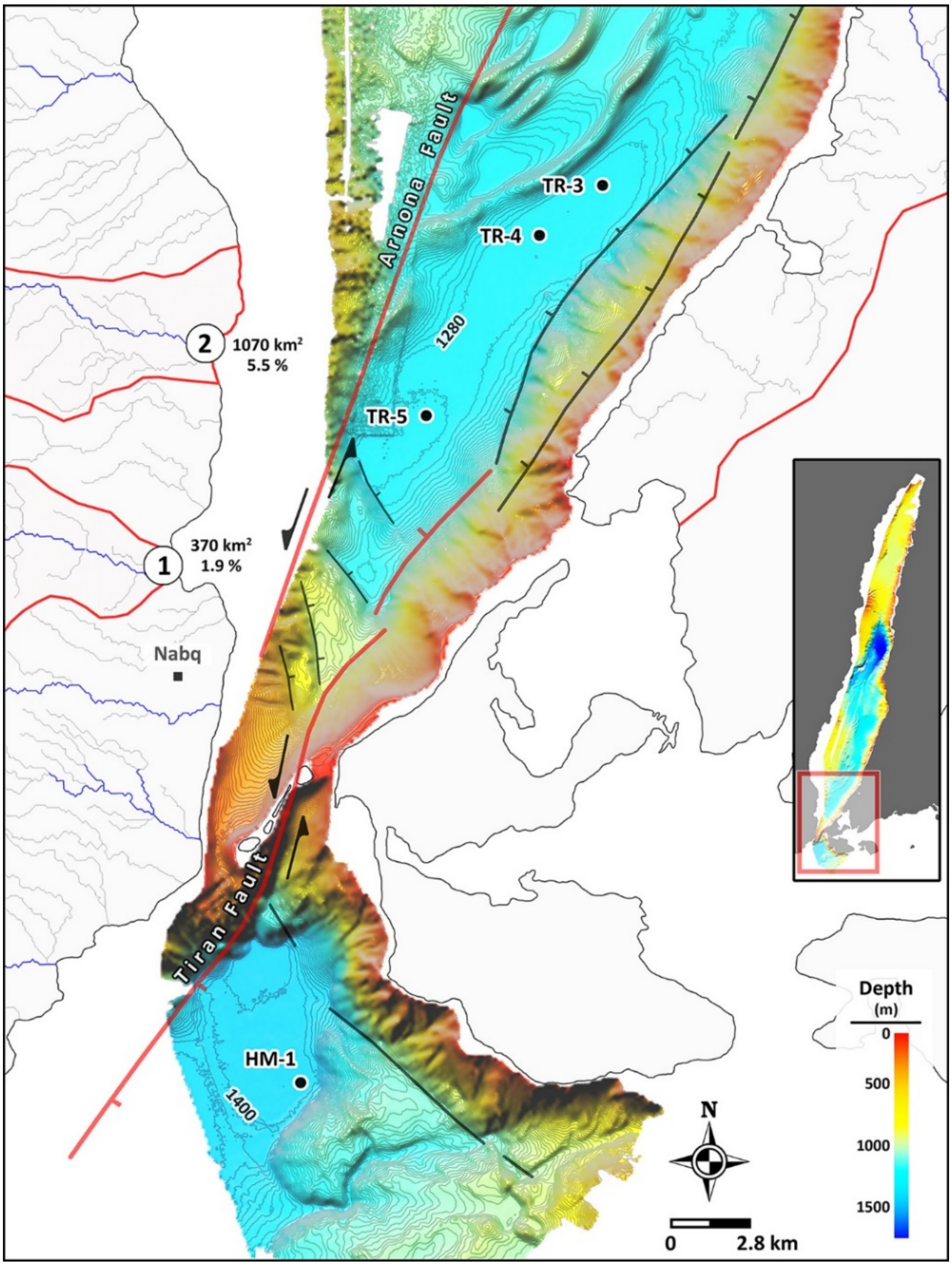

Figure 3.4. Close-up bathymetry of Tiran and Hume Deeps and the sediment cores taken from corresponding deeps (TR-3, TR-4, and TR-5 are from Tiran Deep; HM-1 is from Hume Deep) (Contour interval is 10 m). Sub-catchment areas indicated by 1 and 2 cover an area of 367 km^2 and 1071 km^2, accounting for 1.9% and 5.5% of the total catchment, respectively. These are the two main sources of sediment influx into the Tiran Deep.

Among different types of coring systems, a multi-corer system was used in this study. Multi-corer is an instrument containing several sediment tubes (Figure 3.5a). The working principle of this multi-corer tool is based on taking multiple core samples by placing a weight on the system and pushing it from the research vessel towards the seafloor at a constant rate. With this system, it is possible to take 8 cores at once, which have an undisturbed sediment-water interface. However, when 8 tubes are used with the multi-corer, the maximum sediment length that could be retrieved cannot exceed 20 cm (Figure 3.5a). In order to increase the sediment amount retrieved by each core tube, 2 tubes instead of 8 were placed to the multi-corer (Figure 3.5b). The tubes were arranged opposite to each other to maintain the balance of the multi-corer system. By placing 2 tubes instead of 8 and keeping the same weight and penetration rate on the system, the pressure exerted by the tubes on the seafloor is four times increased, resulting in greater penetration depth for each tube. In this way, the length of retrieved sediment increased up to 45-50 cm.

The last major seismic activity of the Gulf of Aqaba was the 1995 M_W 7.2 earthquake. To find the traces of this recent earthquake, the top levels of the cores must be undisturbed. The cores retrieved by the multi-corer system, have a clean water-sediment interface (Figure 3.5b,c), confirming no sediment loss and undisturbed sampling at the top of the cores.

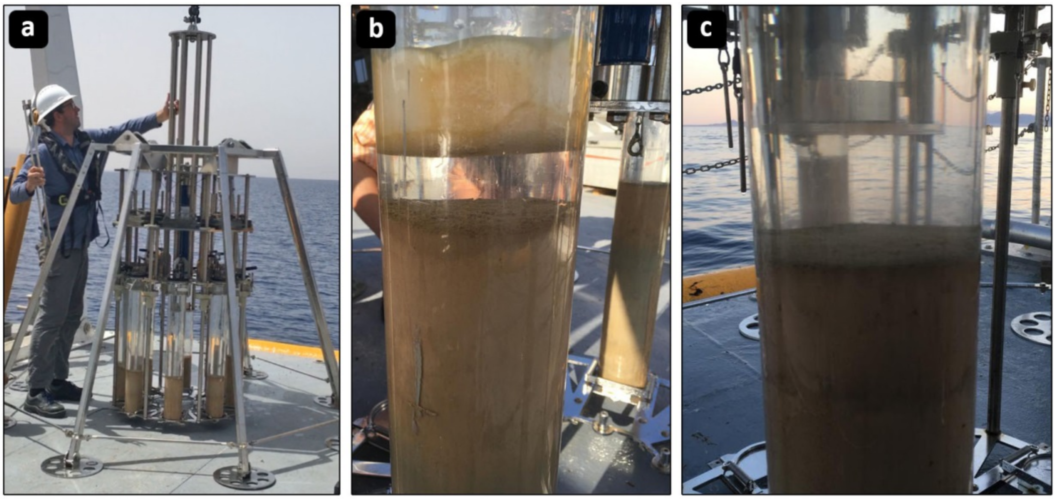

Figure 3.5. a) Multi-corer system used in this study. b) 2 sediment cores placed opposite to each other to provide balance and increase penetration depth. b & c) A photo proving the clarity of the water-sediment interface with no sediment loss or deformation.

3.2 Core Splitting and U-Channel Extraction

The cores taken from the Gulf of Aqaba during the cruise carried out from 20 May to 7 June within the scope of the GAST project were brought to METU Sediment Coring and Analysis Laboratory. First of all, the cores were cut in half in the core cutting laboratory. As shown in Figure 3.6a, the cores were placed horizontally on the platform containing the cutting discs, and the cores were cut in half at a constant rate. Throughout the cutting process, the cores were fixed to the platform with the help of plastic clamps to prevent damage both to the cores and the sediment inside. One-half of the cores were used for analyses, while the other halves were kept in a cold room with the temperature of 6-7 degrees Celcius, which is close to the temperature of the natural environment of the subaqueous sediments The purpose of keeping sediment cores at this temperature is to protect the sediments from cracking or shrinkage by preventing loss of water content as possible.

U-channels are extracted from each half of the cores. The u-channels that were used in this study are simply the plastic cable channels that are generally used to collect and hide cables. As indicated in Figure 3.6d, u-channels provide more clear and precise results for the ITRAX scanning and radiographic imaging, especially in the identification of microstructures, the content of sedimentary sequence in the cores, and possible soft-sediment deformations (Avşar et al., 2016). The channels used in this study are 4.2 cm wide and 0.8 cm high, allowing a cleaner image quality.

The process of u- channel extraction from the sediment cores is shown step by step in Figure 3.6. First, the surface of the split core (Figure 3.6b) is flattened with a knife-like tool. Then the u-channels are thoroughly cleaned and dried so that they do not cause any external contamination. The core is then placed on the u-shaped wooden apparatus so that it can remain stable during the u-channel extraction process. In the next step, the cleaned u-channels are carefully placed to the exact midline of the core and slowly embedded in the sediment (Figure 3.6c). During the embedding process, the u-channel is slowly pressed from one end to the other with equal force as much as possible. In places where relatively hard sediments such as sand are present, it may not be enough to press by hand. In such cases, a piece of wood is used to exert greater force. In places where soft materials such as clay or mud are found, the u-channels are pressed with less force to balance the embedded depth of the u-channel with other parts. If the u-channel is not evenly embedded in the sediment, one end of the channel may dislodge or shift from the specified mid-level. If the channel slides or dislocates as described above, the sediment will be damaged, and the u-channel extraction process should start from the beginning, which is flattening the core surface with a knife. Therefore, working as carefully as possible while placing the u-channel on the core and embedding it into the sediment eliminates the possible errors that can be experienced during the extraction process. If the embedment depth of the u-channels is about 1-2 mm higher than the channel height, which corresponds to 9-10 mm in this study, it ensures that the u-channel is completely embedded in the sediment.

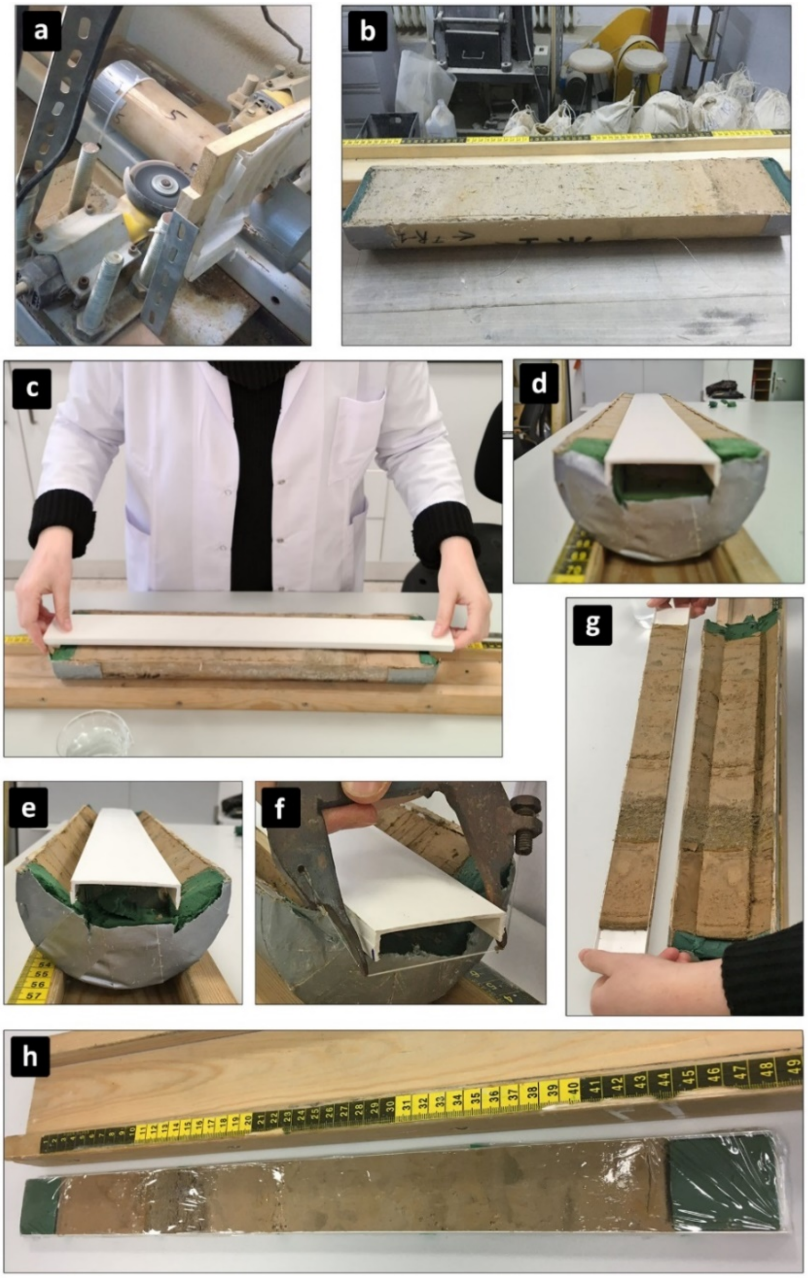

Figure 3.6. Summary of the core cutting and u-channel extraction process. a) Core cutting system used in this study with cutting discs and apparatus for keeping the cores stable. b) A view from the split core inside a transparent pipe. c) Pressing the cleaned u-channel on the split core with alignment to the center. d) U-channel completely immersed in sediment (a cross-sectional view). e) Removal of excess sediment around the u-channel. f) Complete separation of u-channels from the core with fishing line. g) U-channel that is completely separated from the core. h) U-channel covered with a thin plastic sheet to be ready for ITRAX scanning.

After the u-channel is completely embedded in the sediment (Figure 3.6d), any excess sediments outside the u-channel are cut and cleaned with a knife (Figure 3.6e). After the roots of the u-channel are visible on the surface, the channel is cut along the core from one end to the other end with the help of a fish line to separate the channel from the sediment in the core (Figure 3.6f). In this way, u-channel extraction is completed (Figure 3.6g).

The removed u-channel is placed on a clean table and its surface is flattened with a knife. Then, it is covered with a thin plastic sheet and made ready for ITRAX scanning (Figure 3.6h).

U-channel extraction has crucial importance in terms of the reliability and clarity of analyses (Avşar, 2019). If radiographic imaging is done from half cores, it may not be a problem in locations having homogeneous and completely horizontal laminations. That is, the u-channel and half core images will be the same (Figure 3.7a), but such homogeneous and evenly layered locations are extremely rare. Since the main purpose of paleoseismology studies is to find the traces of deformation structures that may occur due to earthquakes, clear detection of these structures is essential. Radiographic imaging made from the half-core cannot give sufficiently clear results about possible deformations. Cross-laminated deformation structures are very likely to occur in cases such as simultaneous sliding of submarine slopes from different directions after ground shaking. These structures can be clearly observed in radiographic images of u-channel, while they appear blur in radiographic images of half-cores, making detections of the structures more difficult (Figure 3.7b). Soft-sediment deformations and turbidites are common indicators used to investigate the traces of earthquakes, and u-channel radiography is a very effective tool in visually revealing these deformations (Migeon et al., 1999; Avşar et al., 2016). If radiographic imaging is performed on both half-core and u channel where soft-sediment deformations are present, the deformations would be more visible in the u-channel radiography than the half-core radiography (Figure 3.7c). In short, physical changes in sediments are more visible in the radiographic images taken from u-channels, compared to a half-core, which highlights the importance of u-channel radiography for paleoseismology studies. Therefore, using u-channel radiography is critical in order to detect even the smallest deformation caused by an earthquake.

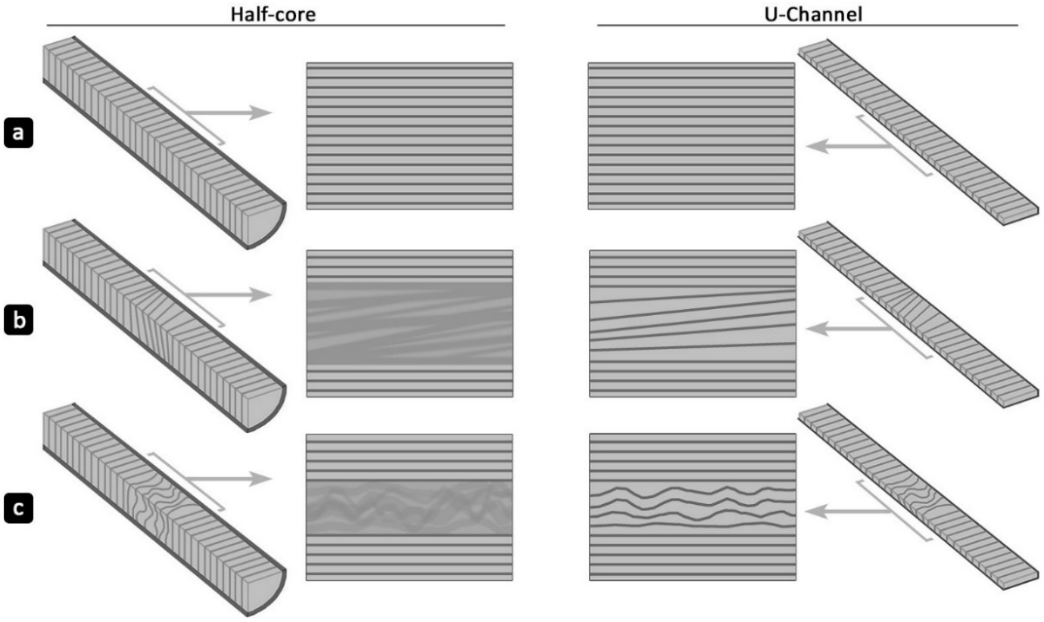

Figure 3.7. Sketches illustrating possible radiographic images taken from half core and u-channel for different types of sediment deformation. a) Undisturbed horizontal lamination. b) Intercalation of inclined laminae. c) Intercalation of undulated soft sediment.

3.3 ITRAX Micro XRF Core Scanning

ITRAX Micro XRF core scanning is one of the most advanced methods used in paleoenvironmental and sedimentological process investigations (Avşar, 2013; Croudace and Rothwell, 2015). In addition, it is widely used in the identification of turbidite geochemistry by provenance analyses. It performs optical and radiographic imaging of sediment cores and, with the X-Ray Fluorescence (XRF) data, it enables the analysis of the relative amounts of elements in the sediments along the cores. In traditional scanning methods, incremental sampling must be done to analyze the sample. Also, conventional techniques involve dried and ground sampling which takes 2 weeks for a 1 m core sample. When complex sample preparation processes are considered, traditional methods are time-consuming and destructive. Instead, ITRAX Micro XRF scanning is utilized as a very rapid and non-destructive method (Croudace and Rothwell, 2015; Croudace et al., 2006; Avşar, 2013). In addition to providing information about the elemental profile of the scanned sediments, it also helps to interpret the paleoenvironment. X-Ray images are useful for understanding the bulk density of sediments along the cores. That is, higher density appears as darker, while lower density appears as lighter (Avşar, 2013; Yeniçeri, 2020). Also, when the ITRAX data is used for turbidites investigations, it provides a rapid and non-destructive characterization of textural grading, bioturbative mixing, and identification of geochemically distinct marker beds within sediment cores (Rothwell et al., 2006).

The ITRAX micro XRF scanner is a large device containing several functional parts (Figure 3.8a). The device includes a central measuring tower consisting of an X-ray focusing unit and a range of sensors. These sensors are an optical-line camera, a laser topographic scanner, an X-ray line camera to measure the transmitted X-rays and a high count-rate XRF detection system. The most important and functional parts of the ITRAX system are summarized in Figure 3.8 - b.

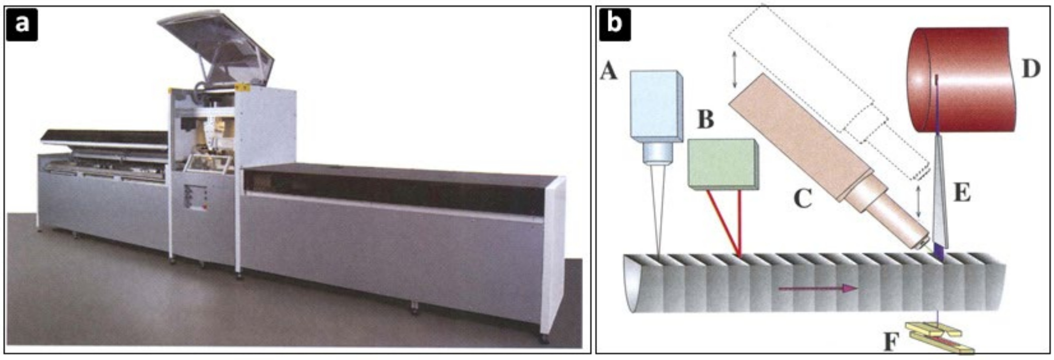

Figure 3.8. a) A photo from the ITRAX Micro XRF core scanning device. b) Parts included in the ITRAX Micro XRF system (Croudace et al., 2006). A - optical-line camera, B - laser triangulation system, C - motorized XRF Si-drift chamber detector, D - 3 kW X-ray tub, E - flat-beam X-ray waveguide, and F - X-ray line camera.

Within the scope of this study, 23 sediment cores were taken and 18 of them were scanned at 0.05 cm resolution. ITRAX micro-XRF scanning was performed in the

ITRAX Laboratory at the Marine Research Department of the General Directorate of Mineral Research and Exploration (MTA).

Since ITRAX measurements are made directly from the bulk sediment surface on u-channels, it is affected by many factors such as water content, organic matter content, grain size changes, and porosity. Also, dwell time is a very important factor affecting the measurements, and determining the optimum dwell time positively affects the quality and budget of the analysis to be made (Avşar, 2013).

ITRAX calculates the concentrations of elements in terms of counts per second (cps) during the dwell time. In other words, throughout the ITRAX scanning, the device sends X-rays for each measured point on the core, resulting in the plot of the incident X-ray energy versus the intensity of photon emission in the sample. The incident X-ray emission intensity of the sample is expressed in counts per second (cps) and interpreted as the elemental concentrations along the core. However, the concentrations of different elements cannot be directly compared to each other as they depend on many factors and their cps scales can greatly differ. Therefore, all element concentrations should be standardized before comparison. A very simple formula given below is used for the standardization process. The cps value calculated for each element is used as the data value (x) in this formula. After subtracting the mean value (μ) of the elemental dataset from the cps values, it is divided by the standard deviation (σ) of the elemental dataset. When this is applied for all elements, the entire dataset is standardized and different elements become comparable.

$$z = \frac{x - \mu}{\sigma}$$

Where,

z: Standardized value, x: Data value, μ: Mean value of dataset, σ: Standart deviation of the dataset

Interpreting the standardized cps values as an absolute proxy in paleoenvironmental and paleoclimatic studies leads to erroneous conclusions. Instead, using inter-element ratios obtained from the standardized values is preferred to compare data properly (Croudace et al., 2006; Rothwell et al., 2006; Avşar, 2013).

3.4 Magnetic Susceptibility (MS) Measurement

Advanced science and technology enable continuous and non-destructive measurements of the physical properties of sediments in many fields of studies such as paleogeography, paleoenvironment, paleoclimatology, or paleoseismology (St-Onge, 2007). Magnetic susceptibility is one of the most used and well-known measurement types among continuous and non-destructive methods. This is used to correlate cores taken from a region and interpret climatic variations or changes in depositional environments from the past to the present (Verosub & Roberts, 1995; Hounslow & Maher, 1999; Larrasoaña et al., 2008).

The magnetization value of sediments is closely related to the magnetic minerals they contain. When looking at the changes of these magnetic minerals along the core, it is seen that this change can be used as a correlation tool between cores (Goldfinger et al., 2011; Avşar, 2013; Bernhardt et al., 2015). Apart from providing information about mineral content, the magnetic susceptibility variation along the core also shows clear results in terms of lithological and depositional environments.

The Bartington MS2E surface sensor was used in 0.5 cm intervals to perform the measurements of magnetic susceptibility (MS) along the 17 sediment cores which have a roughness less than 1 mm. The results were obtained in x10^{-6} SI in the measurements completed using 2 second time interval.

Before starting the measurement, it is essential to cover the core with a thin plastic sheet, as the sediment in the cores causes contamination at the tip of the sensor, and cleaning the sensor each time makes it impractical. In the next step, the cores covered with a thin plastic sheet are aligned to the zero position on a u-shaped board with a ruler (Figure 3.9b & Figure 3.9c). Normally, no rule proposes to use of such an item to measure magnetic susceptibilities of surfaces. However, this board is quite useful because it keeps the core fixed while taking magnetic susceptibility measurements. Otherwise, cores will move or shift due to the roundness of the bottom. The other triangular-shaped board (Figure 3.9b & Figure 3.9c) is designed to ensure that the sensor reaches the sediment properly and does not shift the measured level. In addition to this triangular-shaped board, thanks to a nail (Figure 3.9c) added to the system, the distance of this nail to the sensor was adjusted so that the magnetic measurements were not affected, making sure that the levels were measured without any shifting. Since the sensor was calibrated before starting the measurement on each core (Figure 3.9a), it was ensured that the study would give reliable results. The most accurate way for measurement is immersing the sensor at least 1-2 mm into the sediment. In this way, the device detects the true magnetic value of the sediment. If it is not pressed sufficiently, the tip of the sensor does not make full contact with the sediment and since it is a very sensitive device, it will show a different value than it is.

Figure 3.9. Magnetic susceptibility measurement in sediment cores using the Bartington MS2E surface sensor. a) Calibration process repeated for each core before starting the measurement. b) Magnetic susceptibility measurement by one end of the sensor attached to the computer and the other end touching the sediment surface. c) Triangular-shaped wooden apparatus that ensures proper contact of the sensor with the sediment. The nail indicating the measured level is indicated with a red circle.

Another point to be considered when taking magnetic susceptibility measurements is that this is a temporary measurement type. That is, it shows the instant magnetization, if repeated measurements are taken from the same point, it is observed that this value changes in small amounts. Therefore, it is best to measure as soon as the core is taken without allowing the sediment in the core to dry out or to be exposed to oxygen.

3.5 Grain Size Analysis

In turbidite paleoseismology, the grain size of the sliding dense sediment cloud is different from the grain size of the sediment already deposited on the seafloor. In other words, sediments that slide by turbidity currents and settle down according to gravitational segregation are expected to show a fining upward sequence of sediments deposited on top of relatively coarser-grained bottoms (Shanmugam, 1997; Nakajima & Kanai, 2000). The grain size of the sediment that is dragged off the submarine slopes and deposited in relatively far offshore places changes depending on the intensity of the ground shaking. Therefore, while tracing the earthquake-induced turbidites, it is useful to carefully examine the grain size changes in sediment cores.

The grain size analysis was applied in 10 of the sediment cores so that to examine at least one core from each sub-basin. First, the cores were sampled at 1 cm or 0.5 cm intervals depending on the thickness of the distinct turbidites in the core. For example, since the ELT-1 core taken from the Eilat basin contains very thick turbidites that can be seen very clearly both on radiographic and optical images, it is more time-efficient to sample it at 1 cm intervals. On the other hand, at the DK-2 core, the radiograph images clearly show quite thin event layers. Therefore, at this core, a 0.5 cm sampling interval was preferred in order to avoid missing any event horizon. Following the sampling, the ‘wet sediment’ samples in each cm interval were weighed and the results were noted. The weighed wet sediment pieces were put in 100-ml-beakers and washed by distilled water. The washing process was performed by using a magnetic stirrer for 5 minutes, ultrasonic bath for 5 minutes, and magnetic stirrer for 5 minutes, respectively, to prevent clumping or sticking between the particles. After making sure that the sediment is completely dissolved in water, the resulting mixture was washed thoroughly in a 63-µm sieve with distilled water. The particles remaining on the sieve were drained of excess water and left to dry in a 70° oven for 24 hours. After the dried beakers were weighed and tared, the weight of the dry sediment grains was noted as 'dry sediment'. After all these steps, the percentage values of dry sediment and wet sediment weights were calculated, and 'grain size' graphs of the cores were obtained. After the grain size analysis was completed as described above, the same processes were repeated by removing the carbonated organic matter in the sediments. 0.1 M HCl solution was used to dissolve the carbonate in the sediments. In this way, a clastic-based grain size curve was obtained. Thanks to the specific and clear volume of the u-channels, density calculation could also be made by using the data from the sediment slices prepared for grain size analysis.

3.6 Dating of the Cores

Thanks to the recent technological developments, the chronology of a sedimentary sequence can be established more precisely by various independent techniques. The preferred dating methods generally depend on the type of sediment or rock and the purpose of the study. Within the scope of this study, ^{210}Pb and ^{137}Cs dating was used for the most recent sediments and radiocarbon dating was used for the older parts of the sediment cores.

3.6.1 Radionuclide (^{210}Pb and ^{137}Cs) Dating

Revealing a clear chronology in paleoseismology studies has great importance. Especially recent sediments should be dated as precisely as possible because when the uppermost portions of sediment cores are precisely dated, the ages of the whole length cores ages can be determined accordingly. The most widely used dating technique for the most recent sediments (0-150 years) is ^{210}Pb and ^{137}Cs dating (Lockhart, 2000; Xiang et al., 2002; Mizugaki et al., 2006; Schottler & Engstrom, 2006; Hubert-Ferrari et al., 2017; Avşar, 2019). ^{210}Pb is a natural radioactive isotope of one of the radionuclides formed during the decay of ^{238}U in the atmosphere. The half-life of the ^{210}Pb is 22.3 years and it makes it easier to observe the decay process for particularly recent sediments.

^{210}Pb dating has proven to be a very reliable method especially in stable environments with uniform sedimentation. Many studies have shown that it also gives good results in non-uniform sedimentation (Appleby, 2001). Two simple models called CRS (constant rate of ^{210}Pb supply) and CIC (constant initial concentration) are used in many studies. CRS is the most widely used one. The main principles of this model were tested and proved in 3 Finnish lakes (Appleby et al., 1979). Since these lakes are annually laminated (varved), results of ^{210}Pb dating were validated by counting varves in the lake sediments. On the other hand, the CIC model is generally preferred in areas where the CRS model is invalidated by an abrupt discontinuity in the sediment record (Appleby, 2001).

To validate the dating results of the lead isotope, at least one independent dating technique should be applied. One of the most widely used independent dating techniques is the use of ^{137}Cs which is an artificial radionuclide having approximately 30 years half-life. The fallout of ^{137}Cs to the atmosphere is caused by nuclear weapon tests between the years 1954-1963. The most recent ^{137}Cs fallout is related to the 1986 Chernobyl accident. After this event, the atmosphere is exposed to lots of ^{137}Cs. Therefore, sediments recording the 1986 Chernobyl accident give this certain age accordingly (Appleby, 2001). In short, the sudden increase in the amount of the cesium isotope corresponds to the very accurate and precise dates of nuclear weapon tests between 1954-1963 and the 1986 Chernobyl accident. Therefore, when the sediments in the cores are dated by this method, the date 1986 can be captured with great precision in the proximal locations to the accident location, Chernobyl.

As a part of this study, sample preparation for radionuclide dating was done according to certain rules. First of all, because ^{210}Pb and ^{137}Cs dating has been a viable method since the 1960s, samples were taken from levels that were considered to be recent, which corresponds to approximately 10-15 cm depth from the top of the cores. Secondly, sampling was performed from bulk sediments, at the levels represented by background sedimentation. The sampling was carefully made to avoid levels of any event deposits such as turbidites.

3.6.2 Radiocarbon Dating

Radiocarbon dating, introduced by a chemist named Willard Libby in 1946, is a method that determines the ages of the ones living organisms by measuring the amount of ^{14}C (radiocarbon), which is the radioactive isotope of the carbon, in their bodies when they die. The basic principle of radiocarbon dating is based on some chemical reactions and calculations among the isotopes of carbon. The other two stable isotopes of carbon are ^{12}C and ^{13}C (Alves et al., 2018).

^{14}C is an unstable and weakly radioactive isotope that is continuously produced in the upper layers of the atmosphere. There is a continuous formation of ^{14}C in the atmosphere by cosmic rays hitting the nitrogen atom. It is rapidly oxidized and released into the atmosphere as carbon dioxide. Plants, animals, humans, and many other living organisms continue their lives by assimilating ^{14}C, which is present in the atmosphere as carbon dioxide. Since the ^{14}C exchange between the biosphere and the living organism stops when these organisms die, the amount of ^{14}C in their bodies begins to decrease over time according to the radioactive decay laws. Considering the amount of ^{14}C in the atmosphere is almost constant and knowing the decay rate of ^{14}C, the ^{14}C remnant measured in the dead organism, would reveal the date of the last period the organism had last lived.

The most commonly used dating method, especially for recent sediments, is radiocarbon dating. To find out subaqueous events with a precise chronology, many paleoseismology studies all around the world (Migeon et al., 2017; Moernaut et al.,2017; Polonia et al.,2017) include radiocarbon dating. Organic materials used in dating can be of many different species such as charcoal, pollen (Avşar et al., 2014a), leaves and other remains of plants (Monecke et al., 2004; Avşar et al., 2015), foraminifera samples (Goldfinger et al., 2003a, 2007, 2008, 2011; McHugh et al., 2006). Even rare organic materials such as Ephippia of Daphnia (Avşar et al., 2014a) have been used in radiocarbon dating. In particular, planktonic foraminifera is well suited for radiocarbon dating, which was also used in this study. The reason for using planktonic foraminifera in this study was the absence of macro-organisms suitable for dating and the abundance of planktonic foraminifera in the sediments. Besides, when planktonic foraminifers live and die in the water column, they directly participate in the sedimentation of that day and give clear information about their age (Goldfinger et al., 2003a). The ideal sample for radiocarbon dating should be special terrestrial macrofossils such as tree leaves or pollen that are too delicate that cannot be reworked on land or absorb the old carbon in the sea (Monecke et al., 2004).

Some points should be considered if radiocarbon dating will be applied to marine organisms. These points are nothing more than errors that may occur in the dating process. The first one of them is that the age determination of carbonate samples obtained from freshwater systems fed from limestone or old water sources may be inaccurate. Dissolved inorganic carbon found in the structures of crustaceans in these waters or carbonate concentrations from these solutions may also be older than expected. The reason for all these situations is that limestone was formed in a much earlier period and fed them when these resources were formed. The result of an older age than expected due to the presence of older limestone is generally called the 'hard water effect'. The same effect can be seen in dissolved inorganic carbon samples taken from water systems fed from older sources. The general name of these two effects is called the reservoir effect.

The second error that may occur in radiocarbon dating can be defined as reworking. If the sample to be used in the dating is a terrestrial material, for example, it may be a material formed on land and dropped into the sea by transportation, it is likely that it has been subjected to transportation and erosion for some time. To illustrate, a piece of wood may be transported and eroded on land many times and fell into the sea or lake through streams. If this piece of wood is used as a sample in radiocarbon dating, it will yield an older result than expected because that piece of wood has been subjected to erosion on land, which indicates it is a reworked material. Sometimes, the same problem can be observed in aquatic organisms, like benthic foraminifera, that are also quite susceptible to reworking as if they were terrestrial materials (Goldfinger et al., 2003a; Avşar, 2013).

Within the scope of this study, planktonic foraminifera samples were collected from 18 sediment cores for radiocarbon dating. Among these planktonic foraminifera samples consisting of mixed species, *Trilobatus sacculifer* (Brady, 1877) and *Globigerinoides ruber* (d'Orbigny, 1839) could be identified. The main reason for the use of planktonic foraminifera is their abundance in cores. Also, when making this selection, it is taken into account that they are sensitive to transport and erosion since they are floating in the water. On the other hand, since the cores are stratigraphically correlated in mm scale, the same stratigraphic level in different cores is expected to be of the same age according to simple geology rules. To test this case, one sample was collected from the top 1 cm of all cores and sent to the laboratory for dating.

Foraminifera samples were collected from the levels that were background sedimentation meaning that outside of the 'event' levels. Otherwise, if foraminifera samples were collected from turbidites, they would give very irrelevant and older ages. Because turbidites are not sediments that form under stable conditions in a certain depositional environment. Instead, they are a mixture of sediments that originated from noncontemporary events and formed in different locations. Therefore, when dating the core, date samples should be collected from background sedimentation, and not events levels in order to find a reasonable sedimentation rate and reliable age-depth model. Besides, from the sedimentological point of view, the bottom parts of the submarine events, i.e. turbidites, show a very sharp transition and make it easy to distinguish from background sedimentation. In the light of all this information, the levels at which planktonic foraminifera samples were picked could be easily determined.

To achieve the best results, it is necessary to avoid the above-mentioned errors as much as possible. In this context, organisms that are most suitable for dating should be determined.

After the selection of the correct organic material for radiocarbon dating, the age value obtained must be converted to a calendar year, which is called "calibration", since it has been realized that the age value obtained from the studies conducted using tree rings in previous years is not the same as the calendar age (Pearson & Stuiver, 1986; Björck & Wohlfarth, 2001). There are many reasons for the difference between dendrochronology and calendar years. These can be summarized as geomagnetic and solar magnetic fields, latitude and longitude states, volcanic eruptions, human interferences, and some nuclear tests (Björck & Wohlfarth, 2001; Alves et al., 2018). Also, inconsistency with the calendar age in the age data obtained from aquatic samples can be associated with the change in global ocean ventilation rates (Björck & Wohlfarth, 2001). Several calibration curves such as OxCal v4.2.3, INTCAL09, INTCAL13, Marine 04, INTCAL20, and Marine 20 have been developed in this context and are widely used in many paleoseismology investigations. Marine 20 calibration curve has been used in the present study (Heaton et al., 2020).

The collected planktonic foraminifera samples including *Trilobatus sacculifer* (Brady, 1877) and *Globigerinoides ruber* (d'Orbigny, 1839) are as seen in Figure 3.10. During the sampling process, firstly the levels within the sediment sequence that were decided to be dated were determined. Later, bulk sediment samples were taken from these determined levels. The amount of bulk sediment taken was equal at all levels and was sampled at one-third the volume (calculated on unit length) of a u-channel which corresponds to approximately 1.1 cm^3 in this study. Then, bulk sediment samples cut in 1 cm intervals were dissolved in distilled water by using a magnetic stirrer and ultrasonic bath. The dissolved bulk sediment was passed through a 180-μm sieve and washed completely. At the end of washing, the material remaining on the sieve was examined under a microscope in distilled water. Under the binocular microscope, planktonic foraminifera was carefully collected using a needle-thin instrument and placed in small tubes. While collecting the foraminifera, it was taken care to select undeformed/unbroken ones. Foraminifera samples collected in small tubes were sent to Poznańskie Laboratorium Radiowęglowe in Poland for radiocarbon dating.

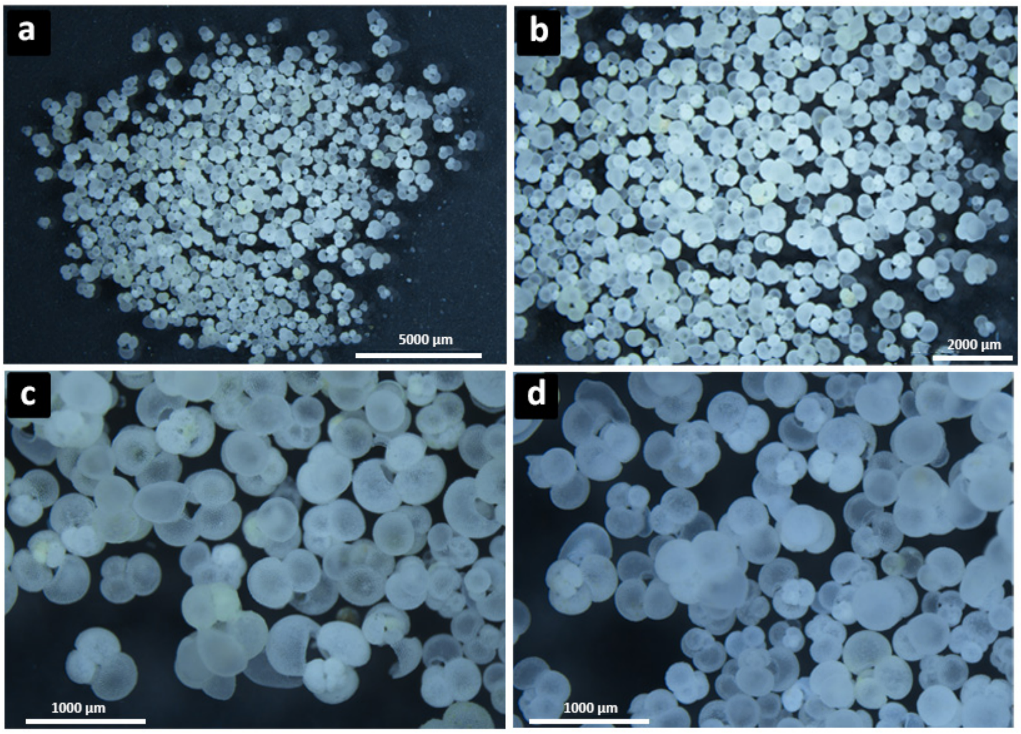

Figure 3.10. Photographs of planktonic foraminifera samples extracted from sediment cores. The photographs were taken under a binocular microscope with different magnifications.

CHAPTER 4

RESULTS

4.1 Diagnostic Properties Used in the Detection of Seismo-turbidites

According to the bathymetry of the Gulf of Aqaba, which is exposed to a dense sediment influx due to a large catchment of 19260 km^2, several submarine landslides were detected in some areas within the gulf. Although the sizes and masses of landslides vary from one to another, almost all are characterized by well-developed scarps and toes (Figure 4.1). Considering that these submarine landslides are particularly concentrated on active fault strands, they might have been related to the earthquakes.

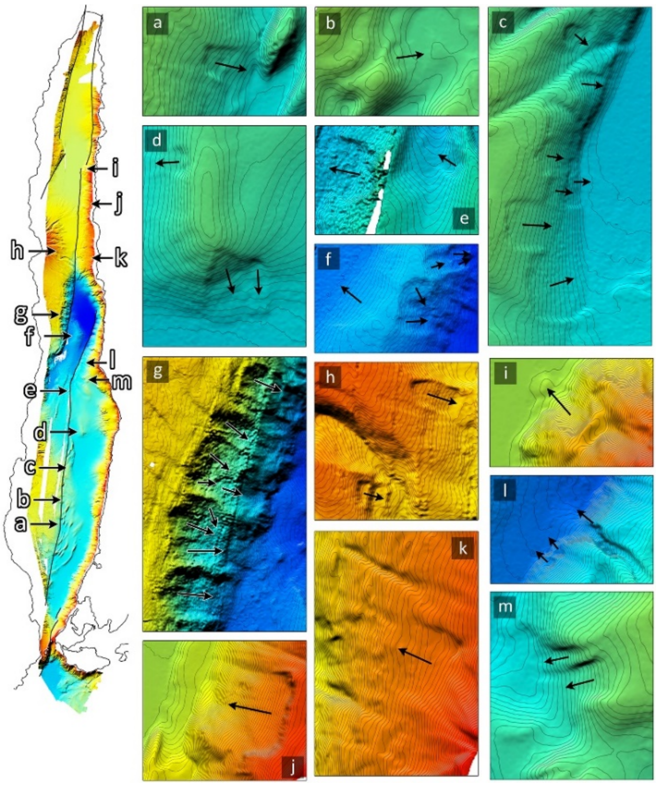

Figure 4.1. Noticeably well-imaged landslides in the close bathymetry of the Gulf of Aqaba. Arrows indicate the flow directions.

The complex nature of the Gulf of Aqaba sediments is shown in Figure 4.2. Background sedimentation consists of brownish silty and clayey units. Since the Gulf of Aqaba is located in a seismically active region, it is susceptible to deformations due to earthquakes. The intense biogenic activity results in highly bioturbated sediments. Sudden event deposits within bioturbated background sedimentation can be noticed by their clear lineaments. All sedimentary anomalies observed in the Gulf of Aqaba sediments are considered as event-deposits.

Close-up view radiography of the DK-1 core taken from the Dakar Deep presents a quite heterogeneous and deformed appearance (Figure 4.2). The type of this heterogeneity can be both earthquake-induced soft-sediment deformations and/or bioturbation-induced deformations. It is also possible that earthquake-induced soft-sediment deformations may be secondarily deformed by bioturbation. In this kind of depositional environment, sediments are expected to have three main components: i) terrigenous clasts, ii) remains of inorganic parts of organisms once lived in the water column, and iii) minerogenic material due to chemical precipitation from the water column. Sediments contain gravel-sized particles that are seen as whitish spots in the radiographic images (Figure 4.2c,f). The lighter appearance of these spots implies that they have lower densities than the surrounding sediments (Avşar, 2013; Yeniçeri, 2020). If these gravels were terrigenous clasts, they would look almost black due to higher density.

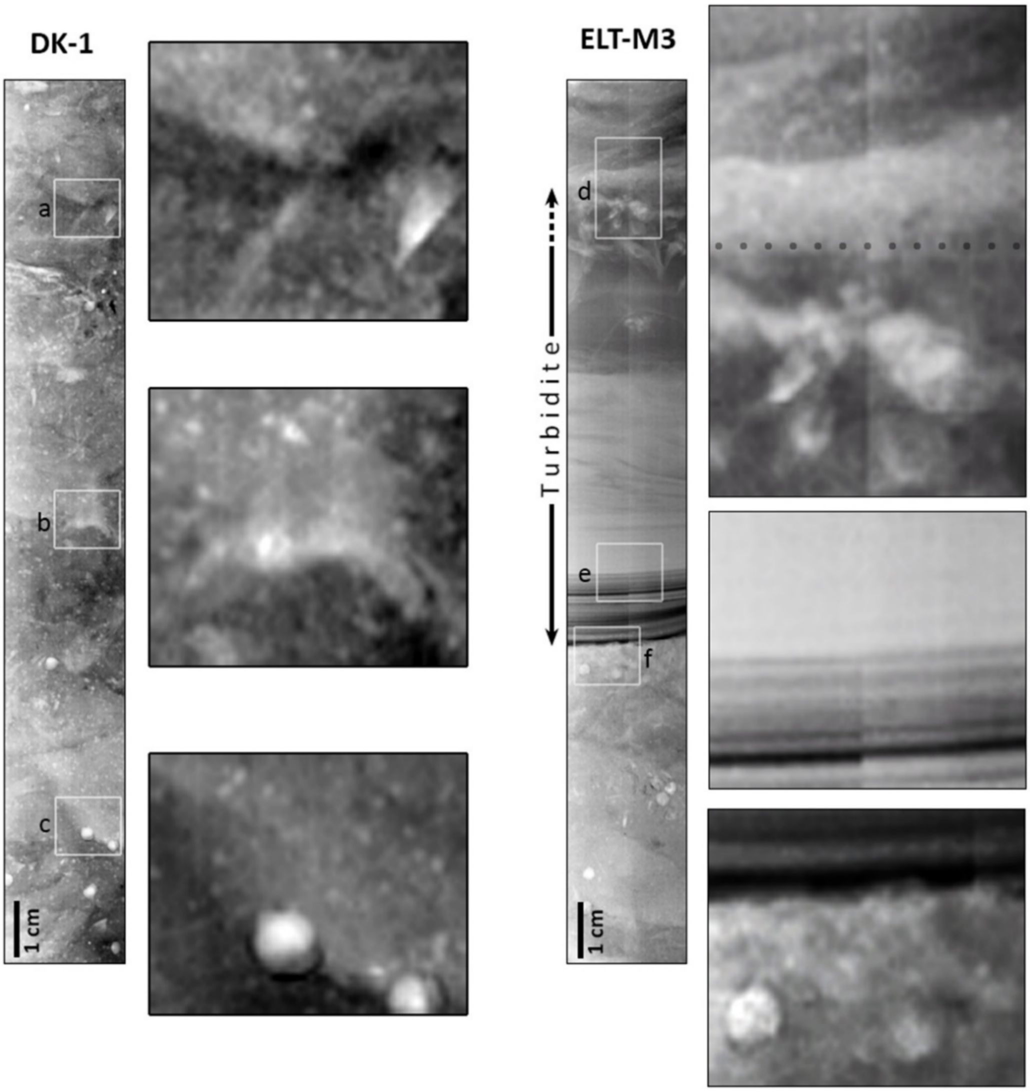

Figure 4.2. A close-up view of the radiographic images of DK-1 and ELT-M3 cores.

Bulk densities of sediments in Eilat, Aragonese, Dakar, Tiran, and Hume deeps were calculated by using u-channels' certain volumes and wet weights of the sediment slices taken for grain size analysis. These procedures have been applied for all levels of sediment taken from 10 of the cores. Results were obtained at 614 different levels with a mean of 1.98 g/cm^3 and a standard deviation of 0.2. Bulk sediment densities varying between 1.58 - 2.38 g/cm^3 were represented by a scatter plot (Figure 4.3).

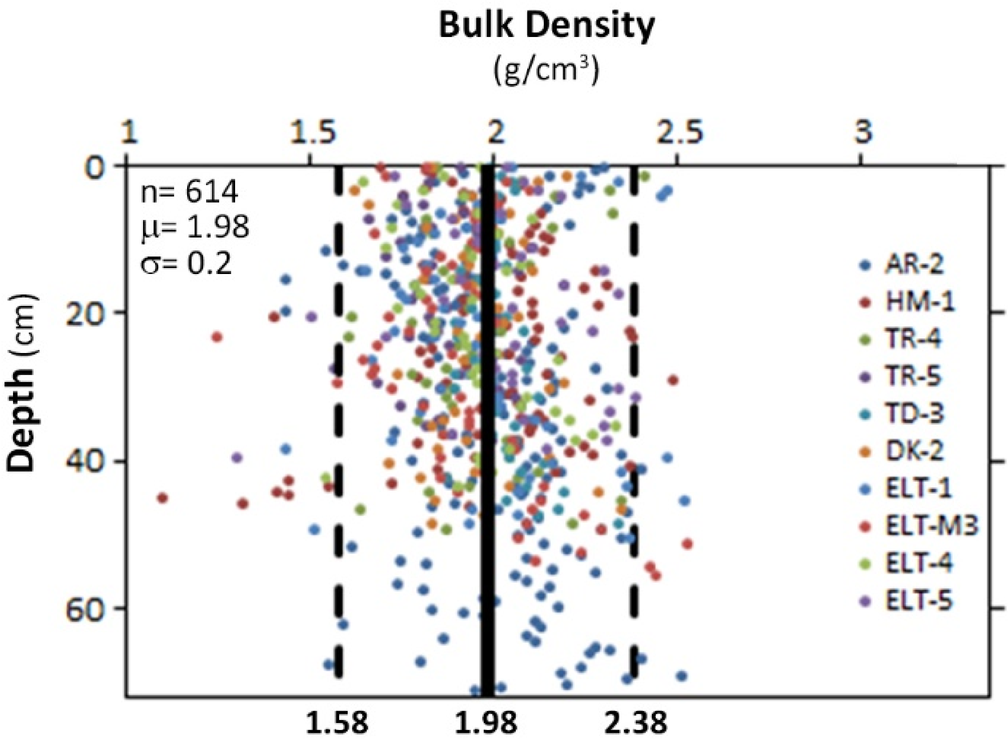

Figure 4.3. The distribution of bulk densities calculated using grain-size data from sub-basins in the Gulf of Aqaba.

Foraminifera shell density is accepted as 1.4 – 1.5 g/cm³ in the literature (Be, 1959; Fok-Pun & Komar, 1983). Compared to the densities of the Gulf of Aqaba sediments, foraminifera has less dense shells, which causes them to be seen in lighter colors on radiographs. For this reason, the whitish spots that are prominent in radiographic images (Figure 4.2c) most likely belongs to a type of foraminifera. If these suspicious spots were mollusks shells, they would appear as almost black spots since their densities are around 2.7 g/cm³ (Rieux et al., 2018).

ELT-M3 core's heterogeneous (bioturbated/deformed) and foraminifera-bearing background sediments contain relatively undisturbed, homogeneous, and foraminifera-free intercalations (Figure 4.2e). These intercalations are most probably mass wasting event deposits that have been identified as turbidites. The turbidite which is characterized by a well-laminated denser base (Figure 4.2f) and a finer and well-laminated medium level and a homogeneous top (Figure 4.2e) composed of relatively less dense materials is distinctly observable within the bioturbated/deformed background sedimentation. Moreover, thanks to the u-channel radiography, even basal erosion (Figure 4.2f) formed by turbidity currents can be easily seen with a visual inspection. Since the turbidites are sudden deposits, they cannot meet the time required for bioturbation. The sediments within turbidity currents contain foraminifera. However, because of their mixing with the turbulence created by these currents and having lower densities than sediments, they are deposited as a thin layer only on top of the turbidite depositions according to gravitational segregation during the re-depositional stage. Hence, they are characterized by undisturbed/unbioturbated and foraminifera-free levels (Figure 4.2e).

Distinct turbidites having distinct turbidite internal structures on radiographic images are presented in Figure 4.4. Turbidites conforming to the classical definition of ‘turbidite’ and deposited according to gravitational segregation are given in Figure 4.4 2,3. Their coarse-grained bases have a lower density than background sedimentation due to their porosity and they look lighter on radiographic images. Therefore, their bottoms are very obvious and distinguished sharply from the background sedimentation. Well-developed laminations are seen in the middle levels of these turbidites (Figure 4.4 2,3). While a homogeneous level was expected to be seen in the upper parts, deformations due to bioturbation existing as a part of the background sedimentation caused the upper limits of these turbidites to lose their clarity. In addition, these two turbidites are foraminifera-free levels implying sudden depositions in such bioturbated and foraminifera-bearing background sedimentation, as described at the beginning.

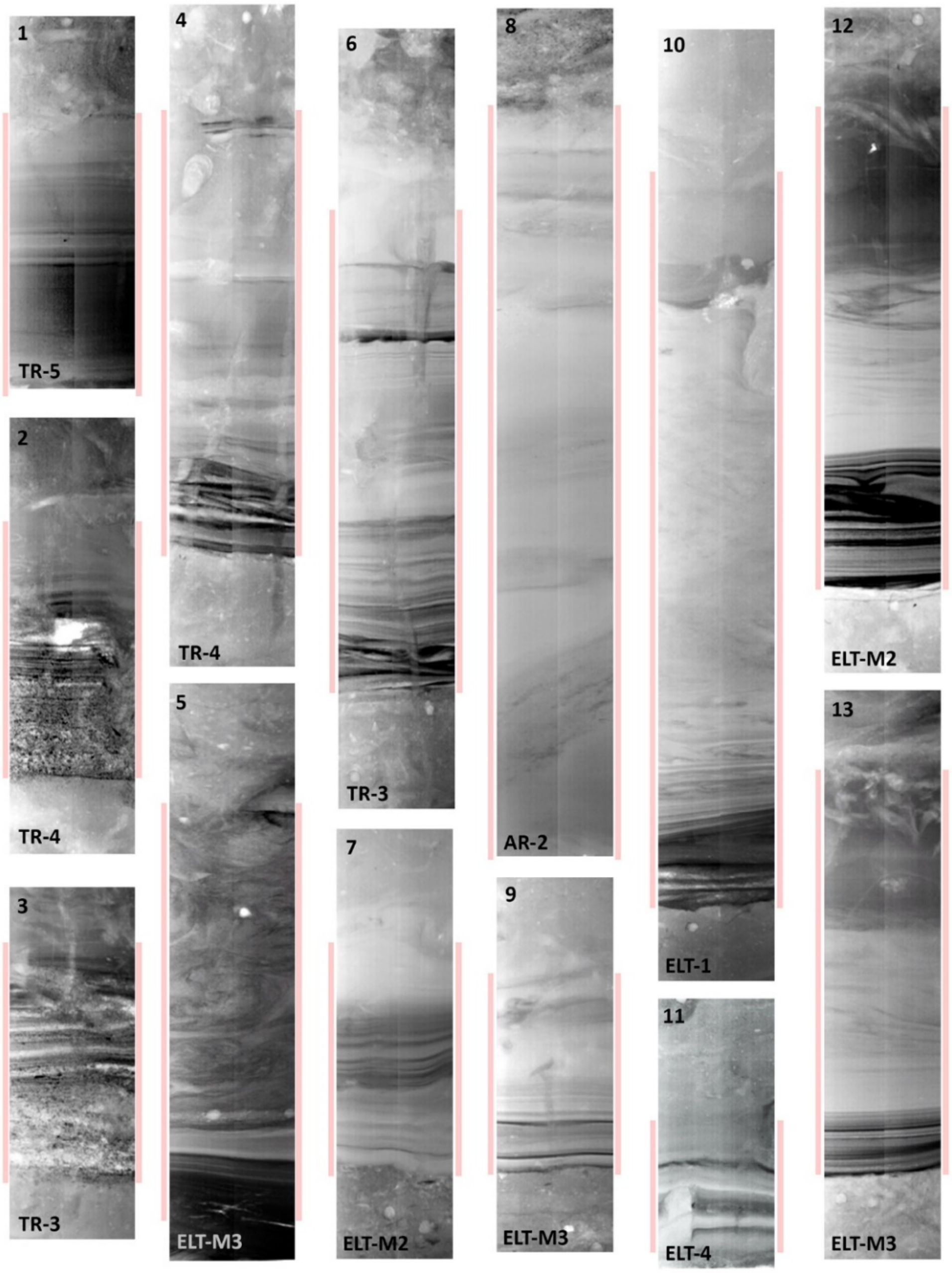

Figure 4.4. Relatively thick and prominent turbidites observed in the Gulf of Aqaba cores. The core names are written on the lower left corners of the insets, and detailed explanations about the numbers on the upper left corners are given in the text.

The levels showing distinct turbiditic features with their well-laminated bases and homogeneous tops are presented in Figure 4.4 1,7-13. They all have well-developed and clear laminations that have not been intensely deformed by various organisms. Besides, since they precipitated according to gravitational segregation, high-density materials have been deposited at the base and relatively low-density materials have been deposited on top of them, which can be explained by the color change from dark to light in the images. In addition, cross-laminations which are characterized by both clear (Figure 4.4 7,10,12) and vague lines (Figure 4.4 8,9,13), are observed in some of these turbidites. These cross layers may show turbidity current direction, or they may indicate simultaneously deposited opposing turbidites. The turbidites shown in Figure 4.4 1,7-13), which are foraminifera-free in the base and middle levels, have been subjected to slight deformations being affected by the bioturbations towards their upper limits. Only one of them (Figure 4.4 13) has been subjected to more intense deformation in its upper levels compared to the others, but still maintains its distinct turbidite internal structure.

In the radiographic images shown in Figure 4.4, there is a third group of turbidites (Figure 4.4 4-6), which are characterized by their exposure to intense deformation and/or bioturbation. For example, in one of these turbidites (Figure 4.4 4), even the well-developed and high-density laminations and cross-laminations at the base of it with a thickness of about 9 cm have been deformed by bioturbation. Similarly, another turbidite (Figure 4.4 5) with approximately the same thickness in this third group also has a quite undulated appearance indicating most probably a water oscillation during an earthquake. Also, the last turbidite (Figure 4.4 6) in this group has been affected by the intense burrowing of its well-developed laminations and consequently, deformed. Despite being subjected to such intense bioturbation and deformation, these three sudden event-deposits (Figure 4.4. 4-6), have preserved their distinctive turbidite internal structures.

Apart from these distinct turbidites which can be identified with their well-developed and graded laminations as a result of gravitational segregation, there also exist some levels that seem like sedimentological anomalies (Figure 4.5). In order to avoid the complexity in radiographic images presented in Figure 4.5, sedimentary anomalies with similar characteristic features are described as a group. In the first group, relatively thinner event-deposits indicating sudden depositions (Figure 4.5 1,4-7,10-13,15,21) can be mentioned. Their blackish linearities (straight laminations and/or cross-laminations) and having no foraminifera indicate that they have been deposited not by normal sedimentation but by gravitational segregation. Since they have a very thin laminated part, they become vulnerable to bioturbation and/or deformation. In other words, since the background sedimentation in the Gulf of Aqaba is characterized by intense bioturbation, possible event deposits that can be observed in the cores start to be affected by these bioturbation activities when the event ceases. If these event-deposits are thin, almost all parts of them might be deformed by the various organisms, like the above-mentioned anomalies (Figure 4.5(1,4-7,10-13,15,21).

In the second group, relatively thicker sedimentary anomalies are seen in Figure 4.5 2,3,17,28. The presence of undisturbed laminations (Figure 4.5 2,17) within these thicker deposits proves that they are turbidites. Although they have signs of being turbidite, there are some unidentified strange forms in the radiographic images and these unidentified forms are large enough to preclude these turbidites' clarity. Moreover, channel-like structures are observed in some of these turbidites (Figure 4.5 2,3), which might have been due to the erosion caused by turbidity currents.

Thirdly, there exist several sedimentary levels (Figure 4.5 8,14,16,18-20,22,26) that appear as linear features. These levels are considered anomalies because they preserve their linearities within such an intensely bioturbated and/or deformed background sedimentation. These linearities can appear as both straight (Figure 4.5 8,16,18,26) and inclined lines (Figure 4.5 14,19,22). Besides, some levels containing radial shapes (Figure 4.5 6,24,26) may also be seen as anomalies since normally they do not exist within the background sedimentation.

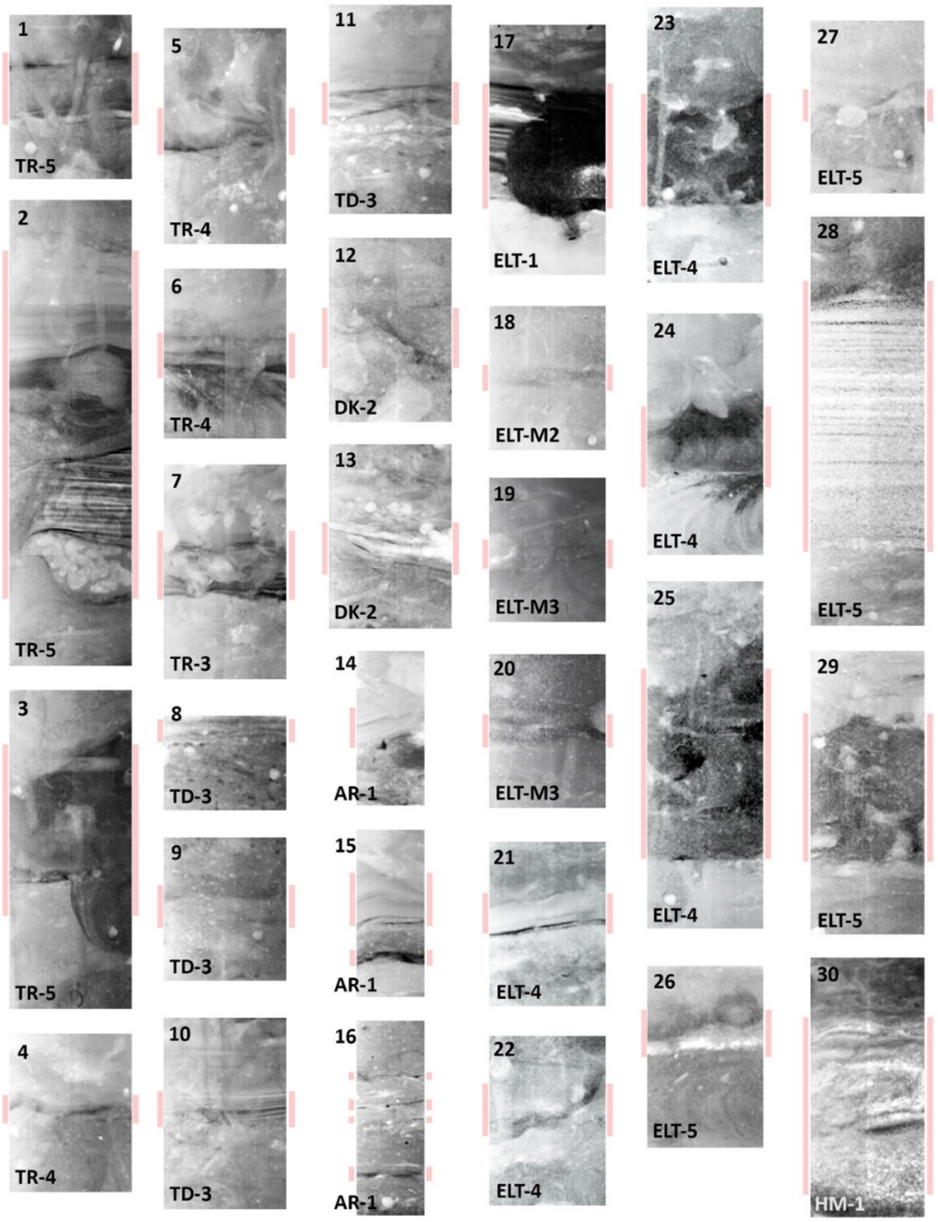

Figure 4.5. Sedimentary anomalies observed within the background sedimentation. The core names are written on the lower left corners, and detailed explanations about the numbers on the upper left corners are given in the text.

As the last group, the most intensely deformed and bioturbated levels (Figure 4.5 23,29,30) attract the attention. Although they are certainly sedimentary anomalies with their complex appearances, nothing very clear can be said about these levels at this stage of the study.

So far, the radiographic imaging results obtained from the Gulf of Aqaba sediments have been summarized. According to these images, background sedimentation has been defined, and distinct and non-distinct event layers as a result of visual inspections have been explained by giving examples from some parts of the cores. Close-up views of radiographic images of all cores are given in the Appendices.

As explained above, a classical turbidite is characterized by a coarse bottom, a fining-upward sequence, and a homogeneous top. It is possible to observe that the grain size of the homogeneous uppermost part is even finer than the background sedimentation. In addition to grain size (GS) increase within a turbidite, it is known that magnetic susceptibility (MS) measurements give higher values in terrestrial mineralogical materials compared to carbonates (Croudace and Rothwell, 2015). Apart from MS and GS measurements, ITRAX scanning provides geochemical information for all cores. Since ITRAX micro-XRF core scanning is affected by several factors such as water content and grain size, inter-element ratios have been used in the present study. Instead of showing all 17 elements measured during the scanning, it has been preferred to present only a few proxy elements that could be useful for the detection of event-deposits over the entire Gulf of Aqaba. In the ITRAX profiles, Zr and Rb have been used as a proxy for terrestrial mineralogical clastics (Rothwell et al., 2006), while Ca and Sr were used as a proxy of carbonate sources. The existence of Ca indicates both marine and terrestrial calcite sources, while Sr is particularly useful in distinguishing foraminiferal calcite (Croudace and Rothwell, 2015). During a sudden event, the terrestrial clastic influx from submarine slopes is directly deposited without allowing biochemicals to precipitate from the water column. For this reason, it is quite possible to see Ca and Sr deficiency as well as an increase in Zr and Rb in the sudden event-deposits. This means that when the ratios of terrestrials to chemicals such as Zr/Ca or Rb/Sr profiles are examined, the levels at which they peak positively provide information about sudden event-deposits (Avşar et al., 2014a; Croudace and Rothwell, 2015). In short, radiographic imaging, Magnetic susceptibility (MS), grain size (GS), and ITRAX scanning have been applied to the sediment cores taken within the scope of this study and used as a proxy for the examination of the turbidites within the Gulf of Aqaba sediments.

The MS, GS, and ITRAX scanning results of TR3, TR4, and TR5 cores taken from the Tiran Deep are shown in Figure 4.6. According to the MS, GS, and/or ITRAX profiles, all suspicious levels giving anomalies within background sedimentation for any reason are indicated by blue bars.

There is a prominent sedimentary anomaly in the first level which is indicated by A in the radiographic image of the TR-5 core (Appendix A), and this anomaly is supported by all other profiles i.e., MS, GS, and ITRAX profiles with weak peaks having small amplitudes (Figure 4.6). A very prominent and thick turbidite is seen in the radiographic image (Appendix A) at the B level. Similarly, this anomaly, which becomes apparent by preserving its turbidite internal structure, makes considerable peaks in all other graphs, supporting that it is an event-deposit. When C and D levels are examined, although there are prominent sedimentary anomalies in the radiograph (Appendix A) and distinct peaks in MS and GS profiles (Figure 4.6), no anomaly in ITRAX profiles can be observed. Finally, looking at the E level in the radiographic image (Appendix A), it is certainly a turbidite with its well-laminated and foraminifera-free internal structure. While this level, which is so obvious in the radiographic image, tends to peak positively in MS and GS profiles, it is interesting that the values in ITRAX profiles tend to decrease (Figure 4.6).

The A level in the TR-4 core is quite a prominent turbidite in the radiographic image (Appendix B) because it has a well-developed and preserved turbidite internal structure and is foraminifera-free. The presence of this turbidite is observed as a negative peak in the MS profile and as a considerable positive peak in the GS profile (Figure 4.6). Among the ITRAX graphs, the Zr/Ca and Zr/Sr profiles interestingly show a negative trend, while the Rb/Ca and Rb/Sr profiles show a positive trend. Both the B and C levels show a distinct and thin sedimentary anomaly on the radiographic image (Appendix B), and all profiles of this anomaly in MS, GS, and ITRAX have thin peaks (Figure 4.6). The D anomaly looks like a disturbed thin turbidite because the laminations that once existed are apparent from some parts of the anomaly. While no signal belonging to D anomaly was observed in MS, Zr/Ca, and Zr/Sr profiles, the same anomaly is observed as weak peaks in GS, Rb/Ca, and Rb/Sr profiles. In the radiographic image (Appendix B) at the E level, one turbidite preserving its internal structure is clearly seen. In addition, at this level, all the other profiles (Figure 4.6) have significant peaks without exception, proving that this level is a turbidite. At the F level, which is the last sedimentary anomaly visible in the TR-4 core, distinct linearity, and radial forms are observed. Similar to the E level, the F level which is found to have a sedimentary anomaly in the radiographic image (Appendix B) is supported by considerable peaks in all other profiles (Figure 4.6).

When the result graphs of the TR-3 core are examined, a remarkable turbidite with its well-developed internal structure that can be a textbook example is observed in the radiographic image (Appendix C) at A level. The GS profile shows a very distinct peak that supports its internal structure having a coarse-grained base and fining upward. On the other hand, in the MS profile, the values have gradually decreased due to the increased porosity depending on the coarsening of grains, and consequently, a negative peak is observed at this level. In all of the ITRAX profiles, considerable peaks are noticeable at this level. When the B level within the TR-3 core is examined, a sedimentary anomaly that once had a turbidite internal structure but now appears to be deformed is observed in the radiographic image (Appendix-C). This anomaly, which has positive and weak peaks in the MS, GS, and Zr/Ca profiles, does not show positive peaks in the Rb/Ca, Zr/Sr, and Rb/Sr profiles, and even tends to peak almost negatively on the Zr/Sr and Rb/Sr profiles (Figure 4.6). Although the next anomaly, C level, is observed as a sedimentary anomaly in the radiographic image and GS profile, no other graph has shown an anomaly signal at this level (Figure 4.6). D level is quite evident in the radiograph (Appendix C) as a thick turbidite that is very clean and preserves its turbidite internal structure. Interestingly, the GS graph has a negative peak at the D level, although the values in the MS and ITRAX profiles tend to increase at this level (Figure 4.6). The E level which is the last anomaly seen in the radiographic image of the TR-3 core shows slight increases in the MS, GS, and ITRAX profiles (Figure 4.6), which supports the existence of an anomaly here.

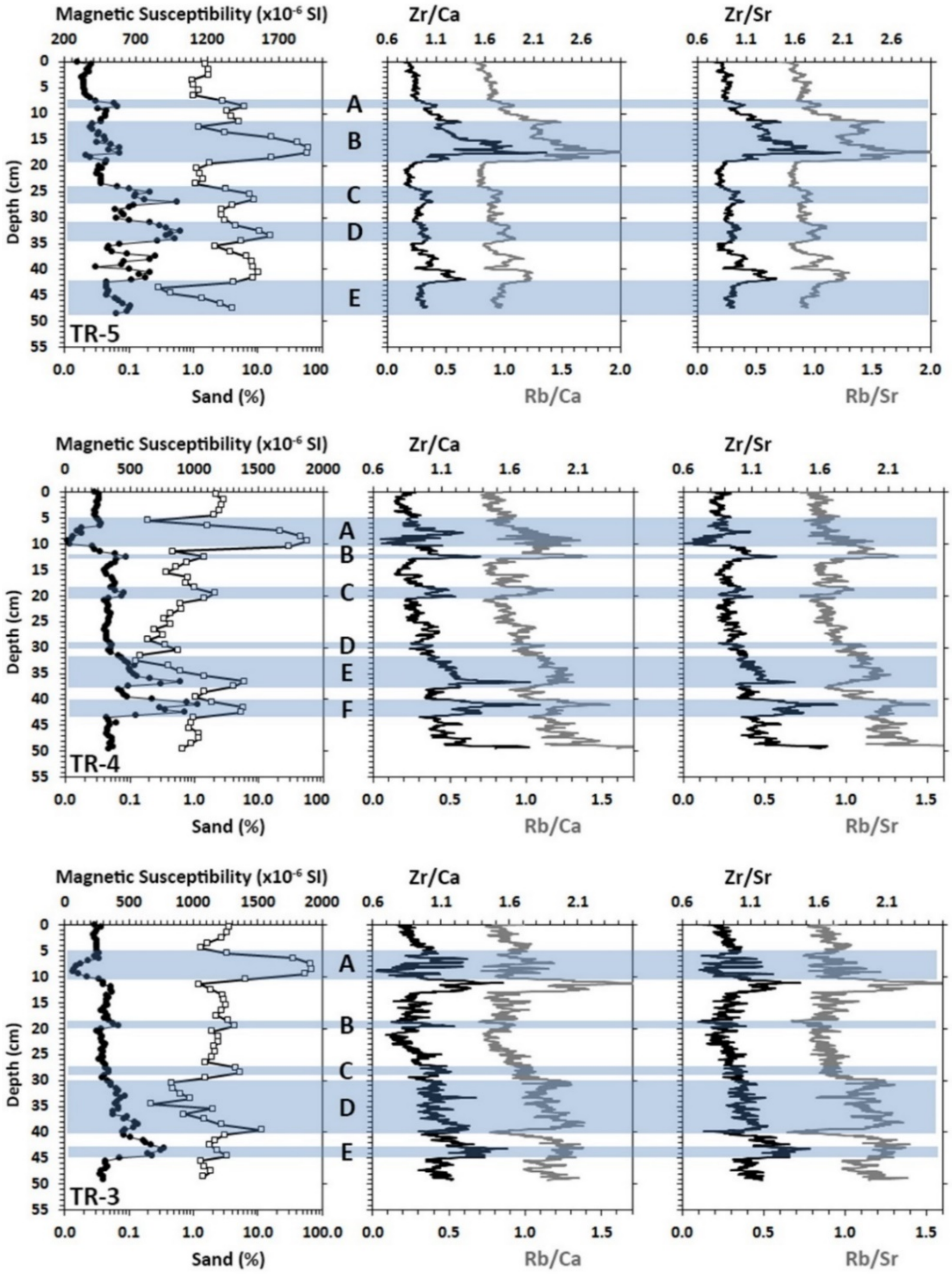

Figure 4.6. Magnetic Susceptibility (MS), Grain Size (GS), and ITRAX Micro XRF Scanning results of (Zr/Ca, Rb/Ca, Zr/Sr, and Rb/Sr profiles) TR-5, TR-4, and TR-3 cores.

ELT-1, ELT-M2, ELT-M3, ELT-4, and ELT-5 cores taken from the Eilat Deep are presented in Figure 4.7 with their MS, GS, and ITRAX profiles. Similar to the results of the Tiran Deep, in the Eilat results, all levels peaking at any proxy, i.e., showing a sedimentary anomaly, are indicated by blue bars as suspicious levels. Each core contains a different number of peaks and depending on these peaks' numbers they all have different numbers of event-deposits that are represented by capital letters like A, B, C, D, and E (Figure 4.7).

In the uppermost part of the radiographic image of the ELT-1 (Appendix D), there is a sedimentary anomaly that is evident by its visible turbidite internal structure. While A level, has considerable anomalies in MS, GS, Zr/Ca, Zr/Sr, and Rb/Sr profiles, there is no indication of an anomaly at this level in the Rb/Ca profile (Figure 4.7). When looking at the B level, which appears as a slight sedimentary anomaly on the radiographic image (Appendix D), it is characterized by a considerable peak on the GS profile and weak peaks on both Zr/Sr and Rb/Sr profiles (Figure 4.7). There is a distinct turbidite in the C level on the radiograph (Appendix D), which preserves the turbidite internal structure with its thick and well-developed laminations and being foraminifera-free. The presence of this turbidite is supported with serious anomalies in all other result profiles (Figure 4.7).

At the top of the ELT-M3 core, there is a very obvious turbidite similar to the one at ELT-1. This turbidite, indicated by level A, shows a classical turbidite internal structure both by having well-developed laminations and being foraminifera-free in such heterogeneous background sedimentation. This turbidite level interestingly tends to peak negatively on MS and GS profiles (Figure 4.7). Also, the A level, which does not seem to be an anomaly according to the Zr/Ca and Rb/Ca profiles, tends to peak positively with the increase of values in Zr/Sr and Rb/Sr profiles (Figure 4.7). The B level observed as a slight anomaly in the radiographic image (Appendix E) is accompanied by an obvious peak only in the MS profile and an increasing trend in the GS profile (Figure 4.7). The remaining graphs show that there is no anomaly at this level. In the radiographic image (Appendix E), level C appears as a well-developed turbidite having a laminated base and foraminifera-free upper levels.

While the GS and MS profiles show a negative trend, all other ITRAX graphs at the same level show a positive trend meaning increasing values (Figure 4.7). The D level, which presents a vague appearance on the radiograph (Appendix-E), proves to be a sedimentary event-deposit with both considerable peaks in MS and GS profiles and minor anomalies in Rb/Ca and Rb/Sr profiles (Figure 4.7). The last anomaly observed in the ELT-M3 core appears at the E level. Undulations towards the upper parts of this level, which is an obvious turbidite with its well-laminated base on the radiograph (Appendix E), are striking. Besides, the level E has significant peaks in all other proxies which are MS, GS, and ITRAX (Figure 4.7), indicating an anomaly.

ELT-M2 is the shortest core taken from the Eilat Deep, so only two events have been recorded. The first event in the ELT-M2 core is indicated by A and presents an image of turbidite that is perfect enough to be a textbook example (Appendix F). Although there is a dramatic decrease in MS, Zr/Sr, and Rb/Sr profiles (Figure 4.7), the increase in Zr/Ca and Rb/Ca profiles (Figure 4.7) supports the existence of a turbidite at this level. The second anomaly observed in the ELT-M2 core is indicated by B and it presents a very clear turbidite internal structure in the radiographic image (Appendix F), like the anomaly indicated by A.

One sedimentary anomaly which is characterized by very obvious and clear linearity and foraminifer-deficiency is seen in level A of the ELT-4 core's radiographic image (Appendix G). This sedimentary anomaly presenting such a clean turbidite appearance on the radiograph is represented by negative peaks in all the MS, GS, and ITRAX profiles (Figure 4.7). The B, C, D, and E sedimentary anomalies detected in the radiographic image of the ELT-4 core (Appendix G) are supported by showing anomalies in all other MS, GS, and ITRAX profiles as well (Figure 4.7). Finally, the G level is quite typical turbidite, with obvious laminations and foraminifera-deficiency visible on the radiograph (Appendix G). While all other profiles also have an increasing trend supporting that there is an anomaly at this level, no anomaly can be observed in the GS profile (Figure 4.7).

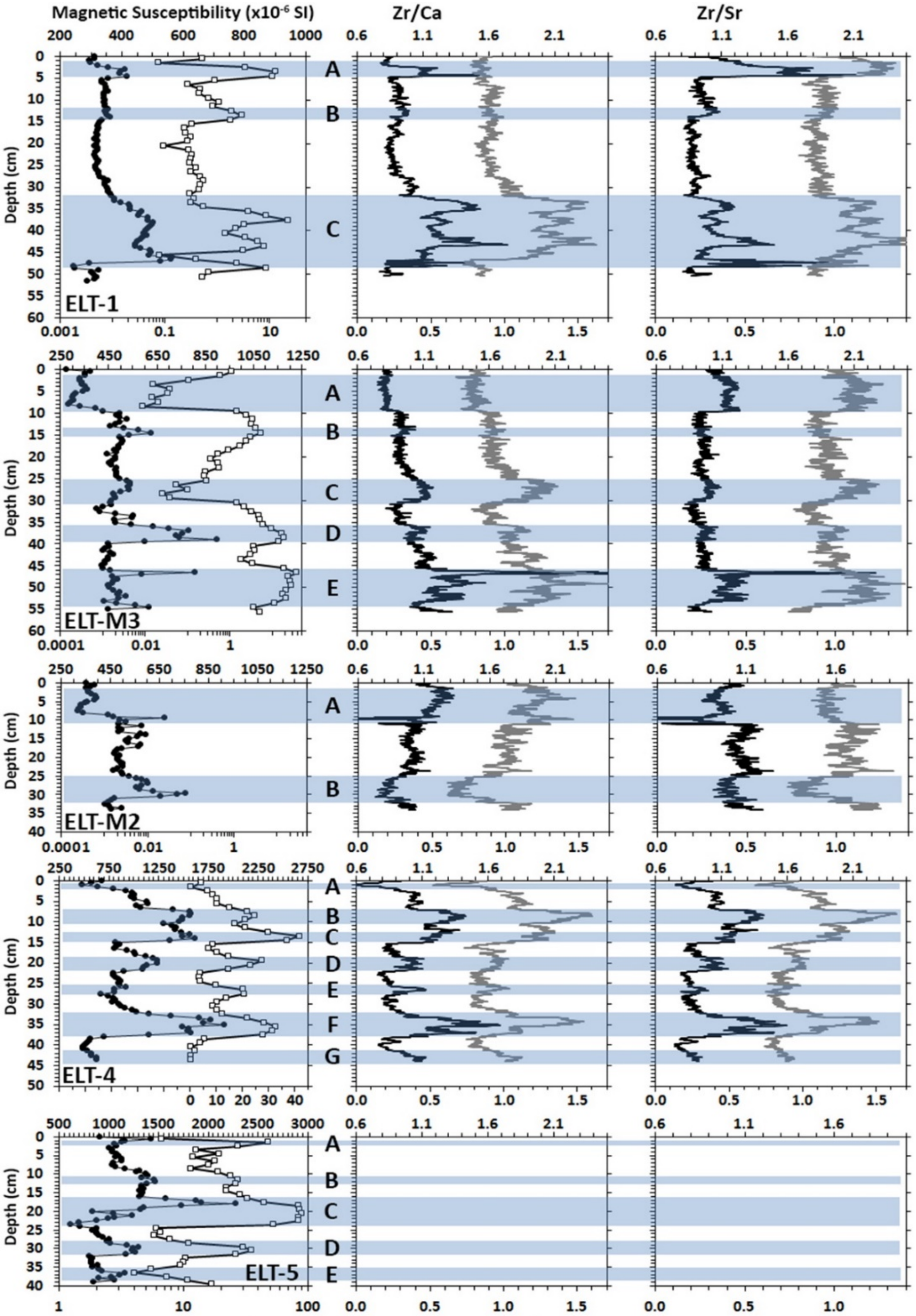

Figure 4.7. Magnetic Susceptibility (MS), Grain Size (GS), and ITRAX Micro XRF Scanning results (Zr/Ca, Rb/Ca, Zr/Sr, and Rb/Sr profiles) of ELT-1, ELT-M2, ELT-M3, ELT-4, and ELT-5 cores.

ITRAX has not been measured in the ELT-5 core so, only MS and GS profiles are available. The prominent anomaly at the uppermost level of the ELT-5 core is characterized by whitish linearity and another darker linearity above it. This prominent sedimentary anomaly also is represented by considerable peaks in both MS and GS profiles (Figure 4.7). Level B appears as an anomaly in the radiographic image (Appendix H) and appears as weak peaks in MS and GS profiles. Looking at level C in the radiographic image of the ELT-5 core (Appendix H), it is definitely a turbidite, with obvious laminations and foraminifera deficiency. This turbidite, which appears so clearly on the radiograph, is represented by quite large peaks in both MS and GS profiles (Figure 4.7). It can be said that there is an obvious sedimentary anomaly at the D level by looking at its image on radiographs (Appendix H) and the increase in MS and GS profiles (Figure 4.7). Finally, a turbidite preserving its internal structure is seen in the E level in the radiographic image of the ELT-5 core (Appendix H). Although the GS profile shows a negative peak, magnetic susceptibility values tend to increase according to the result of the MS profile (Figure 4.7).

MS, GS, and ITRAX profiles of DK-1 and DK-2 cores collected from the Dakar Deep are presented in Figure 4.8. The MS, GS, and ITRAX profiles (Figure 4.8) show a lot of peaks, which proves that DK-1 and DK-2 have recorded more event-deposits. However, in the radiographic images of Dakar cores (Appendices I & J), nothing is clear about turbidites. The DK-1 and DK-2 cores appear heterogeneous as if they are almost completely deformed and/or bioturbated. More clearly, while no level showing any turbidite internal structure is observed in the radiographic images (Appendices I & J), the profiles of MS, GS, and ITRAX give results as if these two cores were composed of fully a turbidite sequence. On the other hand, the peaks of MS, GS, and ITRAX proxies support each other at almost all levels, unlike the radiographic images (Appendices I & J). For example, A, B, E, F, and H events are very obvious in the DK-1 core profiles for three proxies. Similarly, A, C, F, and G events' clarity is noticeable in the DK-2 core profiles for the same proxies (Figure 4.8).

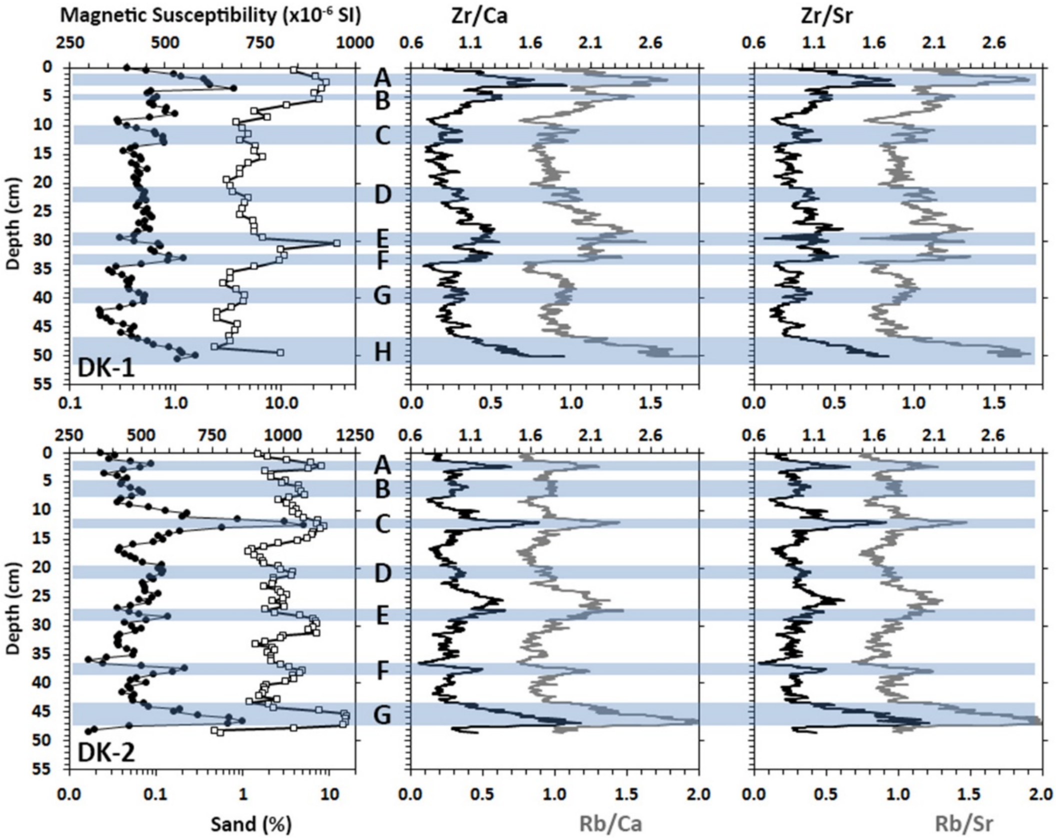

Figure 4.8. Magnetic Susceptibility (MS), Grain Size (GS), and ITRAX Micro XRF Scanning results (Zr/Ca, Rb/Ca, Zr/Sr, and Rb/Sr profiles) of DK-1 and DK-2 cores.

MS, GS, and ITRAX profiles of the Aragonese cores, which are AR-1 and AR-2, are presented in Figure 4.9. AR-1 core is the longest core taken from the Gulf of Aqaba and therefore the most anomalies are observed in this core. While the radiographic image (Appendix K) presents a very heterogeneous appearance, these heterogeneities are accompanied by many peaks in some levels on MS, GS, and ITRAX profiles (Figure 4.9). In this core, unlike the others, it is very clear that the number of levels observed as an anomaly in all of the radiographs (Appendix K) and other profiles (Figure 4.9) is low. Looking at most levels using a single proxy, it is difficult to describe that level as an anomaly. For example, while the anomalies observed at the level C and E appear as considerable peaks in the MS and GS profiles, no signals of anomaly appear in the ITRAX profiles of the same levels (Figure 4.9). On the other hand, all the levels that have peaked in the ITRAX profile and have shown anomalies in the MS and GS profiles. It is seen from the radiographic image (Appendix K) that there are many levels of anomalies, but no clear turbidite is observed that preserves its turbidite internal structure.

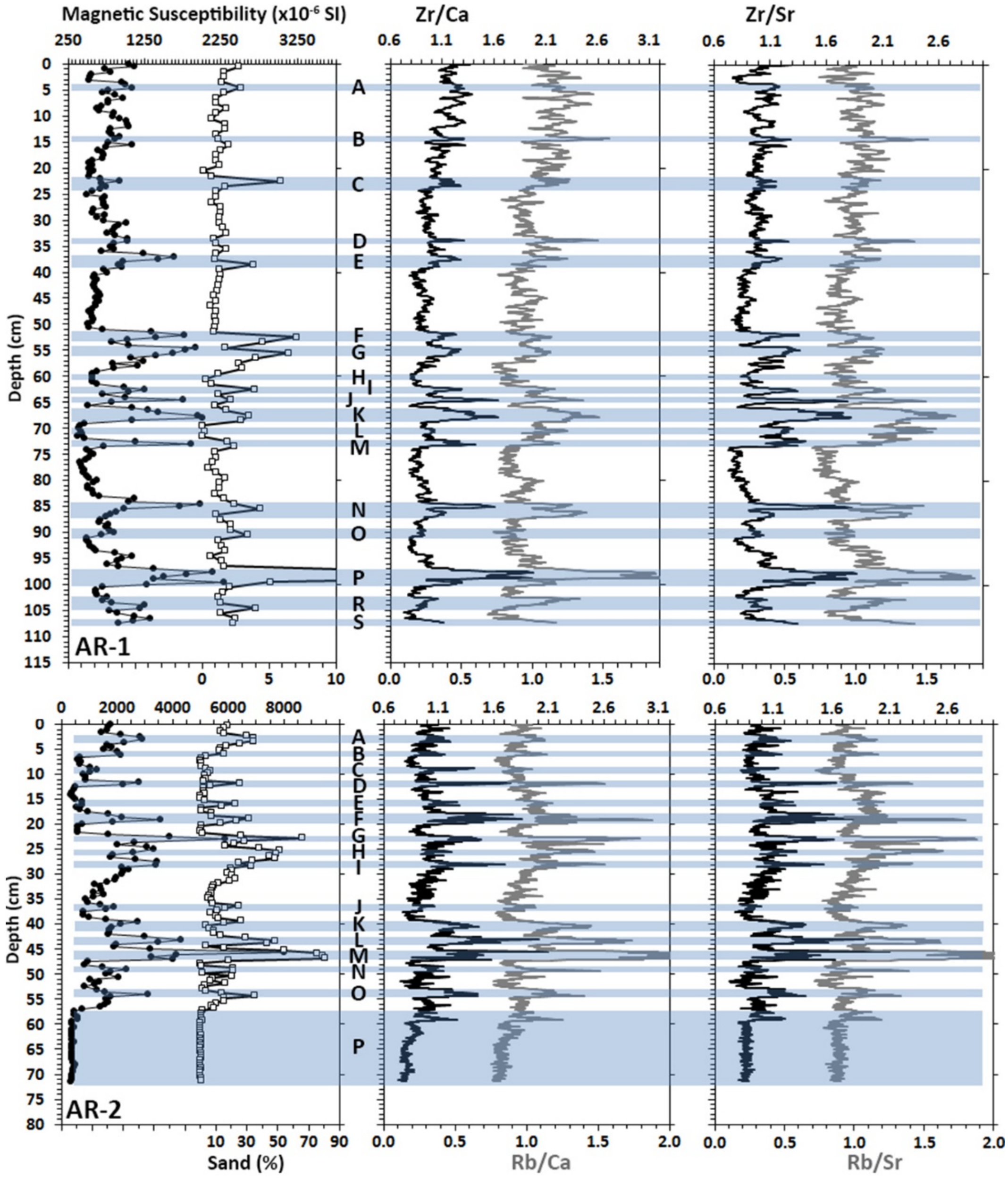

Figure 4.9. Magnetic Susceptibility (MS), Grain Size (GS), and ITRAX Micro XRF Scanning results (Zr/Ca, Rb/Ca, Zr/Sr, and Rb/Sr profiles) of AR-1 and AR-2 cores.

When looking at the AR-2 results, it is seen that the radiographic image (Appendix L) is almost full of turbidite which is supported by all the MS, GS, and ITRAX profiles (Figure 4.9). The frequency of sedimentary anomalies in the AR-2 core is so high that it is almost impossible to distinguish between these anomalies (Figure 4.9).

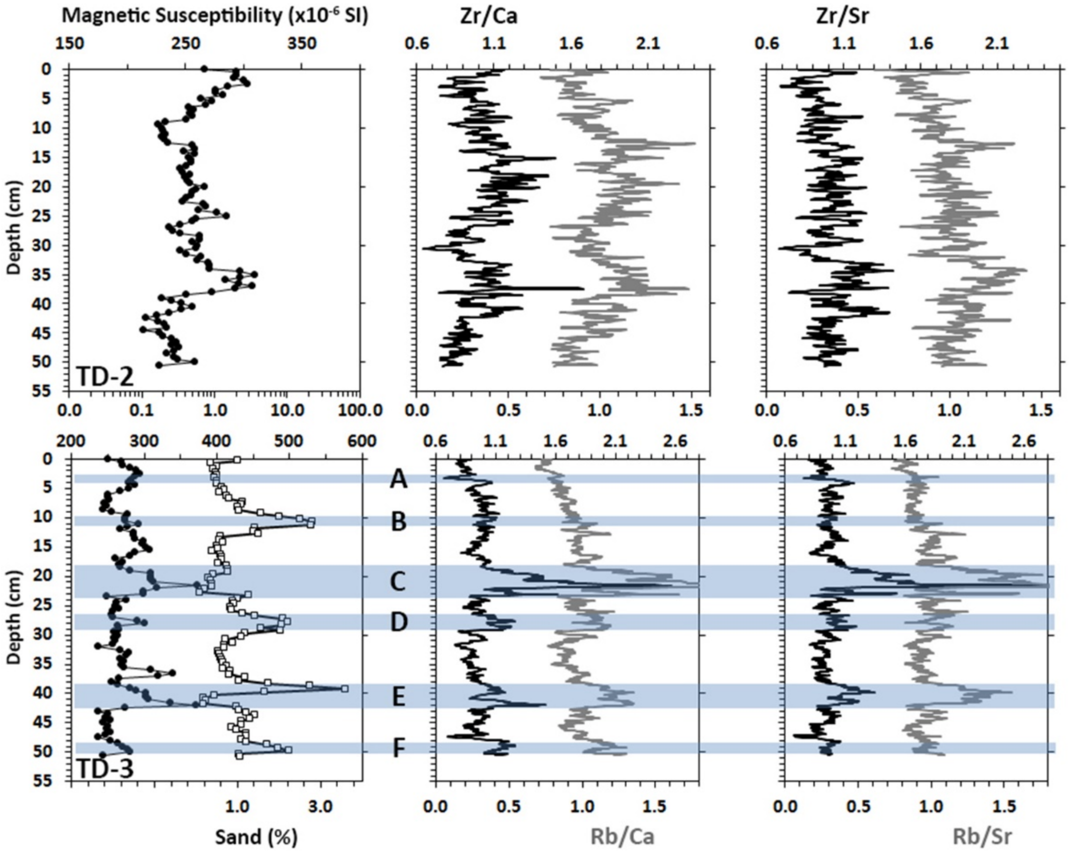

Figure 4.10. Magnetic Susceptibility (MS), Grain Size (GS), and ITRAX Micro XRF Scanning results (Zr/Ca, Rb/Ca, Zr/Sr, and Rb/Sr profiles) of TD-2 and TD-3 cores.

MS, GS, and ITRAX profiles of TD-2 and TD-3 cores collected from an area between Tiran and Dakar deeps are presented in Figure 4.10. As can be seen from Figure 4.10, no anomaly has been detected in the detailed examinations carried out by considering the radiographic image (Appendix M) and MS graph, and ITRAX profiles in the TD-2 core (Figure 4.10). Although both TD-2 and TD-3 appear to almost entirely background sedimentation on radiographs (Appendices M & N), a few sedimentary anomalies could be detected in TD-3 as a result of MS, GS, and ITRAX analyzes performed (Figure 4.10).

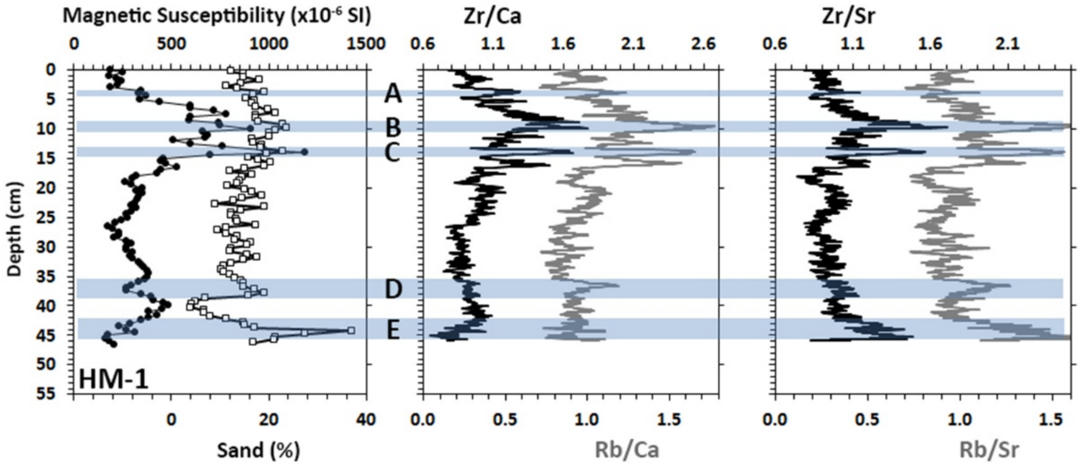

Figure 4.11. Magnetic Susceptibility (MS), Grain Size (GS), and ITRAX Micro XRF Scanning results (Zr/Ca, Rb/Ca, Zr/Sr, and Rb/Sr profiles) of HM-1 core taken from the Hume Deep.

MS, GS, and ITRAX profiles of HM-1 core taken from the Hume basin are presented in Figure 4.11. Similar to TD-2 and TD-3 cores, the radiographic image of the HM-1 core (Appendix O) has also a quite heterogeneous and complex appearance. Although it is not obvious from the radiograph, the five peaks observed in the MS, GS, and ITRAX profiles are sufficient to say that there are five anomalies in this core (Figure 4.11).

In the light of the results obtained, it can be clearly stated that AR-1, AR-2, TD-2, TD-3, and HM-1 cores are not suitable for interpretations in a marine paleoseismology investigation. Because the uncertainty and complexity of the data make it quite difficult to reach a meaningful conclusion.

The summary of the studies on chronology is presented in Figure 4.12. While determining the levels of the samples to be used in dating, great care has been taken to ensure that these levels do not correspond to any event-deposits, since they contain reworked sediments. Figure 4.12 presents the levels of bulk sediment samples collected for radiocarbon and radionuclide dating with respect to sedimentary events. Although efforts have been made to avoid sedimentary events, unfortunately, the bulk sediment sample taken from the bottom of the TD-3 core for radiocarbon dating coincided with an event-deposit (Figure 4.12).

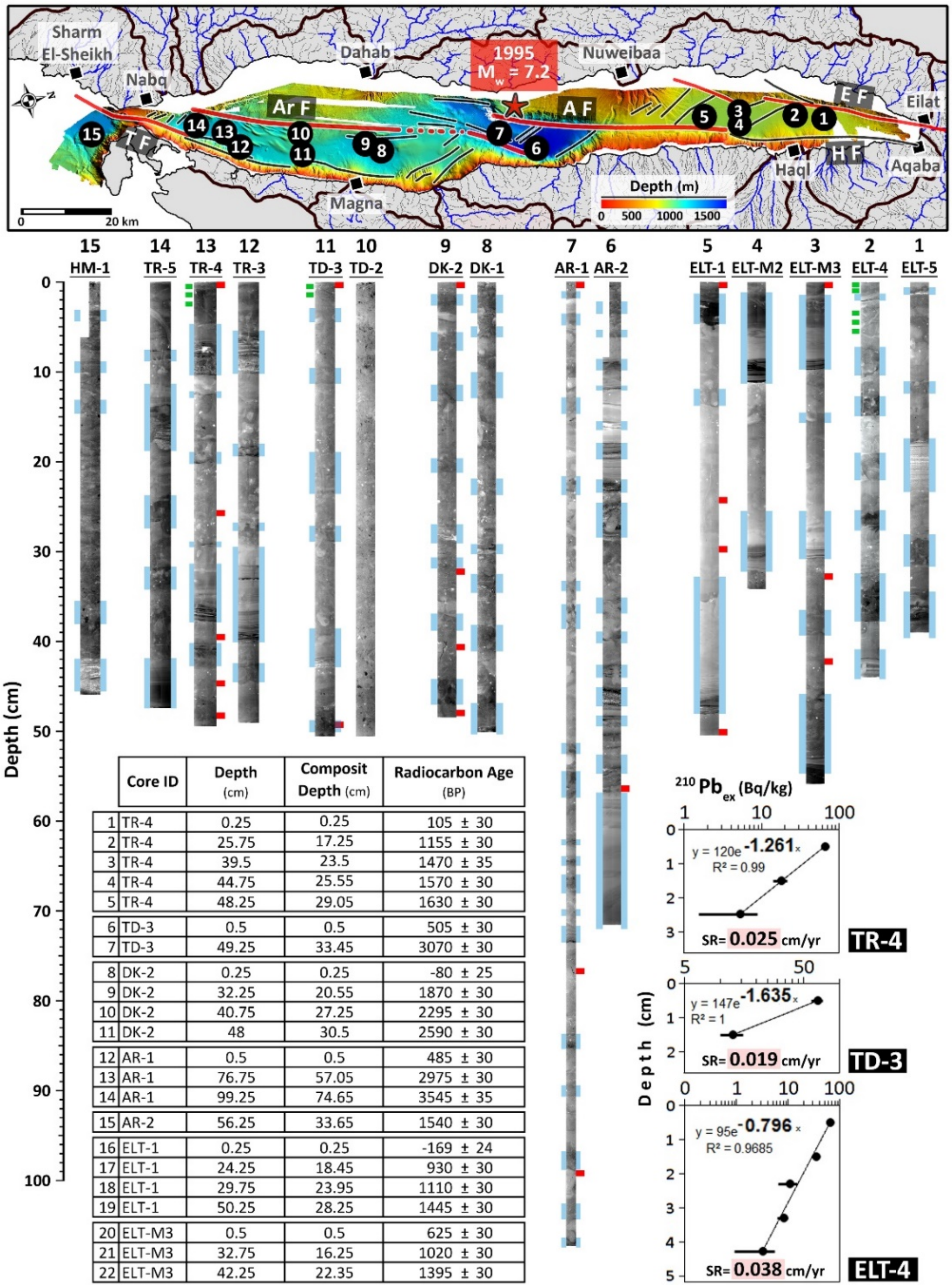

	Core ID	Depth (cm)	Composit Depth (cm)	Radiocarbon Age (BP)
1	TR-4	0.25	0.25	105 ± 30
2	TR-4	25.75	17.25	1155 ± 30
3	TR-4	39.5	23.5	1470 ± 35
4	TR-4	44.75	25.55	1570 ± 30
5	TR-4	48.25	29.05	1630 ± 30
6	TD-3	0.5	0.5	505 ± 30
7	TD-3	49.25	33.45	3070 ± 30
8	DK-2	0.25	0.25	-80 ± 25
9	DK-2	32.25	20.55	1870 ± 30
10	DK-2	40.75	27.25	2295 ± 30
11	DK-2	48	30.5	2590 ± 30
12	AR-1	0.5	0.5	485 ± 30
13	AR-1	76.75	57.05	2975 ± 30
14	AR-1	99.25	74.65	3545 ± 35
15	AR-2	56.25	33.65	1540 ± 30
16	ELT-1	0.25	0.25	-169 ± 24
17	ELT-1	24.25	18.45	930 ± 30
18	ELT-1	29.75	23.95	1110 ± 30
19	ELT-1	50.25	28.25	1445 ± 30
20	ELT-M3	0.5	0.5	625 ± 30
21	ELT-M3	32.75	16.25	1020 ± 30
22	ELT-M3	42.25	22.35	1395 ± 30

Figure 4.12. Chronology chart for the Gulf of Aqaba cores. Radiocarbon results are presented in the lower-left corner of the figure. Radionuclide result graphs are presented in the lower-right corner of the figure. All detected sedimentary anomalies (light-blue bars) and the levels of the samples collected for both radiocarbon (red bars) and radionuclide (green bars) measurements are shown on the radiographic images of the cores.

The results of the radiocarbon measurements of 22 samples are presented as a table in Figure 4.12. Composite depths of the samples have been obtained by excluding the thicknesses of sedimentary event-deposits (Figure 4.12). According to the radiocarbon results, it is seen that the cores cover the sedimentary record for at least the last 1000 years. In other words, the cores have recorded the events that have occurred within the last 1000 years in the Gulf of Aqaba. This means that in addition to the turbidites induced by the 1995 Nuweibaa earthquake, it should be possible to find sedimentary traces of AD 1068, 1212, and 1588 historical earthquakes.

According to the ^{210}Pb decay curve, sedimentation rates at the southern and northern tips of the Gulf of Aqaba resulted in 0.025 cm/yr and 0.038 cm/yr for the TR-4 and the ELT-4 core, respectively (Figure 4.12). Although the number of radionuclide samples collected from the TD-3 core is not sufficient to achieve a statistically meaningful sedimentation rate, it is worthwhile to report the results to compare them with radiocarbon dates in the Discussions chapter. According to the results of the ^{210}Pb decay curve obtained from the TD-3 core, the sedimentation rate is 0.019 cm/yr (Figure 4.12).

In addition to ^{210}Pb dating, ^{137}Cs dating was also done from the bulk sediment samples taken at 1 cm thickness. Normally, the ^{137}Cs decay curve is expected to have a noticeable peak in 1963, when nuclear weapons experiments were carried out, and 1986, when the great Chernobyl disaster occurred. Due to the smoothness of the ^{137}Cs curve, the expected peaks of 1963 and 1986 were observed in an almost indistinguishable state. This smoothness of the ^{137}Cs curve has two reasons; one is that the sampled sediment thickness is too large to obtain a precise dating result, and the second is that the sediments are almost completely mixed due to the intense bioturbation observed throughout the gulf. For all these reasons, the ^{137}Cs curve was not considered during the interpretations.

CHAPTER 5

DISCUSSION

5.1 Classification and Rescaling of Sedimentary Events

According to the common definition of a turbidite, it is known that these are sediments deposited by gravitational segregation from a dense sediment cloud formed due to sudden subaqueous mass movement events. A classical turbidite is characterized by a basal coarse-grained and cross-bedded level overlain by fine-grained almost homogeneous foraminifera-free sediments. This kind of property is expected to be reflected by measured proxies as well. However, along the cores taken from the Gulf of Aqaba, measured proxies do not always obey our sedimentological expectations regarding turbidites.

ELT-M3 core is one of these cores giving unexpected results. One well-developed turbidite, like a textbook example, is seen in the radiographic image at level A in the ELT-M3 core (Figure 5.1a, Appendix E). Unexpectedly, grain-size (percentage of sand) at the bottom of this turbidite is finer than the background sediments. The reason is most probably related to the location where the core was taken (Figure 5.1c). There is a scarp, which is obvious by its high-relief nature, in the left side of the ELT-M3 core location, and this scarp most probably acts as a barrier to stop sediment influx from the west to the core-site. Therefore, the blocked coarse grains could not form the expected coarse-grained base structure in the turbidite at level A. In addition, a closer look reveals that the grains of the turbidite at level A is even finer than the background sedimentation. Although this is not always the case, sometimes it may be possible to see turbidites that have finer grains than the background sedimentation. This is most probably due to the deposition of turbidity currents by gravitational segregation. Background sedimentation is a mixture of coarse and fine grains, various organisms, and chemicals precipitating from the water column. However, when a sudden event occurs, these mixed sediments are re-mixed with the effect of the current and then deposited according to their specific gravities by gravitational segregation. Therefore, the particles with the highest specific gravity deposited first, and the ones with the lowest specific gravity deposited lastly, and form a turbidite. Also, there is no rule that sediments with high specific gravity will always be coarse-grained. Indeed, the events indicated by A and C in the ELT-M3 core are good examples of an exceptional case where the availability of sediments even finer than the background sedimentation in turbidites may be possible. A similar situation may be observed in magnetic susceptibility measurements. Since magnetic susceptibility measurements are porosity dependent, it is possible to say that anything that affects the porosity of the sediment also affects its magnetic susceptibility. Normally, as the grain size increases, the porosity of the sediment increases. However, sediments that have special characteristics, like clay, sometimes do not follow this rule. Although the grain size of clay is very small, its porosity is higher contrary to what is expected (Croudace and Rothwell, 2015). Therefore, while the GS profile tends to decrease in sedimentary environments containing clay, MS measurements, which are affected by the high porosity, also decrease. The events indicated by A and C in the ELT-M3 core are two events that exemplify this situation. As can be seen in Figure 5.1a, decreasing grain size at both levels accompanies decreasing magnetic susceptibility values.

In addition to all these exceptions, sometimes unexpected results may also be encountered in the ITRAX profiles. Since ITRAX measurements are performed directly from the bulk sediment surface, these measurements may be affected by several factors such as water content, grain size, and porosity. For example, the turbidite at level A in the ELT-M3 core does not show any kind of anomaly in the Zr/Ca and Rb/Sr profiles (Figure 5.1a), while it is very obvious on the radiograph (Appendix E). This is probably due to the increased porosity as described above. Since ITRAX is a semi-quantitative method, it should not be used as a single proxy to detect turbidites.

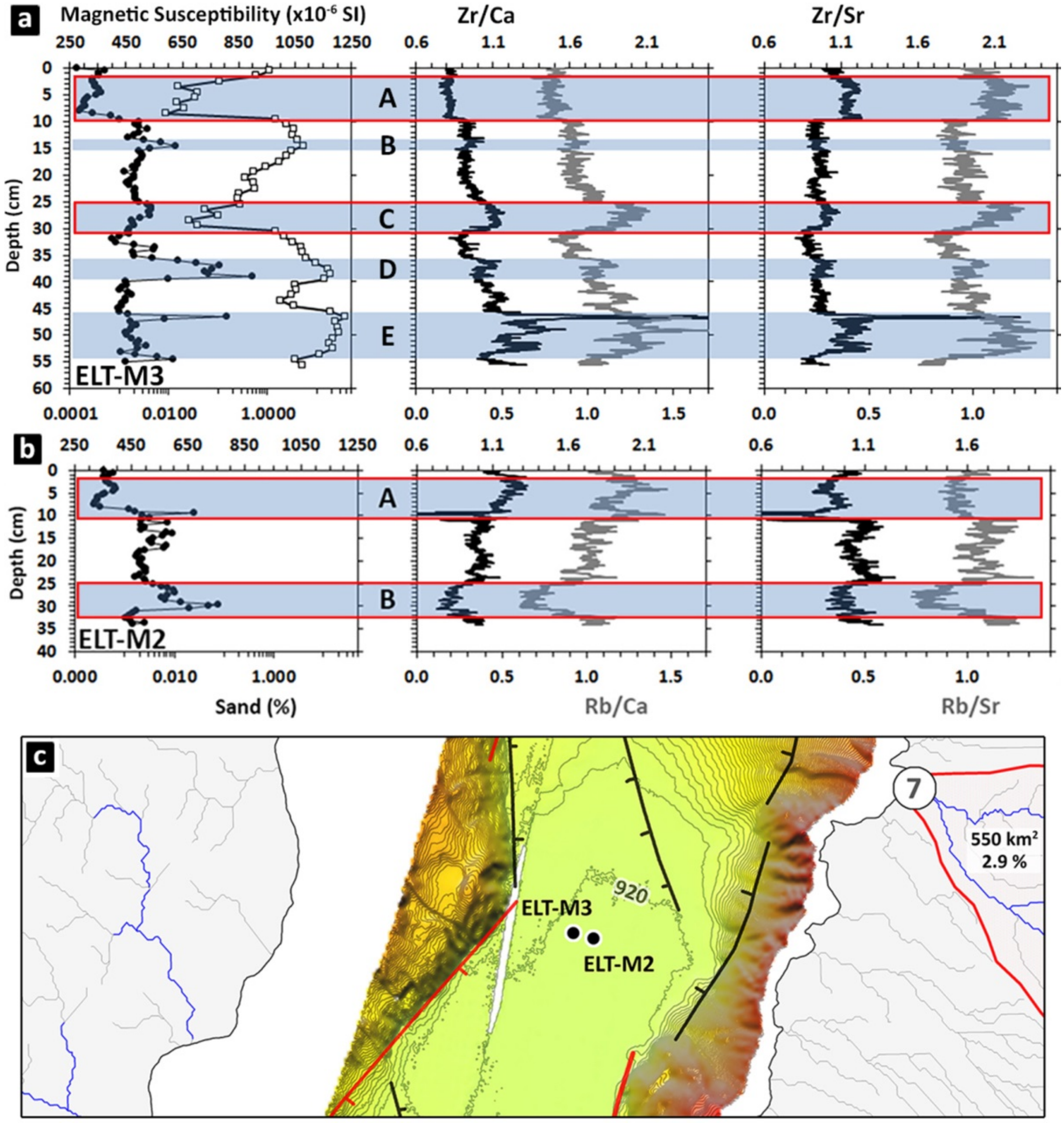

Figure 5.1. MS, GS, and ITRAX profiles of ELT- M3 (a) and ELT-M2 (b) cores. The close bathymetry of the Eilat Deep and the locations of the cores collected from the Eilat Deep (c). Red rectangles represent the levels having unexpected results.

Another example that the only ITRAX measurements are not sufficient in determining turbidites is obvious at levels A and B in the ELT-M2 core (Figure 5.1b). At Level A, a very prominent and thick turbidite is observed in the radiographic image (Appendix F). However, the Zr/Sr and Rb/Sr profiles have tendencies not in the positive direction as expected, but in the opposite direction. Likewise, at level B, there is a trend contrary to what is expected in all of the Zr/Ca, Rb/Ca, Zr/Sr, and Rb/Sr profiles (Figure 5.1b). However, in the radiographic image, there is a very obvious turbidite with its foraminifera-free and well-laminated nature (Appendix F), and it is expected to be seen a positive peak in ITRAX profiles at this level.

A similar situation is observed at level A in the ELT-4 core. At this level, which is certain to be turbidite with its laminated internal structure on the radiograph (Appendix G), the increase in porosity accompanying the decreasing grain size causes negative peaks in the MS profile (Figure 5.2a). Also, ITRAX measurements have been affected by the increasing porosity, which results in a negative peak at the level of turbidite (Figure 5.2a). As can be seen from this example, ITRAX and MS are grain size-dependent measurements and it is not correct to use them as a stand-alone proxy.

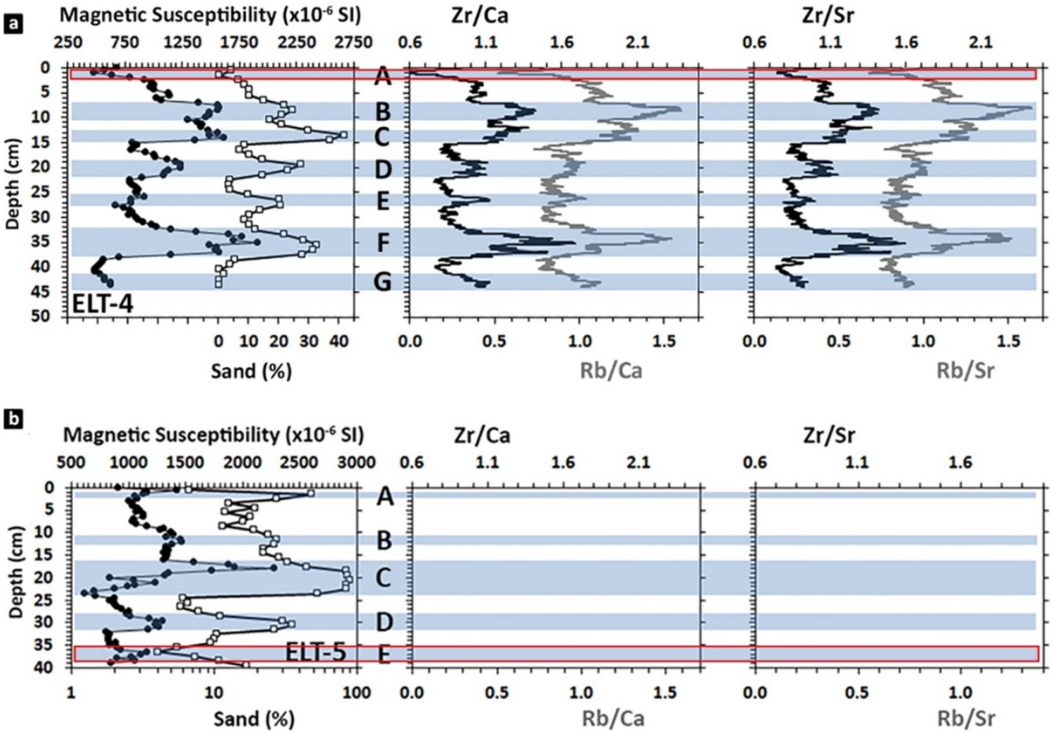

Figure 5.2. MS, GS, and ITRAX profiles of ELT- 4 (a) and ELT-5 (b) cores. Red rectangles represent the levels having unexpected results.

Another unexpected result observed in cores is seen level E at the bottom of the ELT-5 core (Figure 5.2b). Because the top part of this turbidite which is evident in the radiographic image by its internal structure (Appendix H) consists of homogeneous and fine-grained sediments, at the upper boundary of it, the grain size profile also tends to peak negatively. The grain size is fine up to about 37 cm depth and magnetic susceptibility has not yet been affected by porosity. After 37 cm depth, magnetic susceptibility measurements have started to be affected by increasing grain size and porosity and to decrease (Figure 5.2b). A careful look at the radiograph shows that it retains its foraminifera-free and cross-laminated internal structure even at the core margin (Appendix H). In other words, the length of the core is not enough to show the coarse-grained part at the base of the turbidite. Besides, both the increase in grain size and the ongoing decrease in magnetic susceptibility are proof that the lower boundary of the turbidite is not observed within the core limits.

The existence of such exceptional situations emphasizes the importance of two things. First, using multi-proxy is the only way to reach the most precise and accurate results, since each proxy is controlled with other proxies. Second, these exceptional results clearly reveal the quite complex nature of the Gulf of Aqaba sediments. Based on paleoseismology study in the Gulf of Aqaba sediments, which have such a complex nature, the main tool to be used in the detection of earthquakes should be determined carefully. For this purpose, the sedimentary features expected to be in a classical paleoseismology study and those observed in the Gulf of Aqaba have been considered separately.

All kinds of deformations caused by ground shaking in sedimentary depositional environments are generally called seismites (Marco et al., 1996). Three main seismites are widely used in marine paleoseismology studies. The first of these is soft-sediment deformations (SSD), and as the name suggests, it is a type of deformation seen in soft-sediments after earthquakes and can be observed in many different forms. The sediments of the Gulf of Aqaba already have heterogeneous and disturbed background sedimentation due to intense bioturbation. In addition, the Gulf is located in such a seismically active region that the cores most probably contain earthquake-induced SSD. In other words, the sediments may have been deformed due to both bioturbation and earthquakes. As another possibility, sediments that have been deformed due to earthquakes may have also been subjected to a secondary deformation by organisms or, conversely, bioturbation-induced deformations may have become more deformed after an earthquake. Considering all these possibilities, it is quite difficult to distinguish earthquake-induced SSD from bioturbation-induced ones. Therefore, SSD is not preferred to be used as a proxy in this study.

Secondly, another seismites which is likely to be encountered in a seismic region is catchment response (CR). Increased sediment yield in basins caused by earthquake-triggered landslides and/or seismically shattered landscapes is known as catchment response (CR) in the literature (Avşar et al., 2014a). It may also be expected to observe CR in the Gulf of Aqaba, however, geochemical implications of it in sediments have not been observed. If there was CR in the Gulf of Aqaba, an obvious ITRAX anomaly would be seen accompanying each of the distinct turbidites. Because of the absence of any geochemical implication for CR, it can be ruled out in the use for turbidite detection.

Thirdly, seismite known as Mass Wasting Deposit (MWD) may be observed after earthquakes (Avşar et al., 2015), which is already abundant in the Gulf of Aqaba cores. The study area is suitable for mass wasting events to be observed due to its big catchment and submarine topography. In short, paleoseismic investigation in the Gulf of Aqaba seems to be done only by using turbidites. In other words, this study is an example of a turbidite paleoseismology investigation.

A semi-quantitative classification and rescaling have been performed for a better understanding of the ground shaking level for different turbidites. Two properties of sedimentary events have been used for classification and rescaling. The first one is the thickness of the turbidites. Thickness variations along a single core can be considered directly proportional to the intensity of ground shaking, which means that earthquakes having high magnitudes result in thicker turbidites. However, it may not be a correct approach to associate the thickness variations in different cores taken from different basins with the intensity of the earthquake. That is, the same level of ground shaking may result in different turbidite thicknesses in different basins. Because the amount of sediment influx to basins and the morphological structure of these basins are different, thicknesses of turbidites in different cores can not be comparable.

It is evident that turbidites in the Eilat Deep are much thicker compared to the ones in the Dakar Deep. In addition, these two basins likely have almost a similar level of seismic hazard, as can be understood from many aspects, such as their location, proximity to active fault branches, or submarine morphologies. Even though their thicknesses differ so much, the DK-2 E and ELT-M2 A turbidites are probably the results of earthquakes having similar intensities. The difference is probably because the sedimentation rate on the slopes of the Eilat Deep is much higher than the slopes of the Dakar Deep. Therefore, the abundance of sediment deposited on the slopes of the Eilat Deep after each successive earthquake is sufficient to form thick turbidites. In order to handle such a thickness problem, "Thickness Weight" for each sedimentary event has been calculated by taking the ratio between the individual thickness of every single event and the average thickness of the events recorded in that core. Only radiographic images have not been used when calculating the thickness of each event in the cores. Although the amplitudes of the peaks in the MS, GS, and ITRAX profiles do not provide clear information on the intensity of the ground shaking, they are very useful in determining the bottoms and tops of the turbidites. As in every stage of the study, for the calculation of turbidite thicknesses, radiographic images, MS, GS, and ITRAX profiles have been evaluated together.

The second property of sedimentary events used for classification and rescaling is the appearances of these events in the radiographic images. In total, 98 sedimentary anomalies have been detected from 15 cores. These sedimentary anomalies have been classified because of the large number of sedimentary events detected and the complexity of the data. Hereby, a better understanding of the cores has been provided by reducing the number of variables, and the complexity of the data has been somewhat simplified. According to this classification, three types of sedimentary events have been determined as “Type A”, “Type B”, and “Type C” (Figure 5.3).

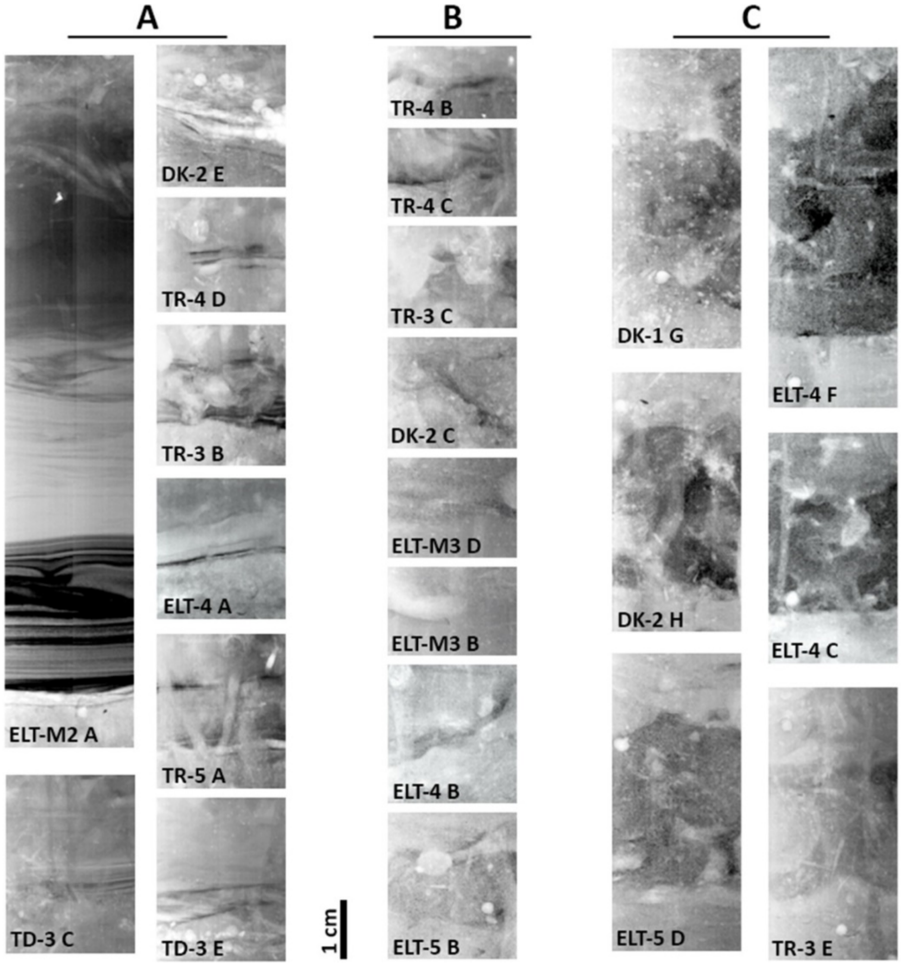

Figure 5.3. Classification of sedimentary events observed in the Gulf of Aqaba cores. According to this classification, Type A, Type B, and Type C are the three main event groups.

The sedimentary events in the group classified as "Type A" are prominent sedimentary anomalies that can be determined as turbidite at first glance on radiographic images (Figure 5.3). Their thickness may be less than 1 cm or may reach up to 10 cm, which implies thickness is not the criterion to be used in the appearance classification. The sedimentary events in this "Type A" group, where laminations are clear on radiographs, noticeable with their non-bioturbated and foraminifera-free nature (Figure 5.3). Although the above-mentioned features can be observed more clearly in sedimentary events thicker than 3-4 cm, the relatively thinner ones of this group also have the same features.

Considering the general characteristics of sedimentary events in the second group, the “Type B” group, it is seen that they are generally thinner than 2 cm and are intensely deformed (Figure 5.3). Besides, although weak implications of the laminated internal structure are seen in sedimentary events in the “Type B” group, it may not be correct to assign these implications as clear laminations due to their intensely bioturbated and deformed nature.

Finally, sedimentary events in the “Type C” group are generally more than 2 cm thick and do not have any laminated internal structure. Despite being thick, sedimentary events in this group attract attention with the foraminifera they contain, as well as being exposed to intense bioturbation (Figure 5.3). Such types of thick and foraminifera containing turbidites probably represent the frequent deposits of several decadal heavy rainy periods that result in intense sediment influx. If these were turbidites formed as a result of a single event, they would not contain foraminifera and would not be affected by bioturbation except only a few centimeters from the top.

At the end of the classification, “Appearance Weight” has been given to every sedimentary event depending on its type and properties. Accordingly, the sedimentary events in the “Type A” group have been assigned 4, the ones in the “Type B” group, 2, and the ones in the “Type C” group, 1 as "Appearance Weight". The final score has been obtained by taking the averages of thickness and appearance weights for each sedimentary event. All the data of this classification and rescaling study are presented in Table 5.1 and Table 5.2.

Table 5.1. Depths, thicknesses, weights, and final scores of the HM-1, TR-5, TR-4, TR-3, TD-3, DK-2, DK-1, and ELT-1 cores.

HM-1							
	Composit Depth	Top	Bottom	Thickness (Av = 2.15)	Thickness Weight	Appearence Weight	Score
A	3.20	3.20	4.50	1.30	0.605	2	1.3
B	7.20	8.50	10.50	2.00	0.930	2	1.5
C	9.90	13.20	14.60	1.40	0.651	1	0.8
D	30.80	35.50	38.00	2.50	1.163	1	1.1
E	34.80	42.00	45.55	3.55	1.651	4	2.8

TR-5							
	Composit Depth	Top	Bottom	Thickness (Av = 4.47)	Thickness Weight	Appearence Weight	Score
A	7.20	7.20	8.80	1.60	0.358	4	2.2
B	9.70	11.30	19.50	8.20	1.834	4	2.9
C	14.20	24.00	27.40	3.40	0.761	2	1.4
D	17.30	30.50	34.30	3.80	0.850	1	0.9
E	25.00	42.00	47.35	5.35	1.197	4	2.6

TR-4							
	Composit Depth	Top	Bottom	Thickness (Av = 3.2)	Thickness Weight	Appearence Weight	Score
A	4.80	4.80	10.60	5.80	1.813	4	2.9
B	6.20	12.00	12.80	0.80	0.250	2	1.1
C	11.70	18.30	20.20	1.90	0.594	2	1.3
D	20.50	29.00	30.00	1.00	0.313	4	2.2
E	22.00	31.50	38.00	6.50	2.031	4	3.0
F	24.00	40.00	43.20	3.20	1.000	4	2.5

TR-3							
	Composit Depth	Top	Bottom	Thickness (Av = 4.18)	Thickness Weight	Appearence Weight	Score
A	5.50	5.50	10.50	5.00	1.196	4	2.6
B	13.00	18.00	19.80	1.80	0.431	2	1.2
C	20.70	27.50	28.50	1.00	0.239	1	0.6
D	21.80	29.60	40.20	10.60	2.536	4	3.3
E	24.10	42.50	45.00	2.50	0.598	1	0.8

TD-3							
	Composit Depth	Top	Bottom	Thickness (Av = 2.97)	Thickness Weight	Appearence Weight	Score
A	2.80	2.80	4.50	1.70	0.573	1	0.8
B	7.80	9.50	11.50	2.00	0.674	1	0.8
C	14.50	18.20	23.50	5.30	1.787	4	2.9
D	18.00	27.00	29.00	2.00	0.674	4	2.3
E	27.20	38.20	43.00	4.80	1.618	4	2.8
F	32.20	48.00	50.00	2.00	0.674	1	0.8

DK-2							
	Composit Depth	Top	Bottom	Thickness (Av = 2.19)	Thickness Weight	Appearence Weight	Score
A	1.30	1.30	2.90	1.60	0.731	4	2.4
B	3.30	4.90	7.80	2.90	1.326	1	1.2
C	6.80	11.30	13.50	2.20	1.006	4	2.5
D	13.10	19.80	21.30	1.50	0.686	1	0.8
E	18.80	27.00	29.00	2.00	0.914	4	2.5
F	20.30	30.50	32.00	1.50	0.686	2	1.3
G	25.30	37.00	38.80	1.80	0.823	1	0.9
H	30.00	43.50	47.50	4.00	1.829	1	1.4

DK-1							
	Composit Depth	Top	Bottom	Thickness (Av = 2.14)	Thickness Weight	Appearence Weight	Score
A	1.20	1.20	3.50	2.30	1.076	2	1.5
B	2.00	4.30	5.80	1.50	0.702	2	1.4
C	6.00	9.80	13.00	3.20	1.497	2	1.7
D	15.00	22.00	23.50	1.50	0.702	2	1.4
E	21.00	29.50	30.50	1.00	0.468	4	2.2
F	23.00	32.50	34.20	1.70	0.795	4	2.4
G	27.30	38.50	41.00	2.50	1.170	1	1.1
H	33.00	46.70	50.10	3.40	1.591	2	1.8

ELT-1							
	Composit	Top	Bottom	Thickness	Thickness	Appearence	Score
A	1.10	1.10	4.90	3.80	0.518	4	2.3
B	8.20	12.00	14.00	2.00	0.273	1	0.6
C	26.20	32.00	48.20	16.20	2.209	4	3.1

Table 5.2. Depths, thicknesses, weights, and final scores of the ELT-M2, ELT-M3, ELT-4, ELT-5, AR-1, and AR-2 cores.

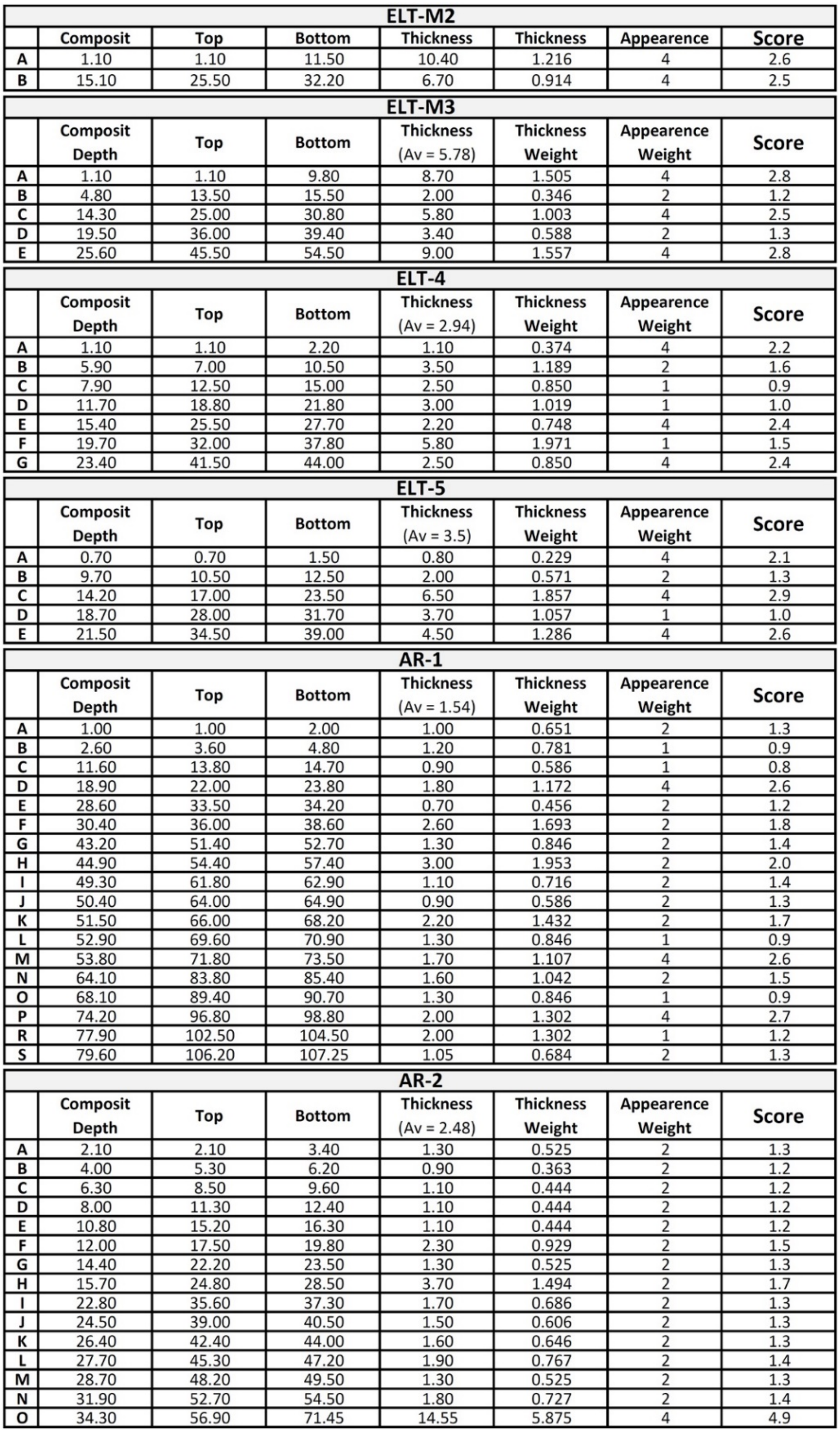

ELT-M2							
	Composit	Top	Bottom	Thickness	Thickness	Appearence	Score
A	1.10	1.10	11.50	10.40	1.216	4	2.6
B	15.10	25.50	32.20	6.70	0.914	4	2.5

ELT-M3							
	Composit Depth	Top	Bottom	Thickness (Av = 5.78)	Thickness Weight	Appearence Weight	Score
A	1.10	1.10	9.80	8.70	1.505	4	2.8
B	4.80	13.50	15.50	2.00	0.346	2	1.2
C	14.30	25.00	30.80	5.80	1.003	4	2.5
D	19.50	36.00	39.40	3.40	0.588	2	1.3
E	25.60	45.50	54.50	9.00	1.557	4	2.8

ELT-4							
	Composit Depth	Top	Bottom	Thickness (Av = 2.94)	Thickness Weight	Appearence Weight	Score
A	1.10	1.10	2.20	1.10	0.374	4	2.2
B	5.90	7.00	10.50	3.50	1.189	2	1.6
C	7.90	12.50	15.00	2.50	0.850	1	0.9
D	11.70	18.80	21.80	3.00	1.019	1	1.0
E	15.40	25.50	27.70	2.20	0.748	4	2.4
F	19.70	32.00	37.80	5.80	1.971	1	1.5
G	23.40	41.50	44.00	2.50	0.850	4	2.4

ELT-5							
	Composit Depth	Top	Bottom	Thickness (Av = 3.5)	Thickness Weight	Appearence Weight	Score
A	0.70	0.70	1.50	0.80	0.229	4	2.1
B	9.70	10.50	12.50	2.00	0.571	2	1.3
C	14.20	17.00	23.50	6.50	1.857	4	2.9
D	18.70	28.00	31.70	3.70	1.057	1	1.0
E	21.50	34.50	39.00	4.50	1.286	4	2.6

AR-1							
	Composit Depth	Top	Bottom	Thickness (Av = 1.54)	Thickness Weight	Appearence Weight	Score
A	1.00	1.00	2.00	1.00	0.651	2	1.3
B	2.60	3.60	4.80	1.20	0.781	1	0.9
C	11.60	13.80	14.70	0.90	0.586	1	0.8
D	18.90	22.00	23.80	1.80	1.172	4	2.6
E	28.60	33.50	34.20	0.70	0.456	2	1.2
F	30.40	36.00	38.60	2.60	1.693	2	1.8
G	43.20	51.40	52.70	1.30	0.846	2	1.4
H	44.90	54.40	57.40	3.00	1.953	2	2.0
I	49.30	61.80	62.90	1.10	0.716	2	1.4
J	50.40	64.00	64.90	0.90	0.586	2	1.3
K	51.50	66.00	68.20	2.20	1.432	2	1.7
L	52.90	69.60	70.90	1.30	0.846	1	0.9
M	53.80	71.80	73.50	1.70	1.107	4	2.6
N	64.10	83.80	85.40	1.60	1.042	2	1.5
O	68.10	89.40	90.70	1.30	0.846	1	0.9
P	74.20	96.80	98.80	2.00	1.302	4	2.7
R	77.90	102.50	104.50	2.00	1.302	1	1.2
S	79.60	106.20	107.25	1.05	0.684	2	1.3

AR-2							
	Composit Depth	Top	Bottom	Thickness (Av = 2.48)	Thickness Weight	Appearence Weight	Score
A	2.10	2.10	3.40	1.30	0.525	2	1.3
B	4.00	5.30	6.20	0.90	0.363	2	1.2
C	6.30	8.50	9.60	1.10	0.444	2	1.2
D	8.00	11.30	12.40	1.10	0.444	2	1.2
E	10.80	15.20	16.30	1.10	0.444	2	1.2
F	12.00	17.50	19.80	2.30	0.929	2	1.5
G	14.40	22.20	23.50	1.30	0.525	2	1.3
H	15.70	24.80	28.50	3.70	1.494	2	1.7
I	22.80	35.60	37.30	1.70	0.686	2	1.3
J	24.50	39.00	40.50	1.50	0.606	2	1.3
K	26.40	42.40	44.00	1.60	0.646	2	1.3
L	27.70	45.30	47.20	1.90	0.767	2	1.4
M	28.70	48.20	49.50	1.30	0.525	2	1.3
N	31.90	52.70	54.50	1.80	0.727	2	1.4
O	34.30	56.90	71.45	14.55	5.875	4	4.9

The final scores are plotted along the Gulf of Aqaba cores in Figure 5.4. Sedimentary events observed in the cores have been rescaled to be comparable for the inter-core and inter-basinal correlations. Accordingly, bigger scores are represented by bigger circles. In other words, the size of a circle is a measure of prominence for the turbidite recorded at the level on which that circle is put. As the circle size gets smaller, this indicates that the effect of the earthquakes corresponding to that circle depth also decreases. Among the cores, the most distinctly recorded turbidite is seen at the bottom of AR-2 (Figure 5.4, Appendix L). Although rescaling makes turbidites in different cores and basins more comparable, a detailed stratigraphical correlation and sediment chronology are still needed to achieve the goal of a proper marine paleoseismology study.

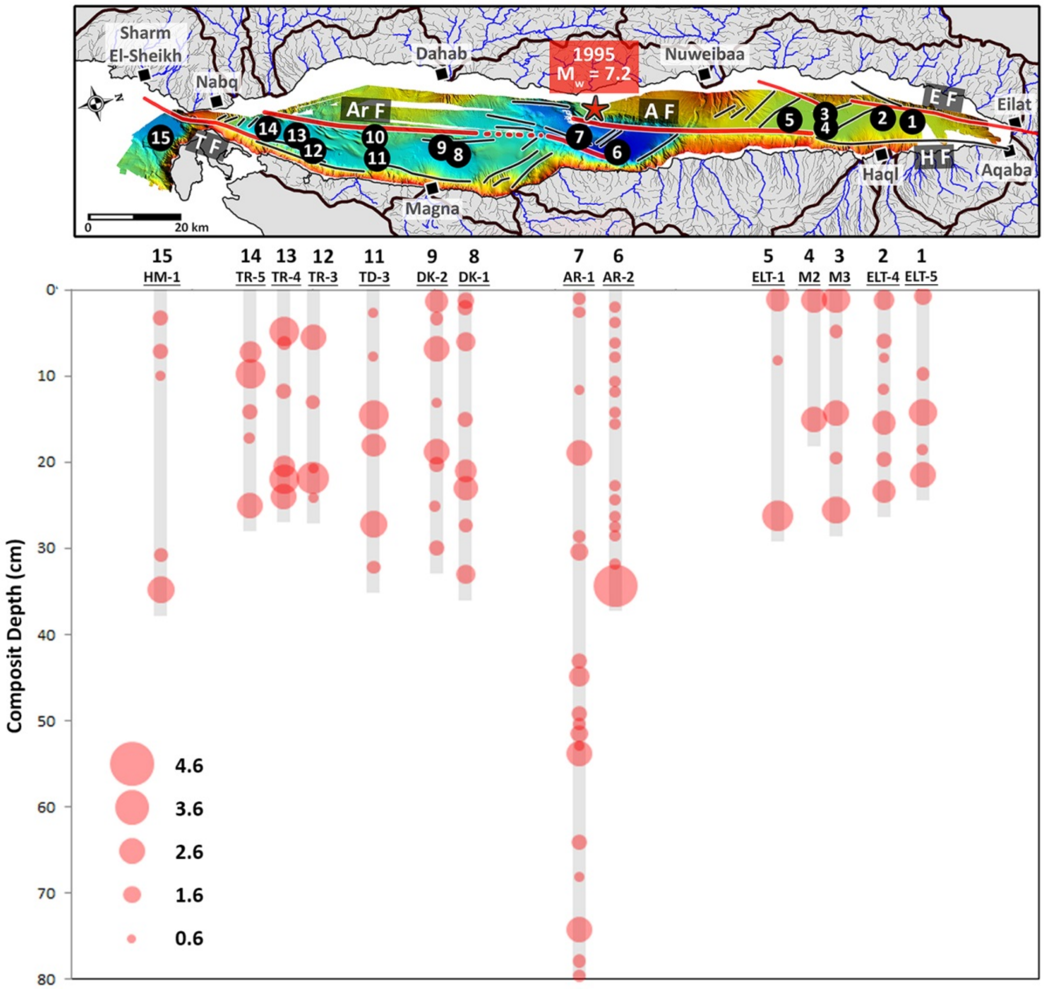

Figure 5.4. Final scores of the sedimentary events in the Gulf of Aqaba. The size of the circles represents their scales determined after the rescaling process.

5.2 Stratigraphic Correlation and Sediment Chronology

Before establishing a proper chronology, the sediment cores taken from the Gulf of Aqaba were stratigraphically correlated. In order to establish a well-grounded correlation, the levels previously determined as event-deposits were excluded from the sedimentary sequences and composit depths were obtained. Then, using MATLAB software, composit depths of all cores were adjusted to the depth of the AR-1 core, which covers the longest sedimentary record. Although MS, GS, ITRAX profiles, and radiographic images were used to determine the turbidite boundaries, the Sr/Ca element ratio was used to stratigraphically correlate the cores. Sr is a marker element representing the biogenic origin, where Ca is an element representing calcium which is found in both detrital and biogenic materials (Croudace and Rothwell, 2015). That is, the Sr/Ca ratio provides information about the relative variation of terrestrial and marine carbonate sources throughout the gulf.

The correlations of DK-2, TD-3, TR-4, and HM-1 cores with AR-1 are presented in Figure 5.5. Stratigraphic levels that were correlated between the cores are shown as gray lines. The depths of these levels are also plotted and presented as small graphes at the right sides of each correlation. These plots show that almost a uniform depth-scale adjustment is generally enough to achieve a reasonable correlation. Since ITRAX scanning provides semi-quantitative results, rather than absolute values along the Sr/Ca profiles, increasing/decreasing trends and fluctuations should be considered during correlations. In order to ease the presentation of the achieved correlation, the AR-1 core was tilted to the right without touching its numerical values (arrow represents the tilting direction and amount in Figure 5.5). The sedimentary events are also presented as black circles on these graphs. It is worth emphasizing that a few cm sediments had been lost at the top of the TD-3 core, probably during the sediment coring process (Figure 5.5).

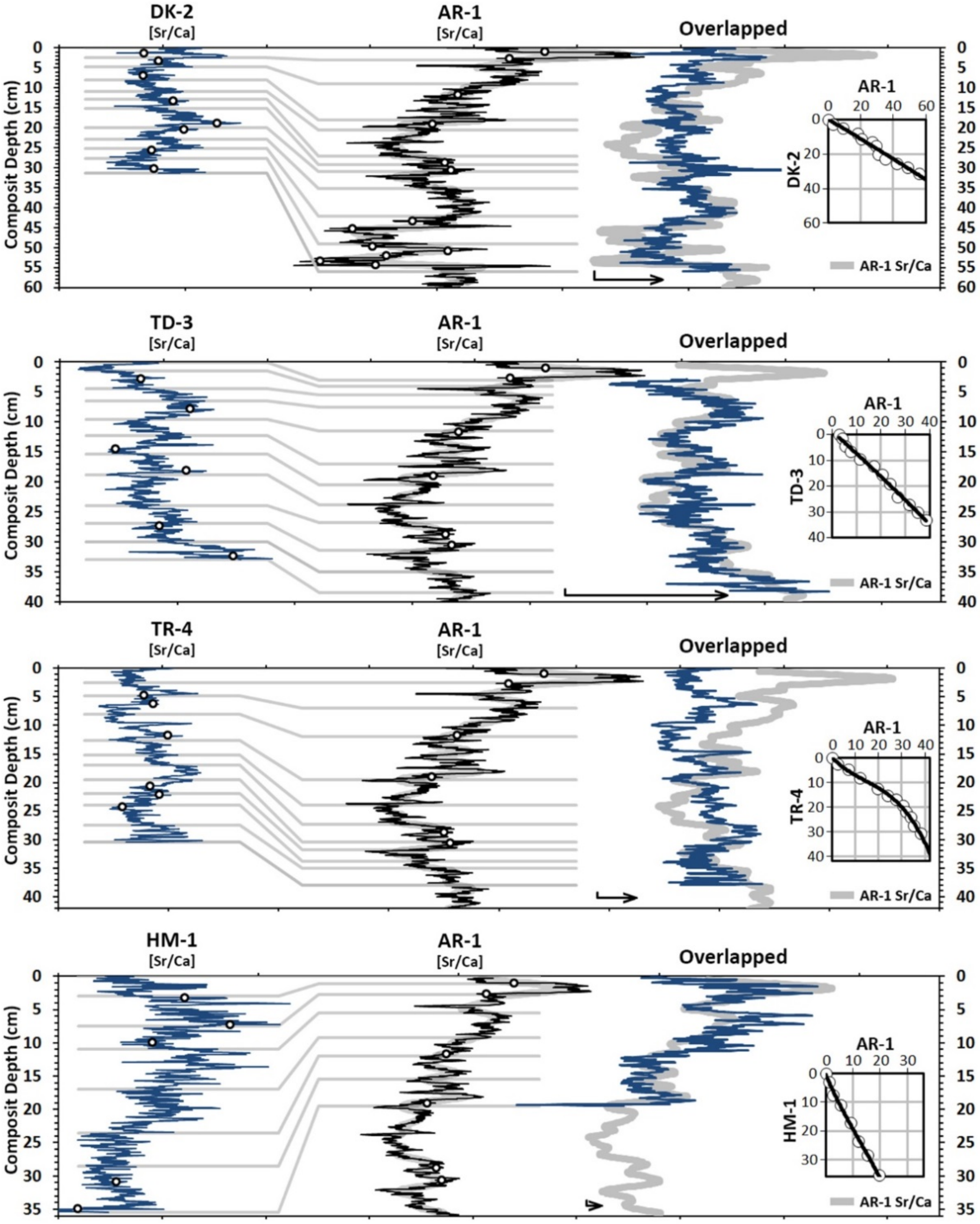

Figure 5.5. The correlation between the cores taken from the south of the AR-1 core-site. (Southern cores are DK-2, TD-3, TR-4, and HM-1). Small insets in the right of the graphs are transfer functions representing depth adjustments.

It is noticed that the correlation between HM-1 and AR-1 is remarkably good at first glance in Figure 5.5. On the other hand, although the Sr/Ca profile of the TR-4 core seems to be very incompatible with the same profile of the AR-1 core, the correlation is observable when the relative increase/decrease trends and fluctuations are taken into account.

The correlation of the AR-2, ELT-1, ELT-M3, and ELT-4 cores that have been collected from the northern part of the AR-1 core location is presented in Figure 5.6. Tie points, plots representing sedimentary events, right tilting of the AR-1 core, and the small transfer functions to the right of the graphs have been prepared with the same logic as the southern cores. While the AR-2, ELT-M3, and ELT-4 composite depths correspond almost exactly to the AR-1 depths, the ELT-1 core has a slight shift, which is most probably related to the sedimentation rate differences of the basins (Figure 5.6). The relative increasing and decreasing trends, and fluctuations in the Sr/Ca profiles of the cores correlate well with the AR-1 core (Figure 5.6). The precision level of the correlations is more evident in the overlapped section. The parallelism between tie points and the fact that the transfer functions are almost straight lines implies that the adjustment of the depths is performed within certain and reasonable limits.

The correlation of all remaining cores with AR-1 is presented in Figure 5.7. As in previous correlations, the depths of all cores have been adjusted to the AR-1, which is the stratigraphically longest core taken from the Gulf of Aqaba. Since the correlation has been made by excluding the sedimentary events from the sequences, it is possible to see that the sedimentation rate remains in a reasonable course in almost all cores. It can be understood from the parallelism between horizontal lines representing tie points (Figure 5.7). The precision level of the correlation is different for each core. For example, the correlation of the DK-1 and ELT-M2 cores with AR-1 is remarkable with the consistency they show in the overlapped section of the graph (Figure 5.7). In addition, the tilting of the AR-1 core enabled the correlation to be seen more precisely. Although the TR-5 and TR-4 cores do not seem to correlate at their tops, when the relative increases, decreases, and fluctuations in the Sr/Ca profiles are examined, it is seen that the correlation is achieved. Since there was no ITRAX scanning in the ELT-5 core, only the event-deposits detected on it were correlated with the ELT-4 core, and the consistency between them was plotted (Figure 5.7).

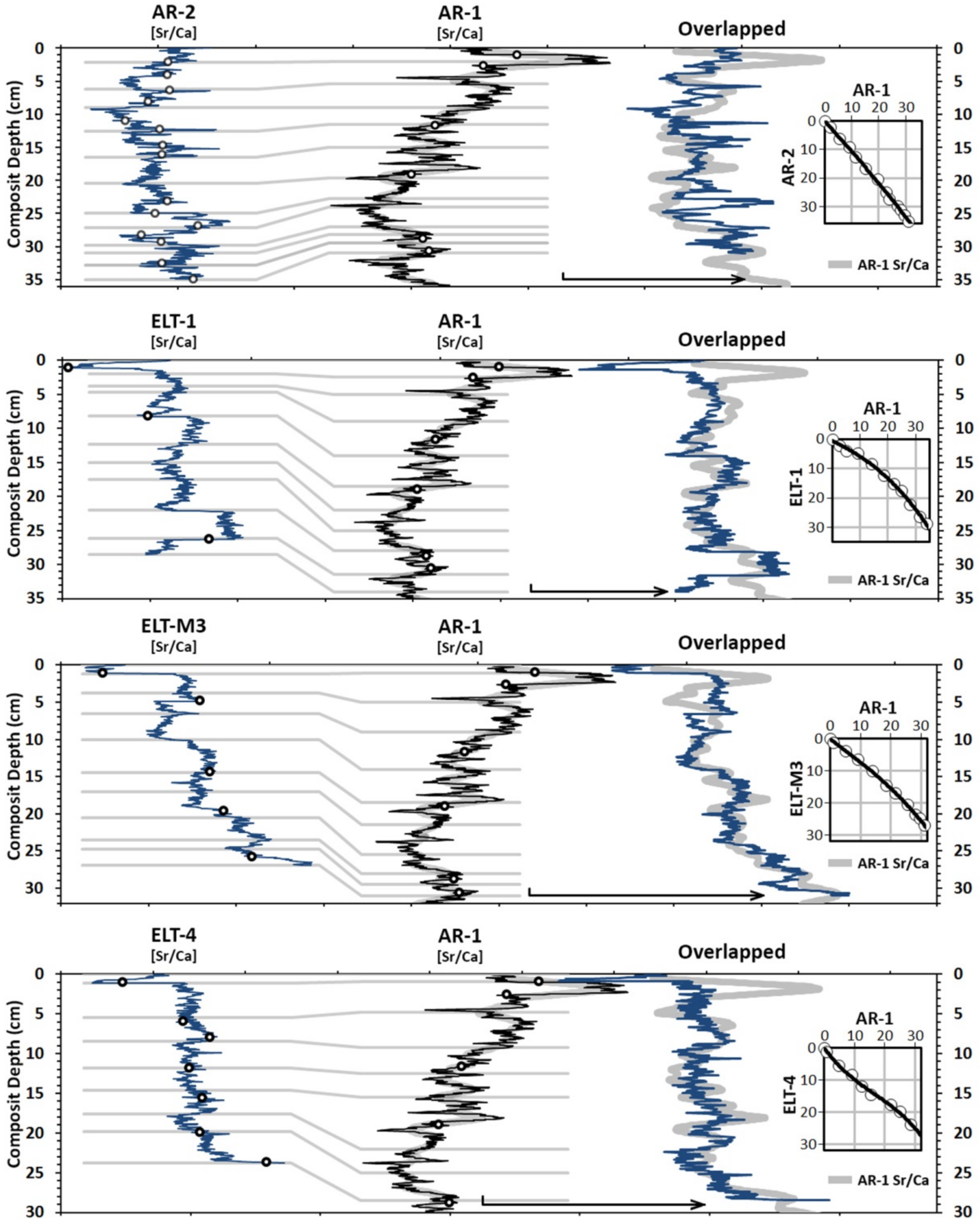

Figure 5.6. The correlation between the cores taken from the north of the AR-1 core-site. (Northern cores are AR-2, ELT-1, ELT-M3, and ELT-4). Small insets in the right of the graphs are transfer functions representing depth adjustments.

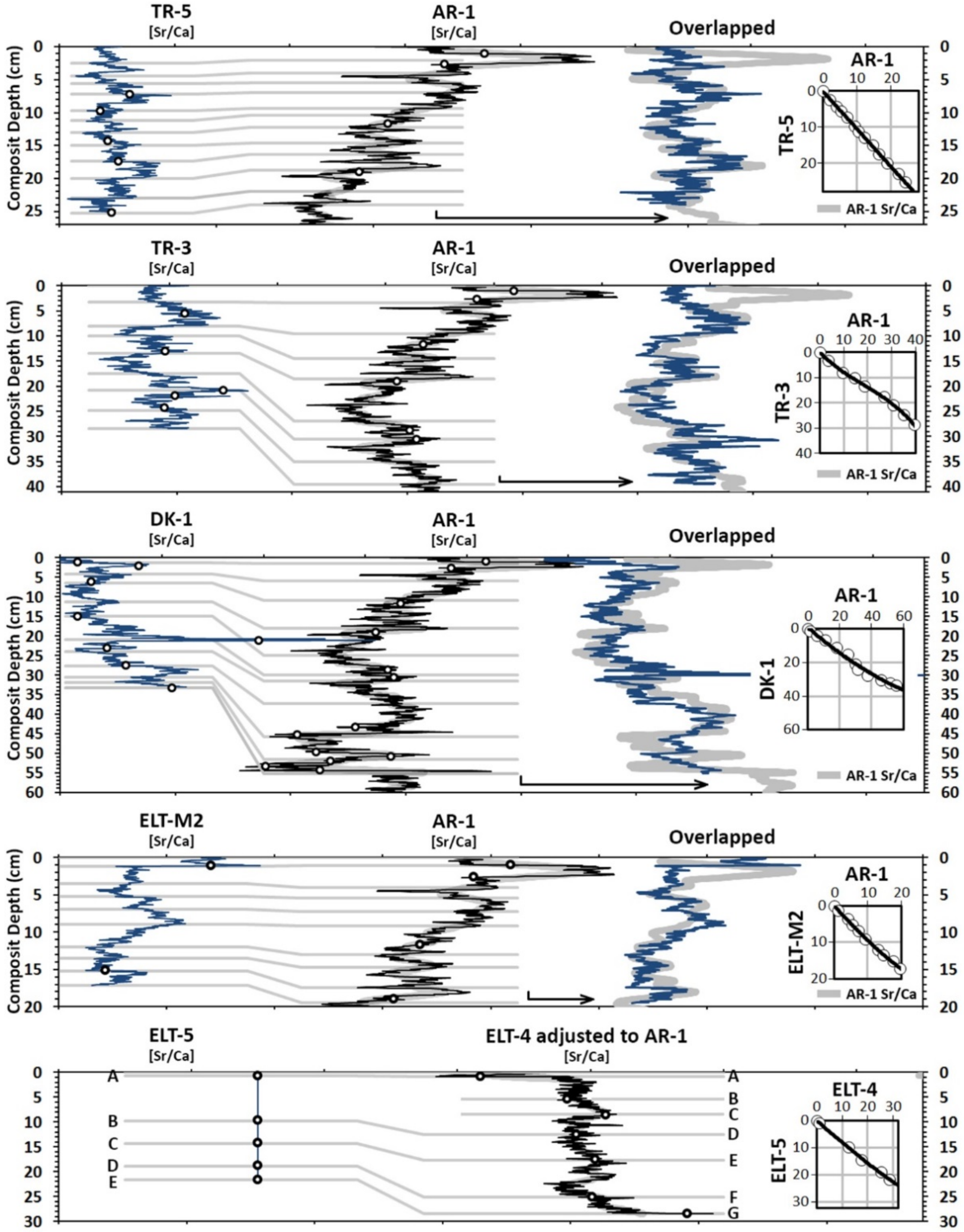

Figure 5.7. The correlation of the remaining cores, which are TR-5, TR-3, DK-1, ELT-M2, and ELT-5. Small insets in the right of the graphs are transfer functions representing depth adjustments.

The correlations between all studied 15 sediment cores were presented in Figure 5.8. Similar to the other correlations, the element ratio Sr/Ca was used in the overall correlation. Levels indicated by gray bars are those considered to correlate significantly, taking into account all proxies used throughout the study.

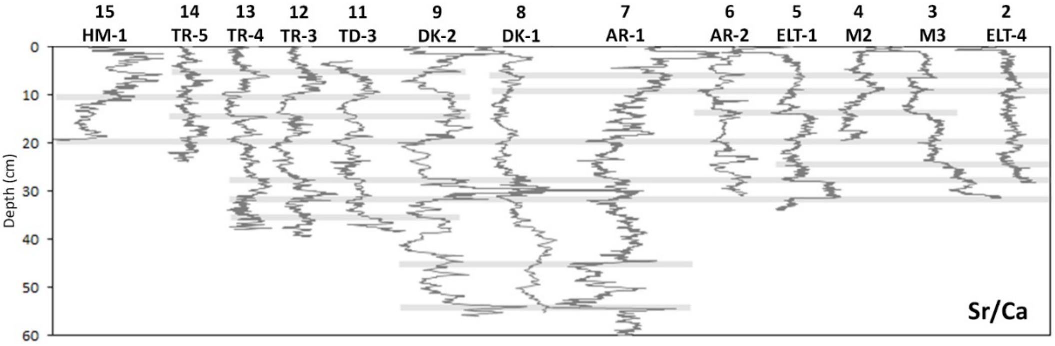

Figure 5.8. The correlation between all sediment cores. It was obtained by using Sr/Ca element ratio.

Planktonic foraminifera samples have been collected for radiocarbon dating from the cores AR-1, AR-2, DK-2, TD-3, TR-4, ELT-M3, and ELT-1, and the age results have been presented as a table in Figure 4.12. In Figure 5.9, the calibrated radiocarbon results are presented. Through Figure 5.9A to 5.9H, the 4th order polynomial best fit and its R^2 are also presented. In Figure 5.9A, the radiocarbon results were calibrated by assuming no atmospheric-marine mixture and there is no deviation from the global Marine 20 calibration curve (i.e., delta_R=0). At this stage it is clearly seen that two of the radiocarbon samples collected from DK-2 and TD-3 cores are reworked, i.e., collected from event-deposits. Figure 5.9B presents the age-depth model without these two samples. R^2 increases from 0.88 in A to 0.98 in B.

R^2 of 0.98 may seem good enough at the first glance. However, there is another point that should be considered at this stage, which is the inconsistency of the age results from ELT-M3 and ELT-1 cores. ELT-M3 and ELT-1 cores, which have a very prominent stratigraphic correlation with both the radiographic images and the MS, GS, and ITRAX profiles, are expected to give the same age results according to basic stratigraphy rules. However, there is almost 400 years difference between the radiocarbon results obtained from ELT-M3 and ELT-1; two gray lines in Figure 5.9B. This difference, which is probably related to reservoir age, should be minimized in order to have a reliable age-depth model. To overcome this problem, as the first step, a delta_R value of 12 ± 51, which was determined for the Gulf of Aqaba (Calib.org), was considered during calibration and the results were re-plotted (Figure 5.9C). This affects neither the graphs nor the R^2s (Both R^2s are 0.98), the inconsistency between ELT-M3 and ELT-1 dates persists. In the next step, the radiocarbon ages obtained from the foraminifera samples extracted from the top of the cores were used as core-specific reservoir ages (Figure 5.9D-H).

In Figure 5.9D, 10% atmospheric and 90% marine carbon mixture (A/M) was assumed, where there is almost no change from Figure 5.9C, i.e., the inconsistency between ELT-M3 and ELT-1 dates still persists. However, as the marine water contribution is increased step by step, from Figure 5.9D to 5.9H, it is seen that the inconsistency almost disappears at A/M=45/55 (Figure 5.9F).

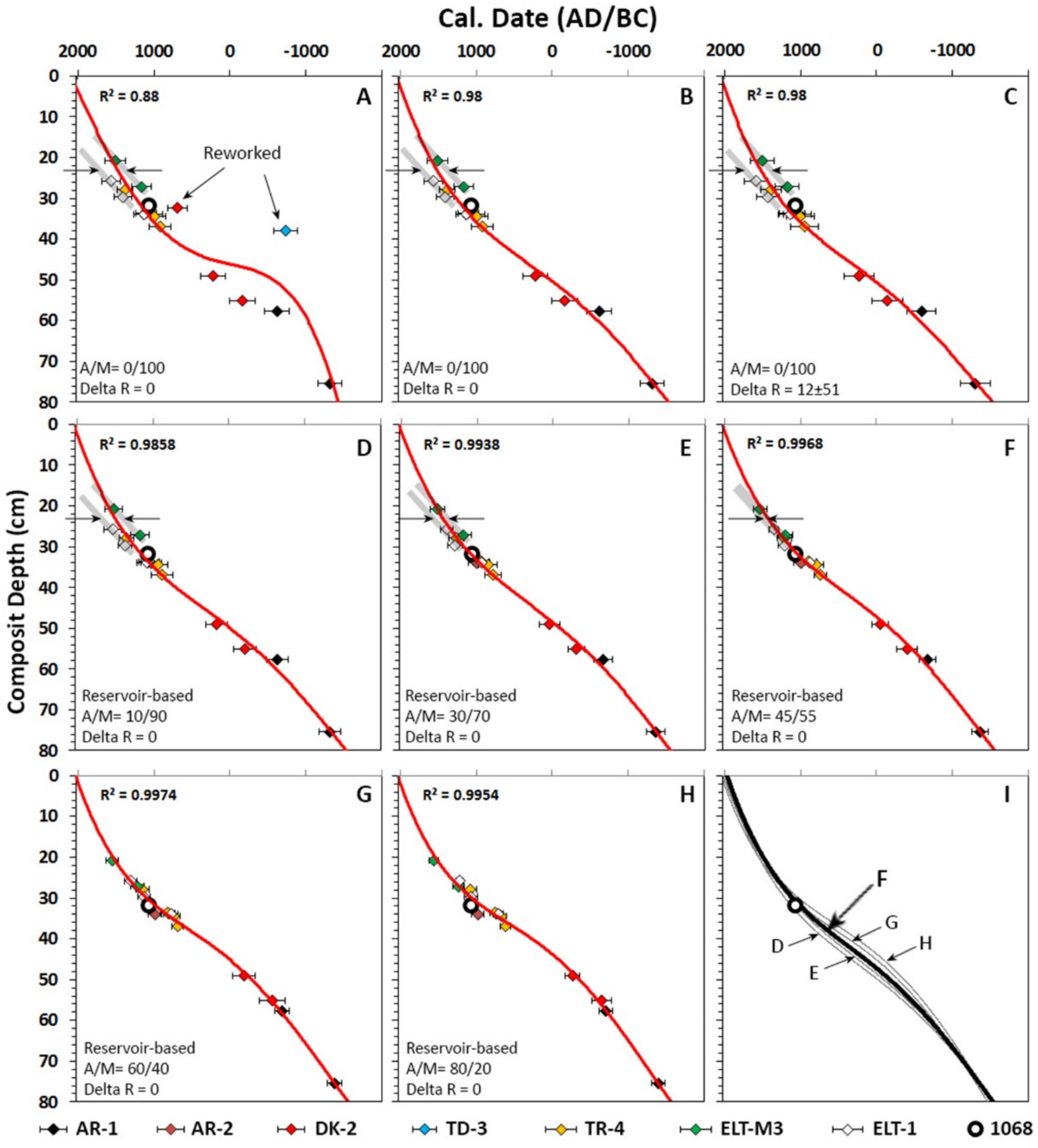

Figure 5.9. Age-depth model improvement by using reservoir age and atmospheric-marine mixing rate of the carbon source.

Looking at the best fits in the E, F, G, and H graphs, it is seen that they almost all contain radiocarbon samples and the R^2 values are considerably precise. Although these four graphs seem to be candidates of age-depth models for this study, it looks like the age-depth model F is the best candidate. The 1068 earthquake is known as the most severe and devastating earthquake affecting a large area around the Gulf of Aqaba region (Ben-Menahem, 1991; Badawy & Horvath, 1999; Klinger et al., 2000;

Zilberman et al.,2005; Ambraseys, 2009; Marco & Klinger, 2014). If it is assumed that the most prominent turbidites in the gulf, ca. at 31 cm depth, are because of the 1068 earthquake, the age-depth model F is the only one that is both precisely passes through 1068 and does not have an inconsistency between ELT-M3 and ELT-1 dates. For this reason, the age-depth model F is used for the sediment chronology in this study.

5.3 Segment-Based Source and Recurrence Interval Interpretations

The distribution of the previously classified and rescaled sedimentary events along the Gulf of Aqaba is presented in Figure 5.10a. Pinkish circles with black dots represent "Type A" turbidites characterized by a basal coarse-grained and cross-bedded level overlain by fine-grained almost homogeneous foraminifera-free sediments. It is obvious that prominent turbidites show a consistent and reasonable alignment along the entire Gulf of Aqaba (Figure 5.10a). The most useful information has been obtained from the cores collected from Tiran and Eilat basins since these two basins have systematically and clearly recorded the turbidites.

The most recent earthquake recorded in the Gulf of Aqaba is the 1995 Nuweibaa Earthquake. Since it was in the instrumental period, much more is known about the 1995 earthquake compared to the historical ones. The Nuweibaa earthquake having a magnitude of 7.2 is not seen in the Tiran cores. Instead, the youngest turbidites recorded in the Tiran Deep dated to the 19th century indicating the AD 1839 earthquake which is less known in the historical records. This event is seen also in the cores taken from the Dakar Deep. Only in Ambraseys (2009), after a severe earthquake in 1840, the restoration that lasted for one year on the walls of the St Catherine monastery on the Sinai Peninsula was mentioned. Considering the location of the monastery, it is expected that the possible traces of the 1839 earthquake may be observed in the central and southern parts of the Gulf of Aqaba. The 1839 earthquake has been observed thinner to the north and thicker to the south in TR-5, TR-4, and TR-3 cores, which indicates that most probably TF is responsible for this event (Figure 5.10a). The sedimentary event, which has been observed almost all along the gulf in the 11th century, most probably belongs to the 1068 earthquake. The severity of the 1068 earthquake mentioned in the literature and the fact that it is observed in almost all of the cores from TR-5 to ELT-M3 indicate that this earthquake may have broken both AF and ArF simultaneously. That is most probably why 1068 was the most devastating earthquake in the Gulf of Aqaba and Strait of Tiran region. Unfortunately, the lengths of the ELT-4 and ELT-5 do not allow observing the 1068 earthquake. Similar to 1839, the turbidites of 1068 have also been observed in TR-4 and TR-3 cores. When TF is considered in this context, there seems to be a recurrence interval of about 800 years from 1839-1068. Considering the slip rate of the DSF which is 5 ± 1 mm/yr (Le Beon et al., 2010), 800 years of recurrence interval seems quite reasonable.

The turbidites of the 1212 earthquake are not seen in the ELT-1 and ELT-M3. However, they are observable in the ELT-4 and ELT-5 cores and get thicker to the north. This indicates that the 1212 earthquake is most probably due to the rupture of EF. On the other hand, turbidites belonging to the 1588 earthquake, which is well known in historical records, were observed in all Eilat cores except for ELT-1. (Figure 5.10). If the 1588 earthquake was caused by EF, it should have appeared in the ELT-1 core. Although some turbidites are observed in HM-1 and TD-3 cores around 1588, only Eilat cores were included in the interpretation of the 1588 earthquake, because the other turbidites are not continuous in the lateral extend i.e., not synchronous. The reason for these turbidites is most probably the normal faults in the Tiran and Dakar deeps. Considering all these constraints, the 1588 earthquake was probably generated by the HF, rather than EF (Figure 5.10).

A hypothetical sketch was drawn to illustrate the recurrence intervals of the fault segments and the northward migration of the earthquakes in the Gulf of Aqaba

(Figure 5.10b). Based on these hypothetical interpretations, it looks like the EF segment is ready to rupture in the near future.

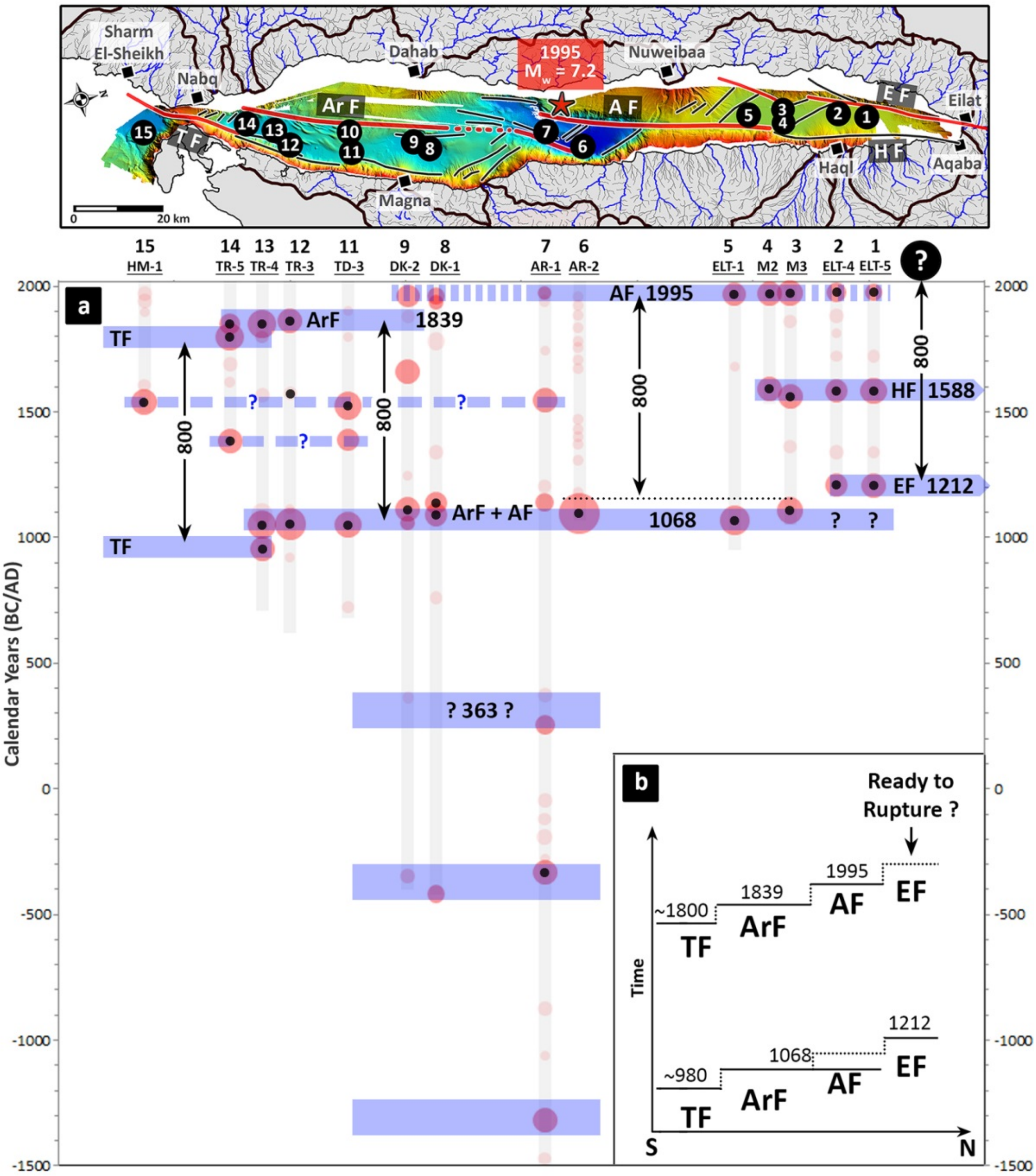

Figure 5.10. a) Segment-based seismic source interpretations. Pinkish circles with black dots represent well-developed and prominent turbidites. Blue bars represent the sedimentary event levels. The recurrence intervals of about 800 years between two consecutive events on the same fault segment are shown by the double-sided arrows. b) Hypothetical sketch illustrating Recurrence interval chart of cores.

In the paleoseismology trenching studies (Klinger et al., 2015; Lefevre et al., 2018), it was stated that 1068 and 1212 earthquakes occurred on the EF. However, sedimentary traces of 1068 and 1212 earthquakes are not seen in the ELT-1 and ELT-M3 cores in the present study. Since the length of the sedimentary record of this study is not enough to enlighten this discrepancy between the turbidite record and the on-land trench studies, longer cores are needed to overcome this problem.

CHAPTER 6

CONCLUSION

The main conclusions that can be drawn from the present study are as follows:

- Working with a multi-core system instead of a single core and establishing a precise stratigraphic correlation of these cores have provided a better understanding of the seismic background of the Gulf of Aqaba sediments and their potential to generate turbidites.
- Because background sediments of the Gulf of Aqaba are full of bioturbations, performing u-channel radiography significantly increased the quality and reliability of the results in the detection of the seismo-turbidites.
- In the light of the data obtained from various analyzes, it has been proven that earthquake-induced turbidites are not always characterized by grain size increase or graded bedding. The importance of using several independent analyzes i.e., multi-proxy investigation, for the exact and accurate detection of seismo-turbidites has been revealed.
- Stratigraphic correlation and sediment chronology play key roles in revealing a paleoseismic record.
- Using site-specific reservoir age is crucial to establish a precise sediment chronology. Thanks to this method that was applied to the Gulf of Aqaba cores, potential dating confusions were avoided.
- Classification and rescaling of sedimentary events made turbidites detected in basins with different sedimentation rates and different morphologies comparable.
- Turbidites triggered by 1068, 1212, 1588, 1839, and 1995 earthquakes have been detected in the sediments of the Gulf of Aqaba.

- Thanks to the classification and rescaling process, significant interpretations could be made regarding the northward migration of the earthquakes in the Gulf of Aqaba.
- The last devastating earthquake that occurred on the Eilat Fault was 1212, and if the recurrence interval of 800 years is as predicted, enough time has passed since 1212. So, this means Eilat and Aqaba cities are most probably have seismic activity in the near future.
- Longer cores are required to enlighten the discrepancy between turbidite records and on-land trench studies.

REFERENCES

Adams, J. (1990). Paleoseismicity of the Cascadia Subduction Zone: Evidence from turbidites off the Oregon-Washington Margin. Tectonics, 9(4), 569–583.

Akyuz, H. S., Altunel, E., Karabacak, V., & Yalciner, C. C. (2006). Historical earthquake activity of the northern part of the Dead Sea Fault Zone, southern Turkey. *Tectonophysics*, *426*(3–4), 281–293.

Al-Tarazi, E. A. (1999). Regional seismic hazard study for the eastern Mediterranean (Trans-Jordan, Levant and Antakia) and Sinai region. Journal of African Earth Sciences, 28(3), 743-750.

Alves, E. Q., Macario, K., Ascough, P., and Bronk Ramsey, C. (2018). The Worldwide Marine Radiocarbon Reservoir Effect: Definitions, Mechanisms, and Prospects. Reviews of Geophysics, 56(1), 278–305.

Ambraseys, N. (2009). Earthquakes in the Mediterranean and Middle East: A Multidisciplinary Study of Seismicity up to 1900. Cambridge: Cambridge University Press.

Ambraseys, N. N., Melville, C. P., and Adams, R. D. (1994). “The Seismicity of the Red Sea”. Cambridge Univ. Press, Cambridge, UK.

Amit, R., Zilberman, E., Enzel, Y., and Porat, N. (2002). Paleoseismic evidence for time dependency of seismic response on a fault system in the southern Arava Valley, Dead Sea Rift, Israel. Geological Society of America Bulletin, 114(2), 192-206.

Amit, R., Zilberman, E., Porat, N., and Enzel, Y. (1999). Relief Inversion in the Avrona Playa as Evidence of Large-Magnitude Historical Earthquakes, Southern Arava Valley, Dead Sea Rift. Quaternary Research, 52(1), 76-91.

Appleby, P. G., Oldfield, F., Thompson, R., Huttunen, P., and Tolonen, K. (1979). 210Pb dating of annually laminated lake sediments from Finland. Nature, 280(5717), 53–55.

Appleby, P.G. 2001. Chronostratigraphic techniques in recent sediments. In: Last, W.M., Smol, J.P. (Eds.), Tracking Environmental Change Using Lake Sediments. Volume 1: Basin Analysis, Coring, and Chronological Techniques. Kluwer Academic Publishers, Dordrecht, The Netherlands, pp. 171-203.

Avşar, U. (2013). Lacustrine paleoseismic records from the North Anatolian Fault, Turkey (Doctoral dissertation, Ghent University).

Avşar, U. (2019b). Sedimentary Traces of Tsunamis in the Aegean Sea during the Last 1500 Years, (Karine Lagoon, W Turkey). Geological Bulletin of Turkey 62(3), 199-220.

Avşar, U., Hubert-Ferrari, A., Batist, M. D., and Fagel, N. (2014a). A 3400 year lacustrine paleoseismic record from the North Anatolian Fault, Turkey: Implications for bimodal recurrence behavior. Geophysical Research Letters, 41(2), 377-384.

Avşar, U., Hubert-Ferrari, A., Batist, M. D., Lepoint, G., Schmidt, S., and Fagel, N. (2014b). Seismically-triggered organic-rich layers in recent sediments from Göllüköy Lake (North Anatolian Fault, Turkey). Quaternary Science Reviews, 103, 67-80.

Avşar, U., Hubert-Ferrari, A., Batist, M. D., Schmidt, S., and Fagel, N. (2015). Sedimentary records of past earthquakes in Boraboy Lake during the last ca 600 years (North Anatolian Fault, Turkey). Paleogeography, Palaeoclimatology, Palaeoecology, 433, 1-9.

Avşar, U., Jónsson, S., Avşar, Ö, and Schmidt, S. (2016). Earthquake-induced soft-sediment deformations and seismically amplified erosion rates recorded in varved sediments of Köyceğiz Lake (SW Turkey). Journal of Geophysical Research: Solid Earth, 121(6), 4767-4779.

Badawy, A., and Horváth, F. (1999). Seismicity of the Sinai subplate region: kinematic implications. Journal of Geodynamics, 27(4–5), 451–468.

Bandy, W. L., Michaud, F., Mortera Gutiérrez, C. A., Dyment, J., Bourgois, J., Royer, J.-Y., Calmus, T., Sosson, M., and Ortega-Ramirez, J. (2010). The Mid-Rivera-Transform Discordance: Morphology and Tectonic Development. Pure and Applied Geophysics, 168(8–9), 1391–1413.

Barjous, M., and Mikbel, S. (1990). Tectonic evolution of the gulf of Aqaba-Dead Sea transform fault system. Tectonophysics, 180(1), 49–59.

Bé, A. W. (1959). A Method for Rapid Sorting of Foraminifera from Marine Plankton Samples. Journal of Paleontology, 33(5), 846-848.

Becker, A., Davenport, C. A., Eichenberger, U., Gilli, E., Jeannin, P., and Lacave, C. (2006). Speleoseismology: A critical perspective. Journal of Seismology, 10(3), 371-388.

Ben-Avraham, Z. (1985). Structural framework of the Gulf of Elat (AQABA), Northern Red Sea. Journal of Geophysical Research, 90(B1), 703–726.

Ben-Avraham, Z., Almagar, G. and Garfunkel, Z., 1979. Sediments and structure of the Gulf of Elat (Aqaba)--Northern Red Sea. Sediment. Geol., 23: 239--267.

Ben-Avraham, Z., Garfunkel, Z., and Lazar, M. (2008). Geology and Evolution of the Southern Dead Sea Fault with Emphasis on Subsurface Structure. Annual Review of Earth and Planetary Sciences, 36(1), 357-387.

Ben-Menahem, A. (1991). Four thousand years of seismicity along the Dead Sea Rift. Journal of Geophysical Research: Solid Earth, 96(B12), 20195–20216.

Bernhardt, A., Melnick, D., Hebbeln, D., Lückge, A., and Strecker, M. R. (2015). Turbidite paleoseismology along the active continental margin of Chile – Feasible or not? Quaternary Science Reviews, 120, 71–92.

Björck, S., and Wohlfarth, B. (2001). 14C chronostratigraphic techniques in paleolimnology. In 1171454392 878393624 W. M. Last & 1171454393 878393624 J. P. Smol (Authors), Tracking environmental change using lake sediments, volume 1: Basin analysis, coring, and chronological techniques (pp. 205-245). Dordrecht, The Netherlands: Kluwer Academic.

Brady, H. B. (1877). Supplementary note on the foraminifera of the Chalk(?) of the New Britain group. Geological Magazine, new ser. 4: 534-536.

Çağatay, M.N., Erel, L., Bellucci, L.G., Polonia, A., Gasperini, L., Eriş, K.K., Sancar, T., Biltekin, D., Uçarkuş, G., Ülgen, U.B., Damci, E., 2012. Sedimentary earthquake records in the İzmit Gulf, Sea of Marmara, Turkey. Sedimentary Geology 282, 347-359.

Croudace, I. W., and Rothwell, R. G. (Eds.). (2015). Micro-XRF studies of sediment cores: Applications of a non-destructive tool for the environmental sciences (Vol. 17). Dordrecht, Netherlands: Springer.

Croudace, I. W., Rindby, A., and Rothwell, R. G. (2006). ITRAX: description and evaluation of a new multi-function X-ray core scanner. Geological Society, London, Special Publications, 267(1), 51–63.

Cui, X., Xing, Z., Yang, F., Fan, M., Ma, Y., and Sun, Y. (2020). A method for multibeam seafloor terrain classification based on self-adaptive geographic classification unit. Applied Acoustics, 157, 107029.

Daeron, M., Klinger, Y., Tapponnier, P., Elias, A., Jacques, E., and Sursock, A. (2007). 12,000-Year-Long Record of 10 to 13 Paleoearthquakes on the Yammouneh Fault, Levant Fault System, Lebanon. Bulletin of the Seismological Society of America, 97(3), 749–771.

De Batist, M., Talling, P., Strasser, M., and Girardclos, S. (2017). Subaquatic paleoseismology: records of large Holocene earthquakes in marine and lacustrine sediments. Marine Geology, 384, 1–3.

Dubertret L. (1932). Les formes structurales de la Syrie et de la Palestine. Académie des Sciences Comptes Rendus 195:65–67

El-Isa, Z. H. (2012). Seismicity and seismotectonics of the Gulf of Aqaba region. Arabian Journal of Geosciences, 6(9), 3437–3449.

El-Isa, Z. H., and Shanti, A. A. (1989). Seismicity and Tectonics of the Red Sea and Western Arabia. Geophysical Journal International, 97(3), 449–457.

Fan, J., Wei, X., Shi, W., Guo, Q., Zhang, S., Xu, H., Song, H., Xu, C., An, W., and Jiang, H. (2020). Response of tree rings to earthquakes during the past 350 years at Jiuzhaigou in the eastern Tibet. Science of The Total Environment, 731, 138714.

Fok-Pun, L., and Komar, P. D. (1983). Settling velocities of planktonic foraminifera; density variations and shape effects. The Journal of Foraminiferal Research, 13(1), 60–68.

Freund, R. (1965). A Model of the Structural Development of Israel and Adjacent Areas Since Upper Cretaceous Times. Geological Magazine, 102(3), 189–205.

Garfunkel, Z. (1981). Internal structure of the Dead Sea leaky transform (rift) in relation to plate kinematics. Tectonophysics, 80(1-4), 81-108.

Girdler, R. W. (1990). The Dead Sea transform fault system. Tectonophysics, 180(1), 1–13.

Goldfinger, C. (2009). Chapter 2B Sub-Aqueous Paleoseismology. International Geophysics Paleoseismology, 119-170.

Goldfinger, C. (2011). Submarine Paleoseismology Based on Turbidite Records. Annual Review of Marine Science, 3(1), 35-66.

Goldfinger, C., Grijalva, K., Burgmann, R., Morey, A. E., Johnson, J. E., Nelson, C. H., Gutierrez-Pastor, J., Ericsson, A., Karabanov, E., Chaytor, J. D., Patton, J., and Gracia, E. (2008). Late Holocene Rupture of the Northern San Andreas Fault and Possible Stress Linkage to the Cascadia Subduction Zone. Bulletin of the Seismological Society of America, 98(2), 861–889.

Goldfinger, C., Morey, A. E., Nelson, C. H., Gutiérrez-Pastor, J., Johnson, J. E., Karabanov, E., Chaytor, J., and Eriksson, A. (2007). Rupture lengths and temporal history of significant earthquakes on the offshore and north coast segments of the Northern San Andreas Fault based on turbidite stratigraphy. Earth and Planetary Science Letters, 254(1–2), 9–27.

Goldfinger, C., Nelson, C. H., and Johnson, J. E. (2003a). Holocene Earthquake Records From the Cascadia Subduction Zone and Northern San Andreas Fault based on precise dating Of offshore turbidites. Annual Review of Earth and Planetary Sciences, 31(1), 555-577.

Goldfinger, C., Nelson, C. H., Johnson, J. E., and Shipboard Scientific Party. (2003b). Deep-water turbidites as Holocene earthquake proxies: The Cascadia subduction zone and Northern San Andreas Fault systems. ANNALS OF GEOPHYSICS, 46(5), 1169-1194.

Gomez, F., Meghraoui, M., Darkal, A. N., Hijazi, F., Mouty, M., Suleiman, Y., Sbeinati, R., Darawcheh, R., Al-Ghazzi, R., and Barazangi, M. (2003). Holocene faulting and earthquake recurrence along the Serghaya branch of the Dead Sea fault system in Syria and Lebanon. Geophysical Journal International, 153(3), 658-674.

Gorsline, D., Diego, T. D., and Nava-Sanchez, E. (2000). Seismically triggered turbidites in small margin basins: Alfonso Basin, Western Gulf of California and Santa Monica Basin, California Borderland. Sedimentary Geology, 135(1-4), 21-35.

Gràcia, E. E., Lamarche, G., Nelson, H., and Pantosti, D. (2013). Preface: Marine and Lake Paleoseismology. Natural Hazards and Earth System Sciences, 13(12), 3469-3478.

Gràcia, E., Vizcaino, A., Escutia, C., Asioli, A., Rodés, Á., Pallàs, R., Garcia-Orellana, J., Lebreiro, S., and Goldfinger, C. (2010). Holocene earthquake record offshore Portugal (SW Iberia): testing turbidite paleoseismology in a slow-convergence margin. Quaternary Science Reviews, 29(9–10), 1156–1172.

Grotzinger, J., and Jordan, T. H. (2010). Understanding Earth (Sixth ed.). W. H. Freeman.

Heaton, T. J., Köhler, P., Butzin, M., Bard, E., Reimer, R. W., Austin, W. E. N., Bronk Ramsey, C., Grootes, P. M., Hughen, K. A., Kromer, B., Reimer, P. J., Adkins, J., Burke, A., Cook, M. S., Olsen, J., & Skinner, L. C. (2020). Marine20—The Marine Radiocarbon Age Calibration Curve (0–55,000 cal BP). Radiocarbon, 62(4), 779–820.

Heezen, B. C., and Ewing, W. M. (1952). Turbidity currents and submarine slumps, and the 1929 Grand Banks [Newfoundland] earthquake. American Journal of Science, 250(12), 849–873.

Hounslow, M. W., and Maher, B. A. (1999). Source of the climate signal recorded by magnetic susceptibility variations in Indian Ocean sediments. Journal of Geophysical Research: Solid Earth, 104(B3), 5047–5061.

Howarth, J. D., Fitzsimons, S. J., Norris, R. J., and Jacobsen, G. E. (2012). Lake sediments record cycles of sediment flux driven by large earthquakes on the Alpine fault, New Zealand. Geology, 40(12), 1091–1094.

Howarth, J. D., Fitzsimons, S. J., Norris, R. J., and Jacobsen, G. E. (2014). Lake sediments record high intensity shaking that provides insight into the location and rupture length of large earthquakes on the Alpine Fault, New Zealand. Earth and Planetary Science Letters, 403, 340–351.

Hubert-Ferrari, A., El-Ouahabi, M., Garcia-Moreno, D., Avşar, U., Altınok, S., Schmidt, S., Fagel, N., and Çağatay, M. N. (2017). Earthquake imprints on a lacustrine deltaic system: The Kürk Delta along the East Anatolian Fault (Turkey). Sedimentology, 64(5), 1322–1353.

Ikehara, K., Kanamatsu, T., Nagahashi, Y., Strasser, M., Fink, H., Usami, K., Irino, T., and Wefer, G. (2016). Documenting large earthquakes similar to the 2011 Tohoku-oki earthquake from sediments deposited in the Japan Trench over the past 1500 years. Earth and Planetary Science Letters, 445, 48-56.

Inouchi, Y., Kinugasa, Y., Kumon, F., Nakano, S., Yasumatsu, S., and Shiki, T. (1996). Turbidites as records of intense palaeoearthquakes in Lake Biwa, Japan. Sedimentary Geology, 104(1-4), 117-125.

Kagan, E. J., Cinti, F. R., Alfonsi, L., Civico, R., and Bar-Matthews, M. (2017). Broken speleothems reveal Holocene and Late Pleistocene paleoearthquakes in Northern Calabria, Italy. Quaternary International, 451, 176-184.

Kanari, M., Niemi, T. M., Ben-Avraham, Z., Frieslander, U., Tibor, G., Goodman-Tchernov, B. N., . . . Marco, S. (2020). Seismic potential of the Dead Sea Fault in the northern Gulf of Aqaba-Elat: New evidence from liquefaction, seismic reflection, and paleoseismic data. Tectonophysics, 793, 228596.

Keeper, D. K. (1984). Landslides caused by earthquakes. Geological Society of America Bulletin, 95(4), 406-421.

Kelsey, H. M., Hull, A. G., Cashman, S. M., Berryman, K. R., Cashman, P. H., Trexler, J. H., and Begg, J. G. (1998). Paleoseismology of an active reverse fault in a forearc setting: The Poukawa fault zone, Hikurangi forearc, New Zealand. Geological Society of America Bulletin, 110(9), 1123-1148.

Klinger, Y., Béon, M. L., and Al-Qaryouti, M. (2015). 5000 yr of paleoseismicity along the southern Dead Sea fault. Geophysical Journal International, 202(1), 313-327.

Klinger, Yann, Avouac, J.-P., Karaki, N. A., Dorbath, L., Bourles, D., & Reyss, J. L. (2000). Slip rate on the Dead Sea transform fault in northern Araba valley (Jordan). Geophysical Journal International, 142(3), 755–768.

Klinger, Yann, Rivera, L., Haessler, H., and Maurin, J.C. (1999). Active Faulting in the Gulf of Aqaba: New Knowledge from the Mw=7.3 Earthquake of 22 November 1995. Bull. Seismol. Soc. Am., 89 (4). (August), 1025–1036.

Korzhenkov, A. M., Avanesyan, M. A., Vardanyan, A. A., and Vergino, E. S. (2016). Traces of strong earthquakes of the 9th century in the ruins of Dvin, ancient Armenian Capital. Seismic Instruments, 52(2), 99-110.

Kozacı, Ö. (2012). Dendroseismology on the central North Anatolian fault, Turkey: Documenting three centuries of surface rupture history using tree rings. Journal of Geophysical Research: Solid Earth, 117(B1).

Larrasoaña, J. C., Roberts, A. P., and Rohling, E. J. (2008). Magnetic susceptibility of eastern Mediterranean marine sediments as a proxy for Saharan dust supply? Marine Geology, 254(3–4), 224–229.

Le Béon, M. et al. (2010). Early Holocene and late Pleisotoce slip rate of the southern Dead Sea fault determined by 10Be cosmogenic dating of offset alluvial deposits. Journal of Geophysical Research, 115, doi:10.1029/2009JB007198.

Le Béon, M., Klinger, Y., Mériaux, A., Al-Qaryouti, M., Finkel, R. C., Mayyas, O., and Tapponnier, P. (2012). Quaternary morphotectonic mapping of the Wadi Araba and implications for the tectonic activity of the southern Dead Sea fault. Tectonics, 31(5).

Lefevre, M., Klinger, Y., Al-Qaryouti, M., Le Béon, M., & Moumani, K. (2018). Slip deficit and temporal clustering along the Dead Sea fault from paleoseismological investigations. *Scientific Reports*, *8*(1), 1–9.

Leithold, E. L., Wegmann, K. W., Bohnenstiehl, D. R., Smith, S. G., Noren, A., and O'Grady, R. (2017). Slope failures within and upstream of Lake Quinault, Washington, as uneven responses to Holocene earthquakes along the Cascadia subduction zone. Quaternary Research, 89(1), 178–200.

Lockhart, W. (2000). Tests of the fidelity of lake sediment core records of mercury deposition to known histories of mercury contamination. The Science of The Total Environment, 260(1–3), 171–180.

Marco, S., and Klinger, Y. (2014). Chapter 7 Review of On-Fault Palaeoseismic Studies Along the Dead Sea Fault. In Z. Garfunkel, Z. Ben-Avraham, & E. Kagan (Eds.), Dead Sea Transform Fault System: Reviews (2014th ed., pp. 183–205). Springer.

Marco, S., Hartal, M., Hazan, N., Lev, L., & Stein, M. (2003). Archaeology, history, and geology of the A.D. 749 earthquake, Dead Sea transform. *Geology*, *31*(8), 665.

Marco, S., Stein, M., Agnon, A., & Ron, H. (1996). Long-term earthquake clustering: A 50,000-year paleoseismic record in the Dead Sea Graben. Journal of Geophysical Research: Solid Earth, 101(B3), 6179–6191.

Masana, E., Martínez-Díaz, J. J., Hernández-Enrile, J. L., and Santanach, P. (2004). The Alhama de Murcia fault (SE Spain), a seismogenic fault in a diffuse plate boundary: Seismotectonic implications for the Ibero-Magrebian region. Journal of Geophysical Research: Solid Earth, 109(B1).

McCalpin, J. P., and Nelson, A. R. (2009). Introduction to Paleoseismology. In 1143870963 860846024 J. P. McCalpin (Ed.), Paleoseismology (2nd ed., Vol. 95, ISSN 0074-6142, pp. 1-27). London, UK: Academic Press.

Mchugh, C., Seeber, L., Cormier, M., and Hornbach, M. (2014). Submarine Paleoseismology Along Populated Transform Boundaries: The Enriquillo-Plantain-Garden Fault, Canal du Sud, Haiti, and the North Anatolian Fault, Marmara Sea, Turkey. Oceanography, 27(2), 118-131.

Mchugh, C., Seeber, L., Cormier, M., Dutton, J., Cagatay, N., Polonia, A., Ryan, W.B.F., and Gorur, N. (2006). Submarine earthquake geology along the North Anatolia Fault in the Marmara Sea, Turkey: A model for transform basin sedimentation. Earth and Planetary Science Letters, 248(3-4), 661-684.

Mendecki, M., and Szczygieł, J. (2019). Physical constraints on speleothem deformations caused by earthquakes, seen from a new perspective: Implications for paleoseismology. Journal of Structural Geology, 126, 146-155.

Migeon, S., Garibaldi, C., Ratzov, G., Schmidt, S., Collot, J.-Y., Zaragosi, S., and Texier, L. (2017). Earthquake-triggered deposits in the subduction trench of the north Ecuador/south Colombia margin and their implication for paleoseismology. Marine Geology, 384, 47–62.

Migeon, S., Weber, O., Faugeres, J. & Saint-Paul, J. (1999). SCOPIX: a new X-ray imaging system for core analysis. Geo-Marine Letters 18, 251–255.

Mizugaki, S., Nakamura, F., and Araya, T. (2006). Using dendrogeomorphology and 137Cs and 210Pb radiochronology to estimate recent changes in sedimentation rates in Kushiro Mire, Northern Japan, resulting from land use change and river channelization. CATENA, 68(1), 25–40.

Moernaut, J. 2010. Sublacustrine landslide processes and their paleoseismological significance: Revealing the recurrence rate of giant earthquakes in South-Central Chile. Tez. PhD thesis, Ghent University, Belgium.

Moernaut, J., Daele, M. V., Heirman, K., Fontijn, K., Strasser, M., Pino, M., Urrutia, R., and Batist, M. D. (2014). Lacustrine turbidites as a tool for quantitative earthquake reconstruction: New evidence for a variable rupture mode in south central Chile. Journal of Geophysical Research: Solid Earth, 119(3), 1607-1633.

Moernaut, J., Van Daele, M., Strasser, M., Clare, M. A., Heirman, K., Viel, M., Cardenas, J., Kilian, R., Ladrón de Guevara, B., Pino, M., Urrutia, R., and De Batist, M. (2017). Lacustrine turbidites produced by surficial slope sediment remobilization: A mechanism for continuous and sensitive turbidite paleoseismic records. Marine Geology, 384, 159–176.

Monecke, K., Anselmetti, F. S., Becker, A., Sturm, M., and Giardini, D. (2004). The record of historic earthquakes in lake sediments of Central Switzerland. Tectonophysics, 394(1-2), 21-40.

Monecke, K., Anselmetti, F. S., Becker, A., Sturm, M., and Giardini, D. (2004). The record of historic earthquakes in lake sediments of Central Switzerland. Tectonophysics, 394(1–2), 21–40.

Mutti, E., Lucchi, F. R., Seguret, M., and Zanzucchi, G. (1984). Seismoturbidites: A new group of resedimented deposits. Marine Geology, 55(1–2), 103–116.

Nakajima, T., and Kanai, Y. (2000). Sedimentary features of seismoturbidites triggered by the 1983 and older historical earthquakes in the eastern margin of the Japan Sea. Sedimentary Geology, 135(1–4), 1–19.

Nelson, A. R., Kelsey, H. M., and Witter, R. C. (2006). Great earthquakes of variable magnitude at the Cascadia subduction zone. Quaternary Research, 65(3), 354–365.

Nelson, C. H., Goldfinger, and S. C.Wol. (1999). Abstract: Cascadia Basin Channel Pathways And Late Holocene Turbidite Event History AAPG Bulletin, 83 (1999), T41E-11.

Niemi, T. M., and Ben-Avraham, Z. (1994). Evidence for Jericho earthquakes from slumped sediments of the Jordan River delta in the Dead Sea. Geology, 22(5), 395.

Orbigny, A. D. d'. (1839). Foraminifères, in de la Sagra R., Histoire physique, politique et naturelle de l'ile de Cuba. *A. Bertrand.* 1-224.

Patton, J. R., Goldfinger, C., Morey, A. E., Ikehara, K., Romsos, C., Stoner, J., Djadjadihardja, Y., Udrekh, Ardhyastuti, S., Gaffar, E.Z., and Vizcaino, A. (2015). A 6600 year earthquake history in the region of the 2004 Sumatra-Andaman subduction zone earthquake. Geosphere, 11(6), 2067-2129.

Patton, J. R., Goldfinger, C., Morey, A. E., Romsos, C., Black, B., and Djadjadihardja, Y. (2013). Seismoturbidite record as preserved at core sites at the Cascadia and Sumatra–Andaman subduction zones. Natural Hazards and Earth System Sciences, 13(4), 833-867.

Pavlides, S., and Caputo, R. (2003). Magnitude versus faults' surface parameters: Quantitative relationships from the Aegean Region. Tectonophysics, 380(3-4), 159-188.

Pearson, G. W., and Stuiver, M. (1986). High-Precision Calibration of the Radiocarbon Time Scale, 500–2500 bc. Radiocarbon, 28(2B), 839–862.

Polonia, A., Nelson, C. H., Romano, S., Vaiani, S. C., Colizza, E., Gasparotto, G., and Gasperini, L. (2017). A depositional model for seismo-turbidites in confined basins based on Ionian Sea deposits. Marine Geology, 384, 177–198.

Polonia, A., Torelli, L., Gasperini, L., and Mussoni, P. (2012). Active faults and historical earthquakes in the Messina Straits area (Ionian Sea). Natural Hazards and Earth System Sciences, 12(7), 2311–2328.

Quennell, A.M. (1956) Tectonics of the Dead Sea rift. In: Asociacion de Servicios Geologicos Africanos. Congreso Geologico Internacional, 20th sesion, Mexico, pp 385–405.

Quennell, A.M., 1958. The structural and geomorphic evolution of the Dead Sea Rift. Quarterly Journal of the Geological Society, 114(1-4), pp.1-24.

Ribot, M., Klinger, Y., Jonsson, S., Avşar, U., Pons-Branchu, E., Matrau, R., and Mallon, F. L. (2021). Active faults' geometry in the Gulf of Aqaba, southern Dead Sea fault, illuminated by multi beam bathymetric data. Tectonics.

Rieux, A., Weill, P., Mouaze, D., Poirier, C., Nechenache, F., Perez, L., and Tessier, B. (2018). Threshold of motion and settling velocities of mollusc shell debris: Influence of faunal composition. Sedimentology, 66(3), 895–916.

Rothwell, R. G., Hoogakker, B., Thomson, J., Croudace, I. W., and Frenz, M. (2006). Turbidite emplacement on the southern Balearic Abyssal Plain (western Mediterranean Sea) during Marine Isotope Stages 1–3: an application of ITRAX XRF scanning of sediment cores to lithostratigraphic analysis. Geological Society, London, Special Publications, 267(1), 79–98.

Sari E, and Cagatay MN., 2006. Turbidites and their association with past earthquakes in the deep Cinarcik Basin of the Marmara Sea. Geo-marine letters 26 (2), 69-76.

Schottler, S. P., and Engstrom, D. R. (2006). A chronological assessment of Lake Okeechobee (Florida) sediments using multiple dating markers. Journal of Paleolimnology, 36(1), 19–36.

Shanmugam, G. (1997). The Bouma Sequence and the turbidite mind set. Earth-Science Reviews, 42(4), 201–229.

Shanmugam, G. (2008). The constructive functions of tropical cyclones and tsunamis on deep-water sand deposition during sea level highstand: Implications for petroleum exploration. AAPG Bulletin, 92(4), 443–471.

Shanmugam, G. (2016). Submarine fans: A critical retrospective (1950–2015). Journal of Palaeogeography, 5(2), 110–184.

Shiki, T., Kumon, F., Inouchi, Y., Kontani, Y., Sakamoto, T., Tateishi, M., Matsubara, H., and Fukuyama, K. (2000). Sedimentary features of the seismo-turbidites, Lake Biwa, Japan. Sedimentary Geology, 135(1–4), 37–50.

Silva, P., Borja, F., Zazo, C., Goy, J., Bardají, T., Luque, L. D., Lario, J., and Dabrio, C. (2005). Archaeoseismic record at the ancient Roman City of Baelo Claudia (Cádiz, south Spain). Tectonophysics, 408(1-4), 129-146.

St-Onge, G., Mulder, T., Francus, P., and Long, B. (2007). Proxies in Late Cenozoic Paleoceanography (Vol. 1, pp. 63-92) (1170972623 878094129 C. Hillaire-Marcel & 1170972624 878094129 A. D. Vernal, Authors). Amsterdam, Netherlands: Elsevier.

Subaşi, Ö. (2015). Natural Disasters in Anatolia in the Eleventh Century. Journal of Turkish Research Institute, (54), 505-535.

Tibor, G., Niemi, T. M., Ben-Avraham, Z., Al-Zoubi, A., Sade, R. A., Hall, J. K., Hartman, G., Akawi, E., Abueladas, A., and Al-Ruzouq, R. (2010). Active tectonic morphology and submarine deformation of the northern Gulf of Eilat/Aqaba from analyses of multibeam data. Geo-Marine Letters, 30(6), 561–573.

Verosub, K. L., and Roberts, A. P. (1995). Environmental magnetism: Past, present, and future. Journal of Geophysical Research: Solid Earth, 100(B2), 2175–2192.

Villamor, P., and Berryman, K. (2001). A late Quaternary extension rate in the Taupo Volcanic Zone, New Zealand, derived from fault slip data. New Zealand Journal of Geology and Geophysics, 44(2), 243-269.

Willis, B., (1938). Wellings' observations of Dead Sea structure. Geological Society of America Bulletin, 49(4), 659–668.

Xiang, L., Lu, X. X., Higgitt, D. L., and Wang, S. M. (2002). Recent lake sedimentation in the middle and lower Yangtze basin inferred from 137 Cs and 210 Pb measurements. Journal of Asian Earth Sciences, 21(1), 77–86.

Yeniçeri, M.T. (2020). Geochemical Traces of Historical Eastern Mediterranean Tsunamis in the Sediments of Ölüdeniz Lagoon, SW Turkey. (MSc Thesis, Middle East Technical University).

Zilberman, E., Amit, R., Porat, N., Enzel, Y., and Avner, U. (2005). Surface ruptures induced by the devastating 1068 AD earthquake in the southern Arava valley, Dead Sea Rift, Israel. Tectonophysics, 408(1-4), 79-99.

APPENDICES

A. Radiographic image of the TR-5 sediment core

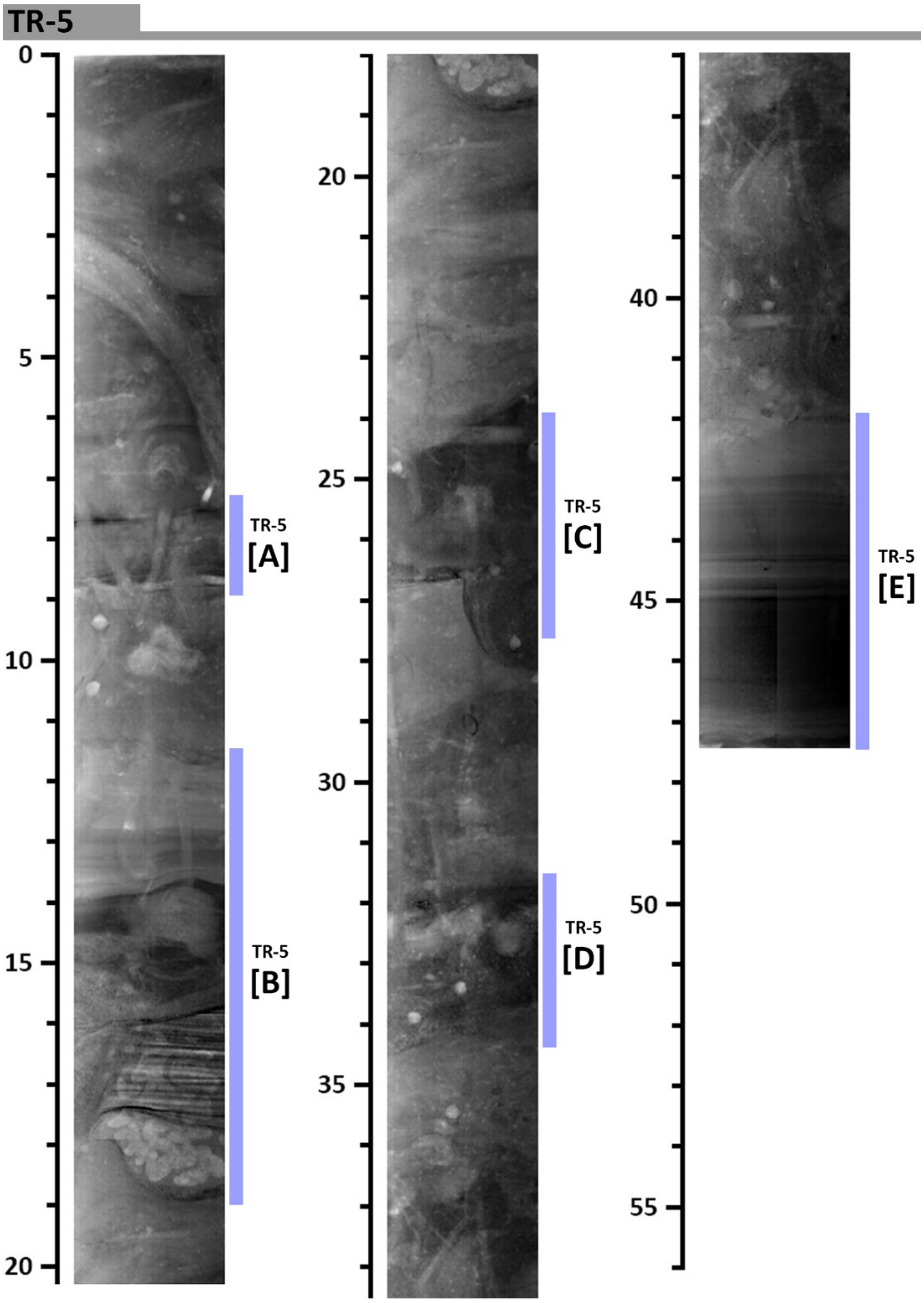

B. Radiographic image of the TR-4 sediment core

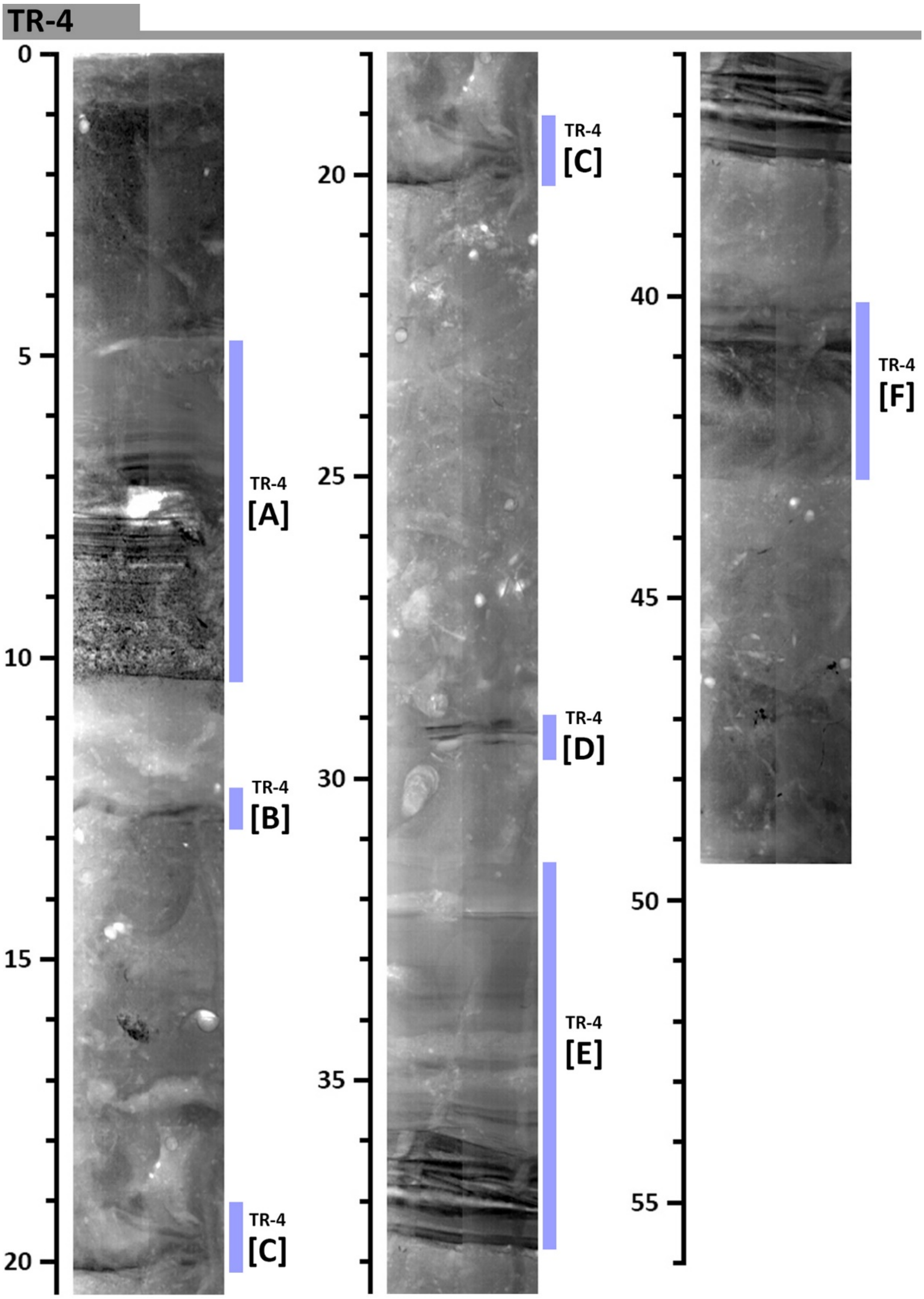

C. Radiographic image of the TR-3 sediment core

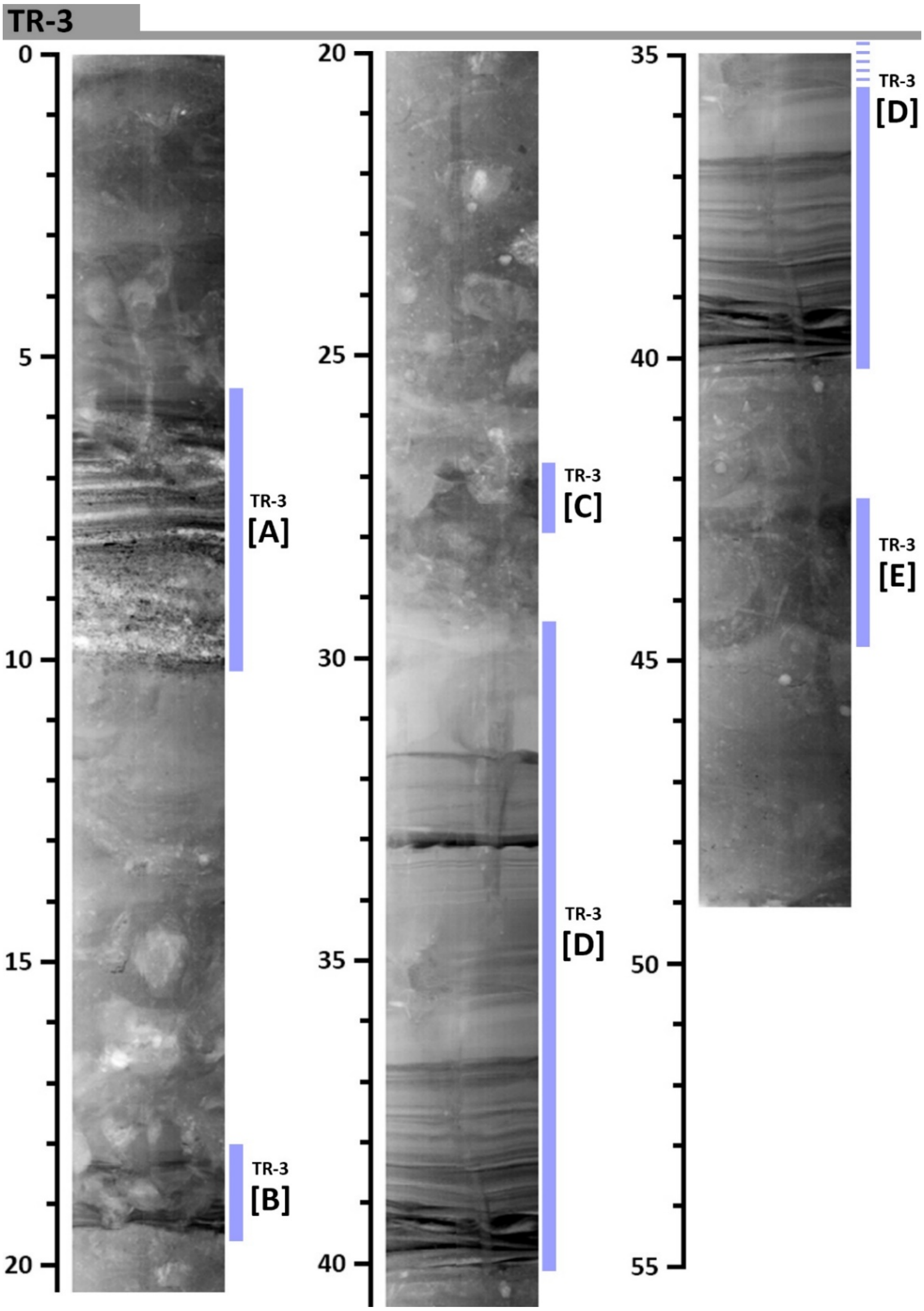

D. Radiographic image of the ELT-1 sediment core

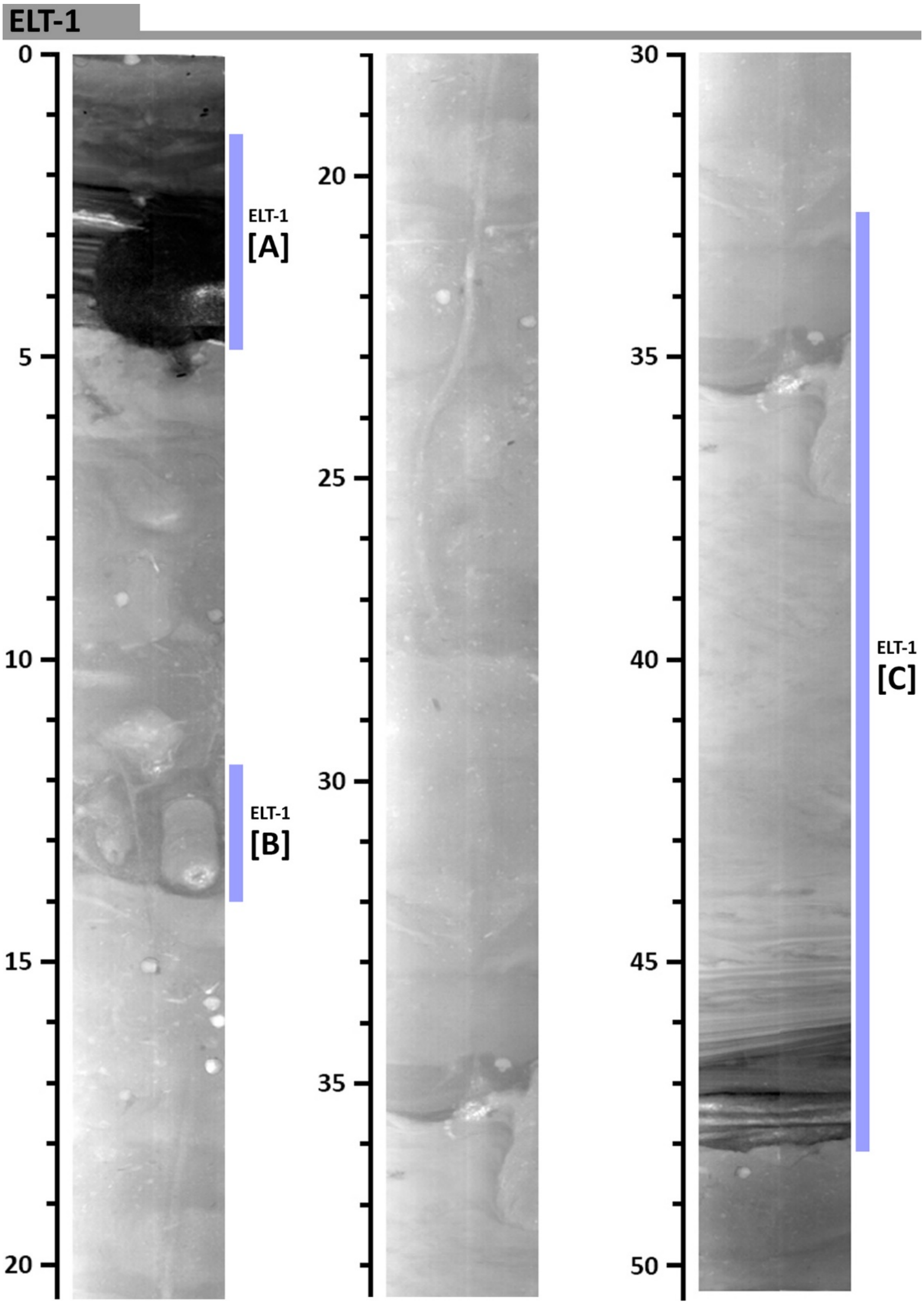

E. Radiographic image of the ELT-M3 sediment core

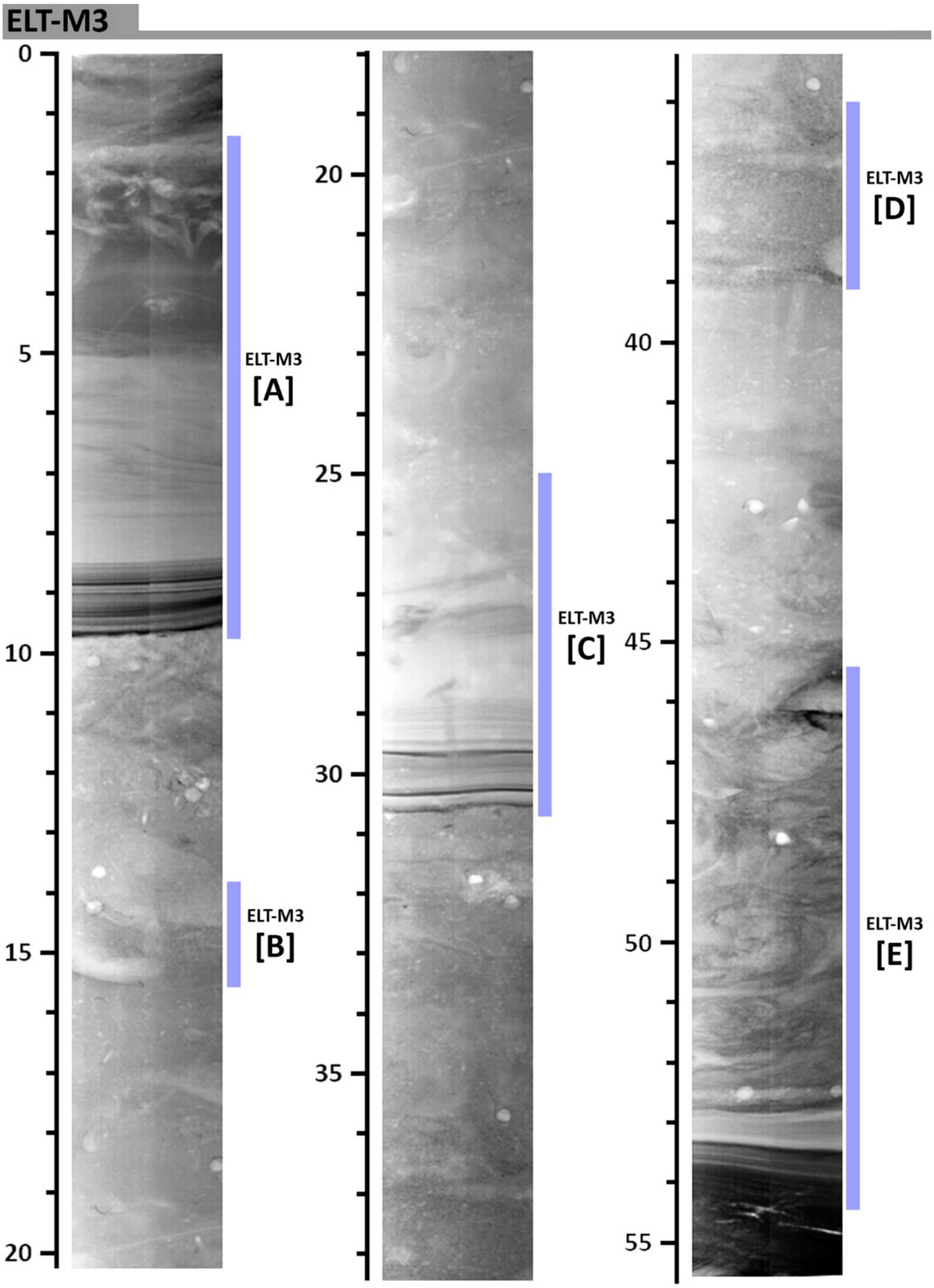

F. Radiographic image of the ELT-M2 sediment core

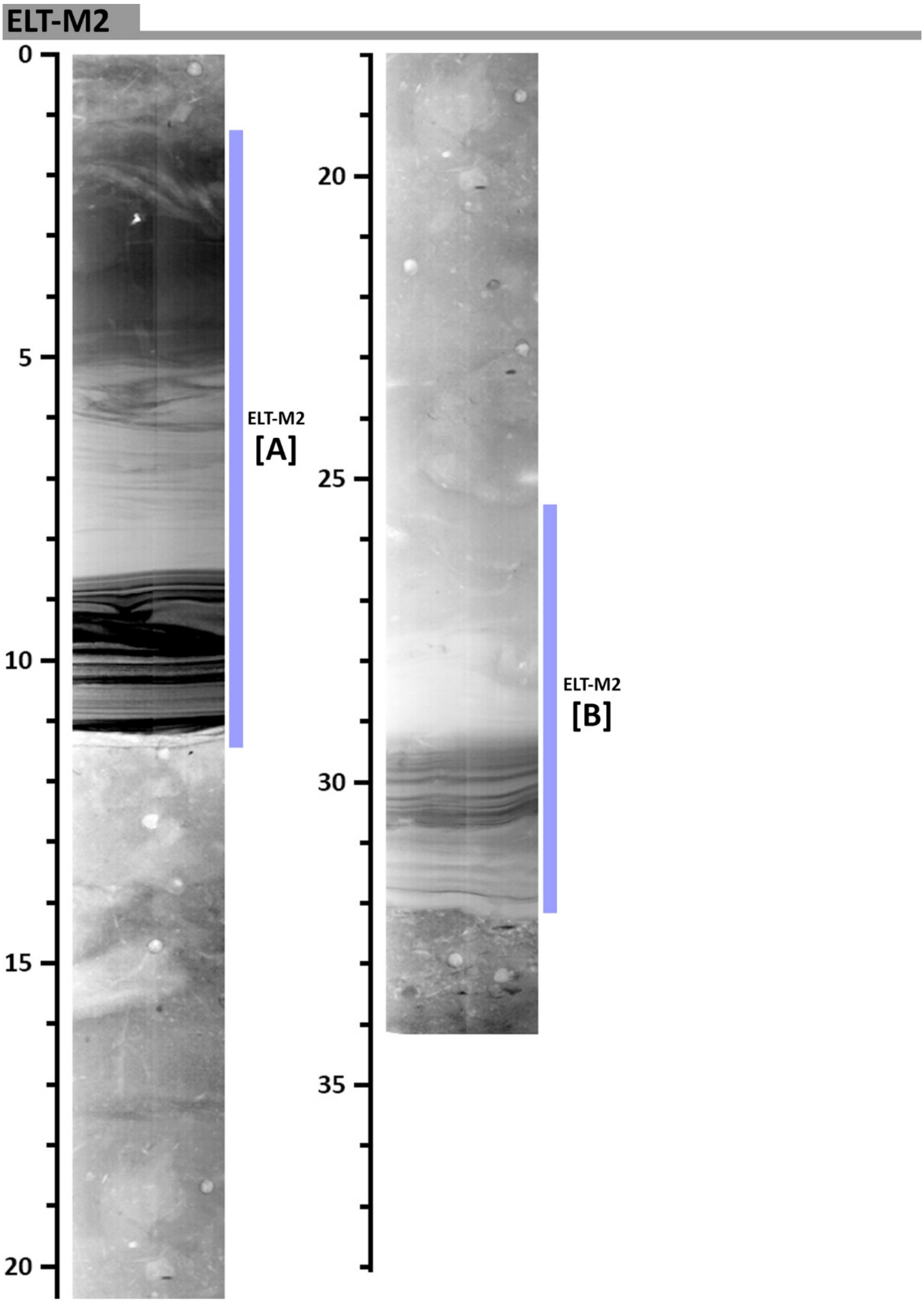

G. Radiographic image of the ELT-4 sediment core

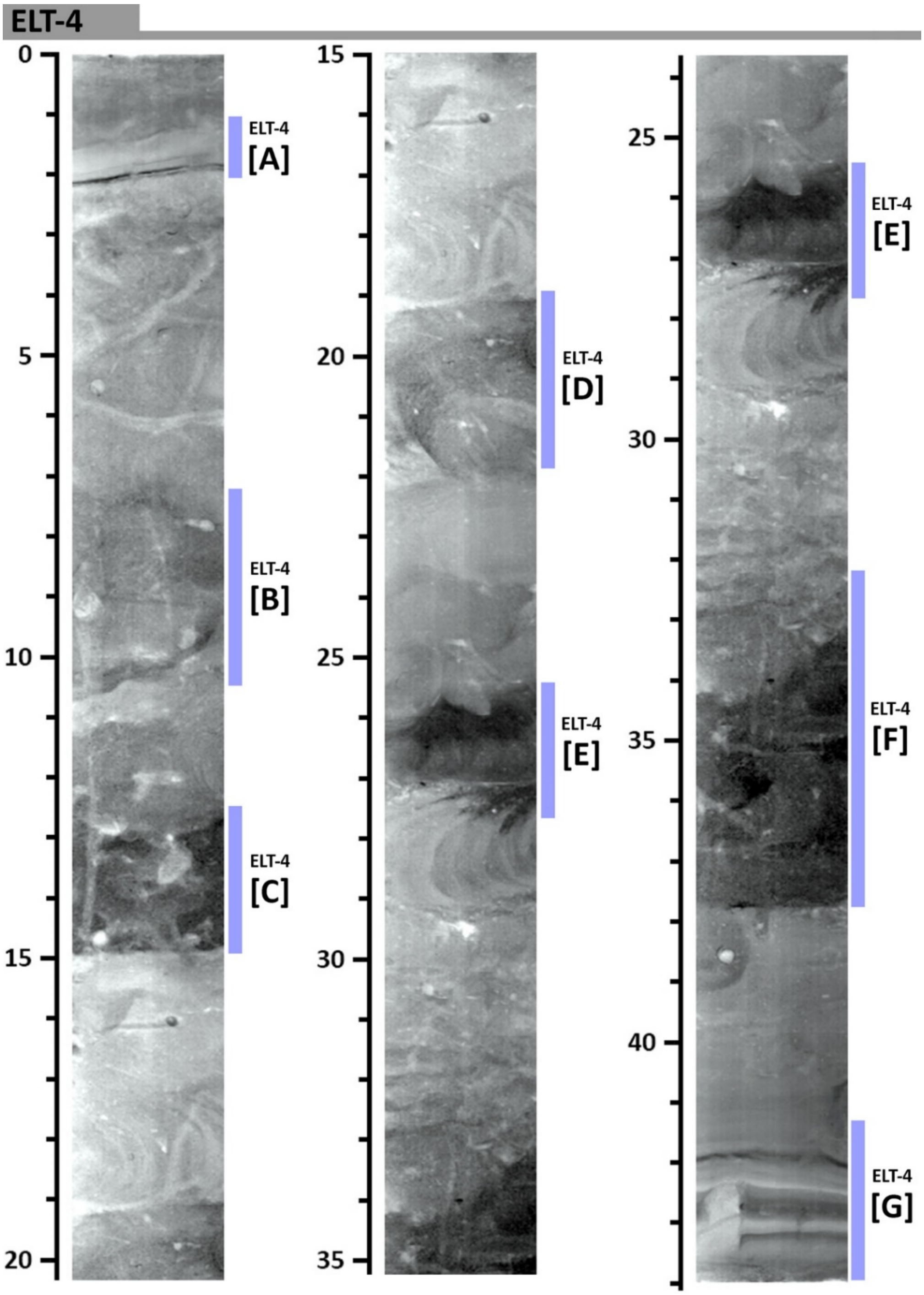

H. Radiographic image of the ELT-5 sediment core

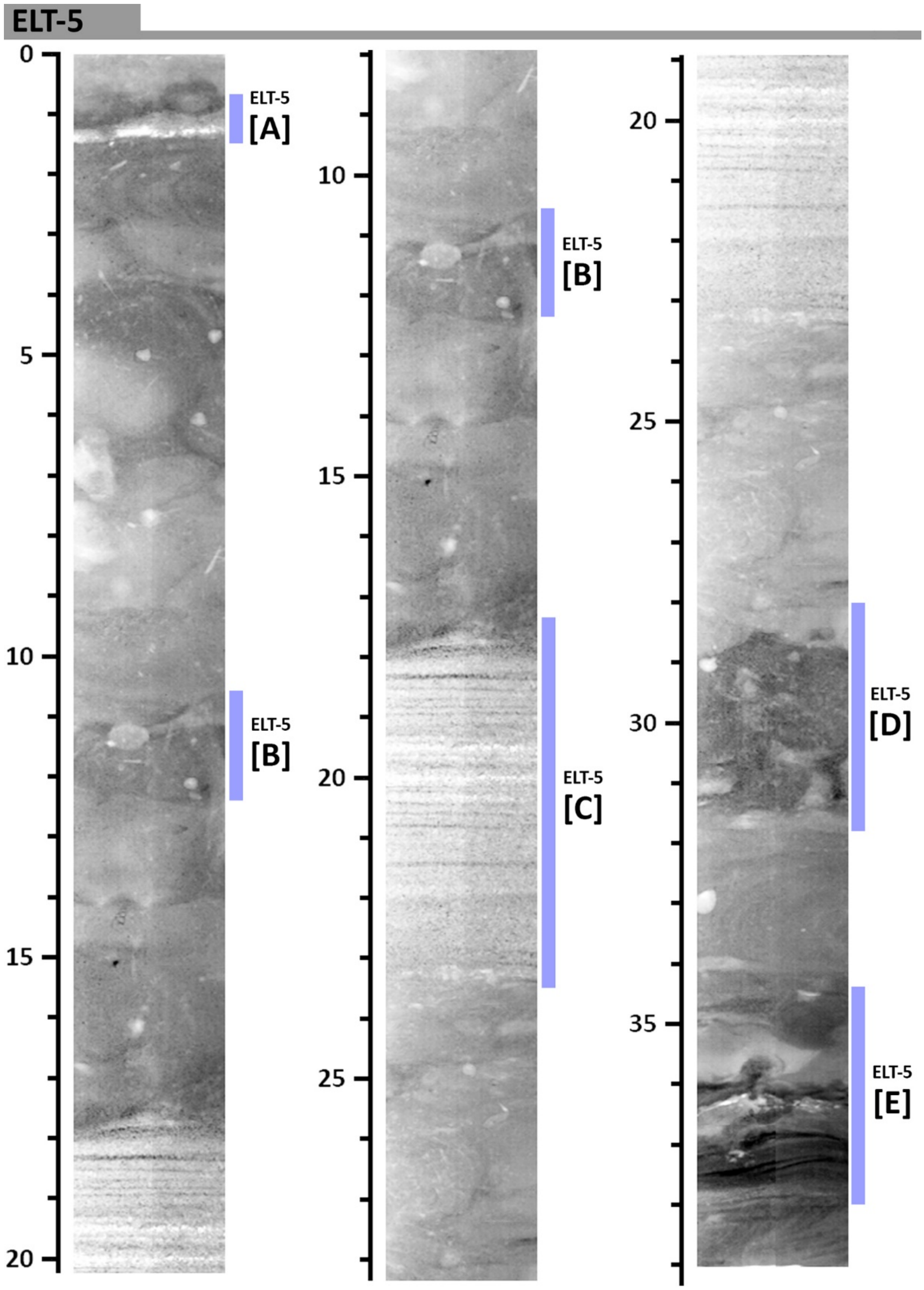

I. Radiographic image of the DK-1 sediment core

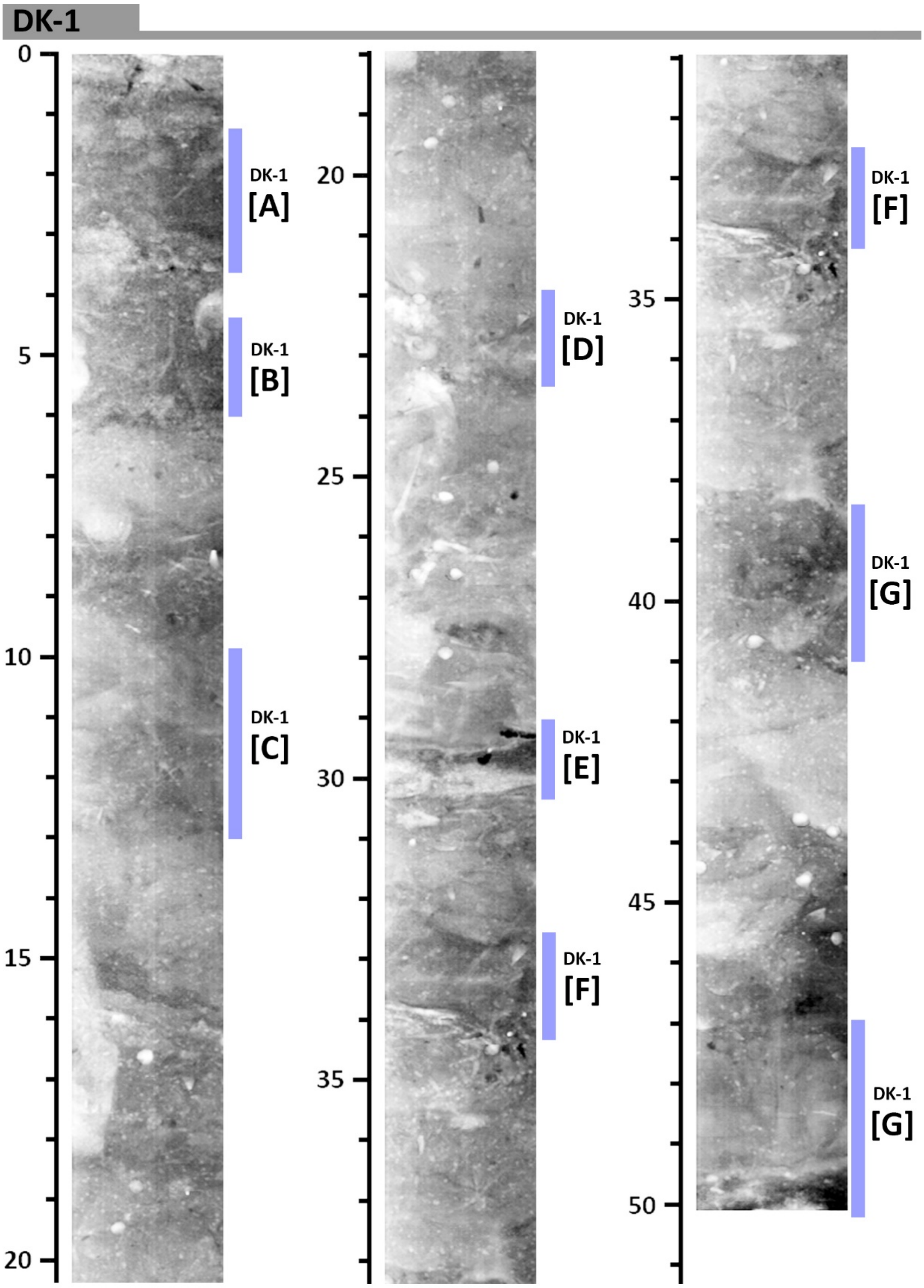

J. Radiographic image of the DK-2 sediment core

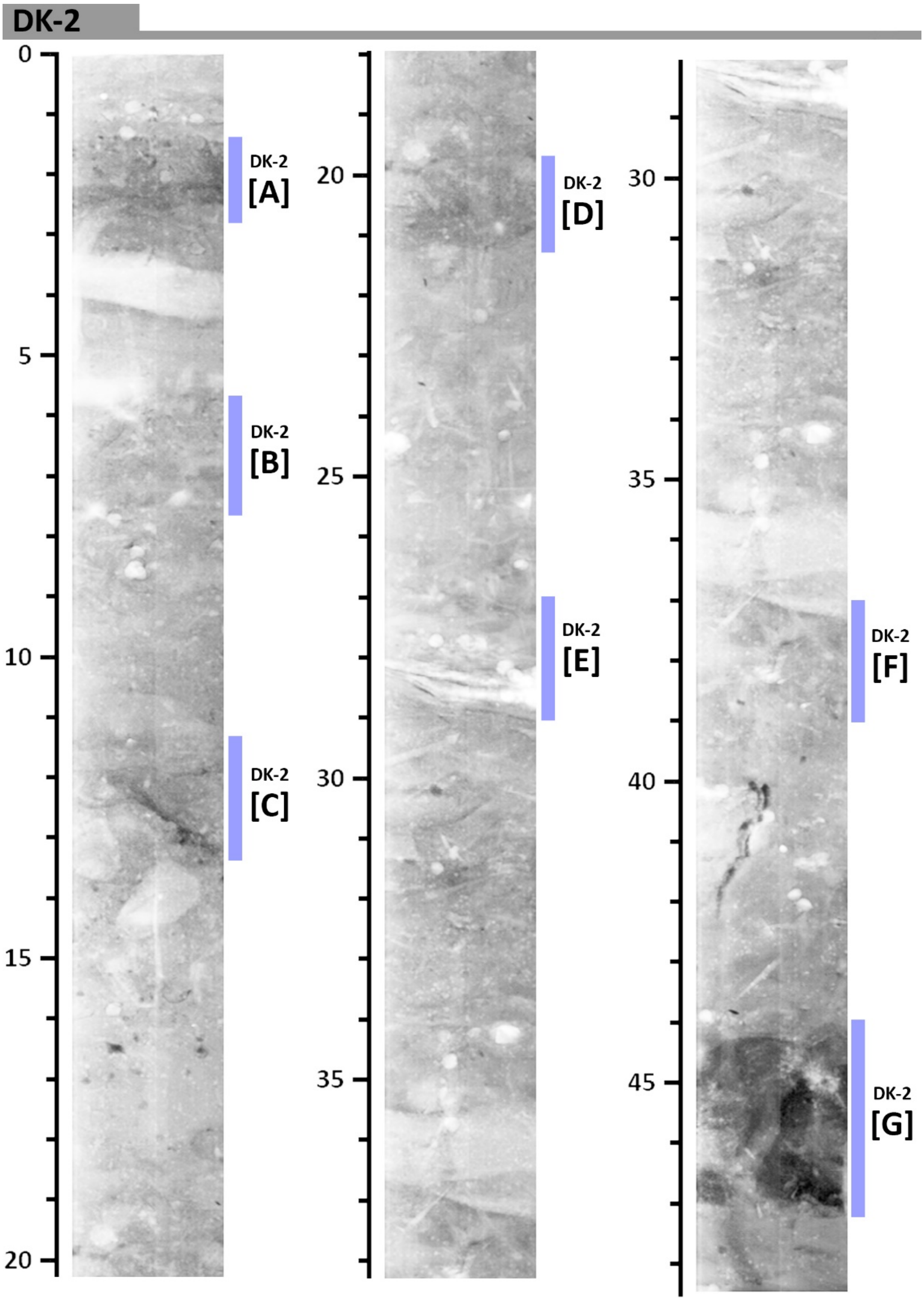

K. Radiographic image of the AR-1 sediment core

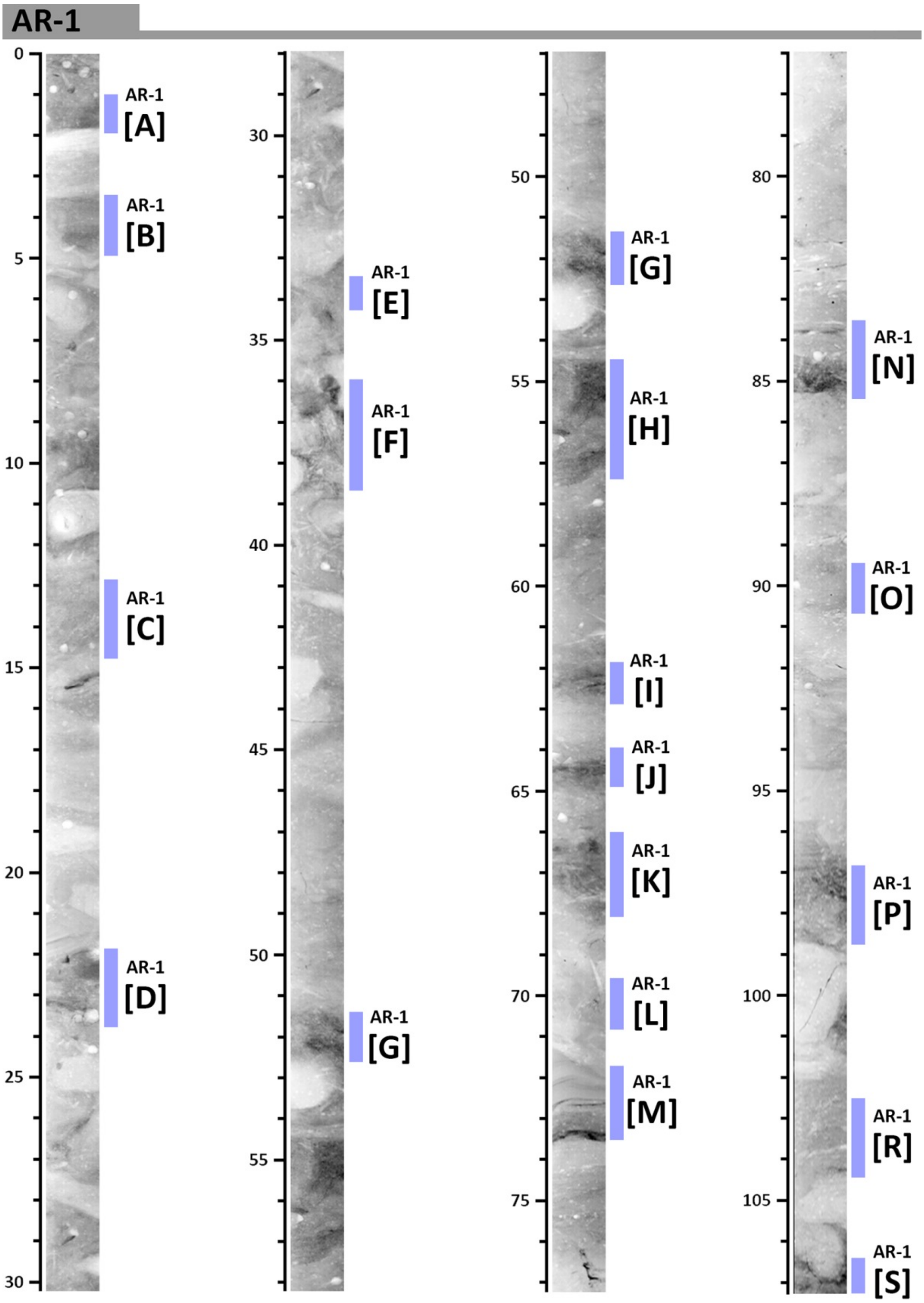

L. Radiographic image of the AR-2 sediment core

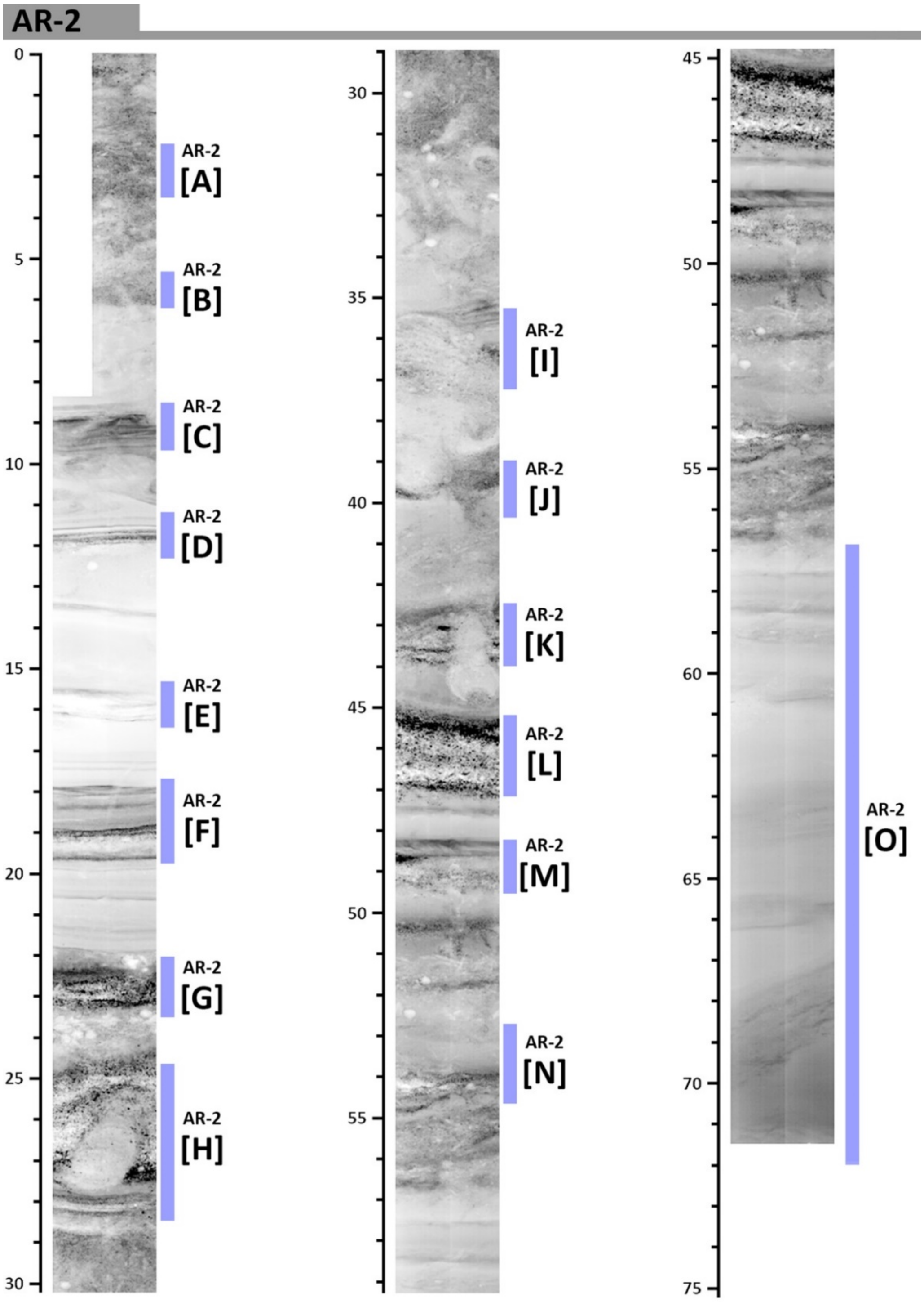

M. Radiographic image of the TD-2 sediment core

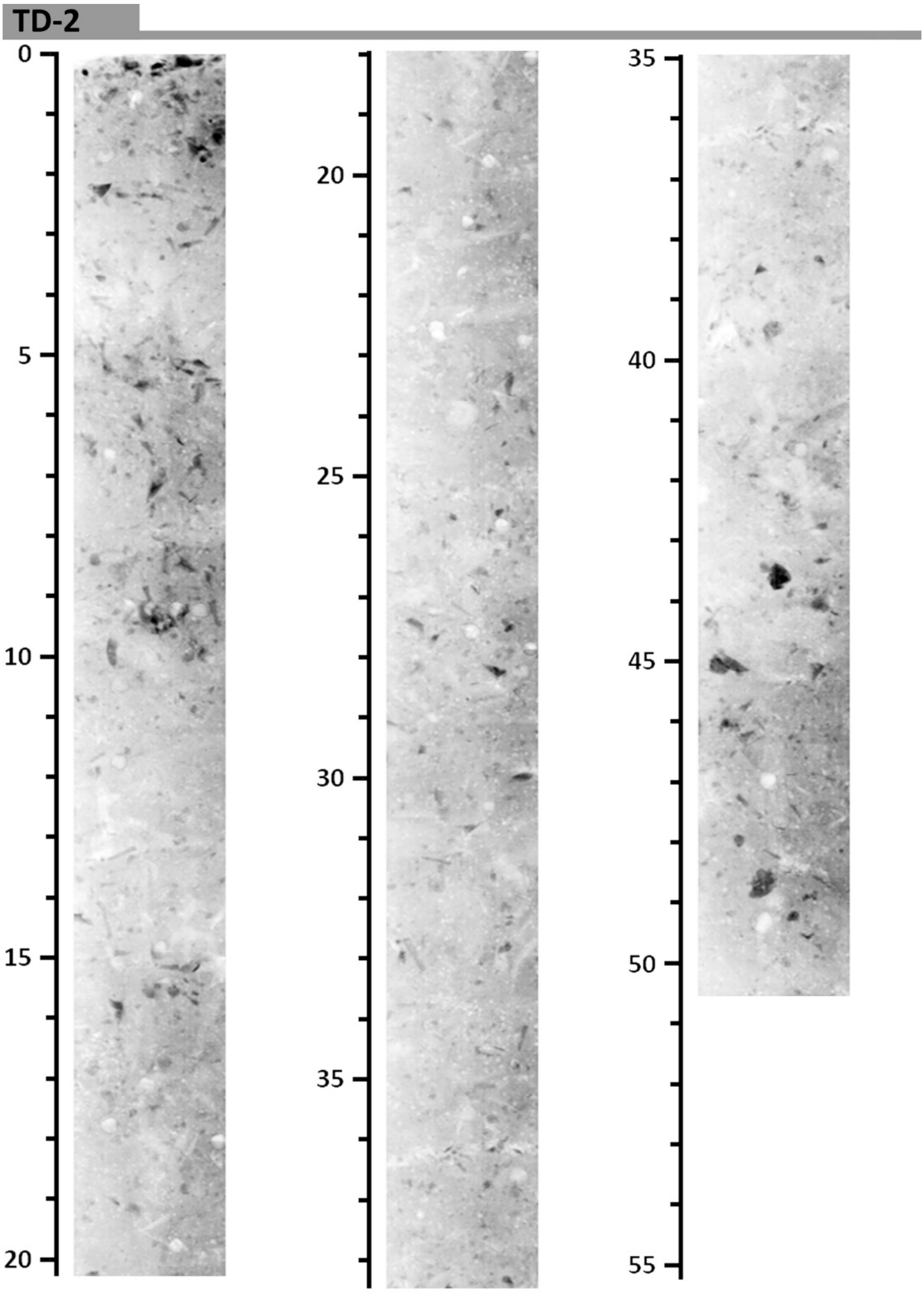

N. Radiographic image of the TD-3 sediment core

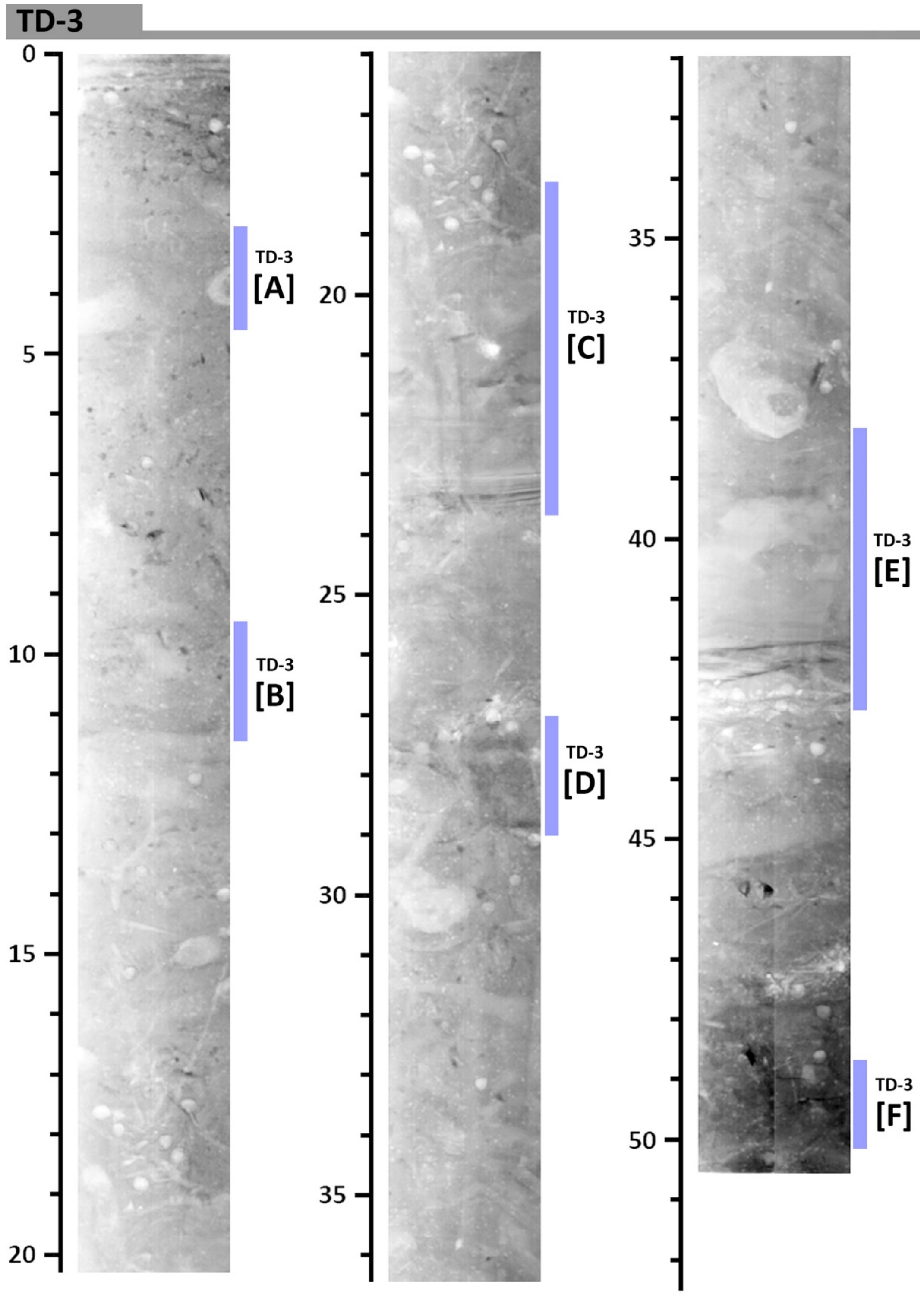

O. Radiographic image of the HM-1 sediment core